Evolution of the pore pressure due to vibratory installation of sheet piles in sand

A B Arun Kumar

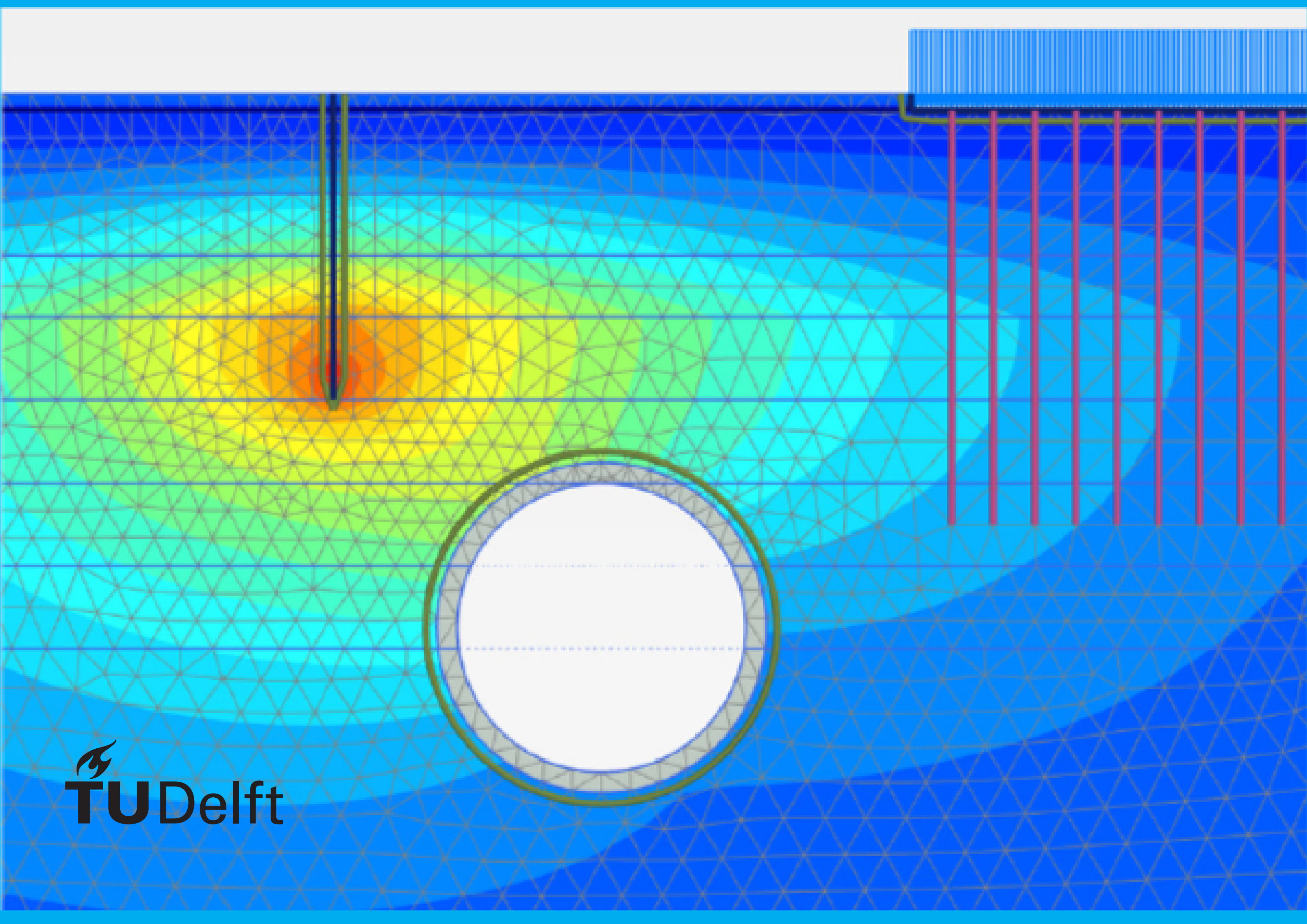

TU Delft

Evolution of the pore pressure due to vibratory installation of sheet piles in sand

by

A B Arun Kumar

to obtain the degree of Master of Science
at the Delft University of Technology,
to be defended publicly on Friday October 23, 2020 at 14:30.

Student number:	4824059	
Project duration:	November 16, 2019 – 23 October, 2020	
Thesis committee:	dr.ir.Wout Broere,	TU Delft,
	ir.drs.R.E.P. (Richard) de Nijs,	TU Delft
	dr.Alice Cicirello,	TU Delft
	Stefanos Gkekas, MSc	Witteveen Bos

This thesis is confidential and cannot be made public until March 31, 2021.

TU Delft

Dedicated to family and friends

Preface & Acknowledgement

"Who is helping you don't forget them. Who is loving you, don't hate them. Who is believing you, don't cheat them"

- Swami Vivekananda

I started my engineering career around tons of steel sheet piles being driven day and night in the projects along the western coast of Singapore. I was always fascinated by various sheet pile installation technique and this interested me to pursue my master thesis in "Evolution of excess pore pressure due to the vibratory installation of a sheet pile by vibratory driving.

I shall begin with God the almighty: without Thee we would never find the right path. I would like to thank my committee chair Dr Wout Broere for his support in guiding and motivating me to successfully pursue my master thesis. His direction helped me to find the right research path.

I thank ir.drs.Richard de Nijs for providing me with a wonderful opportunity to pursue this research thesis at Witteveen+Bos N.V. His insightful comments and tricky question motivated me to widen my research perspectives. My sincere thanks to Dr Alice Cicirello, for her continuous support and encouragement throughout my research period.

I wholeheartedly thank Stefanos Gkekas for putting up with my ideas and always providing me with a stimulating discussion. Without his precious support in unprecedented Corona times, this work would not have been possible. Further acknowledgement is dedicated to ir.Kristina Reinders for her encouragement and support. I thank my colleagues at TU Delft and Witteveen Bos for their motivation and support. My sincere thanks to Kshitij Asthana forever holding my back. I thank my friends and housemates for being there at all times. It is simply too long to list them.

Last but not the least, I would like to thank Mamma, Papa, Bhaiya and Bhabhi for their love and being ever supportive of all the decisions of my life. It has been a wonderful journey with all of you.

Anchal Bhaskar
23rd October 2020, Delft, The Netherlands.

Abstract

Vibratory installation of sheet piles is the most economic and suitable for the sandy soil because of its mechanism. However, the process induces excess pore pressure in saturated conditions leading to subsidence [65]. This research focuses on the development of a tool-based solution to predict the excess pore pressure due to vibratory installation, which shall be verified by the postdiction of Kademuur Damrak measurements. This tool will help engineers quantify the impact of generated excess pore pressure on adjacent structures.

The proposed work attempted to achieve its objective by answering the following main and sub research questions:

How can the existing knowledge on generation and evolution of porewater pressure during vibratory installation be effectively integrated into a model/tool, which verified by the postdiction of Kademuur Damrak measurements, can practically estimate the porewater over-pressure during vibratory installations?

- What are the parameters that influence the dissipation of the excess pore pressure?
- How does the generation and dissipation of excess pore pressure vary in the liquefied zone from non-liquefied?
- How can the vibration attenuation affect the generation of excess pore pressure in the sand?
- What are the limitations and controlling parameters of this model or tool?

The proposed work combines dynamic soil response and transient groundwater flow model to simulate the evolution of pore pressure due to vibratory loading. Based on the degree of modulus degradation due to the vibratory loading the soil, it is zoned into three. This is also termed as a multiscale computational framework. This allows for the formations liquefied and non-liquefied zone. The threshold acceleration of 0.1g - 0.3g must be available for the soil to liquefy [66]. The non- liquefied zone is fed by the groundwater flow from the liquefied zone.

According to the Theis equation, head response due to constant pumping in an aquifer is influenced by the rate of discharge (V), storativity(S) and transmissivity(T), distance from the source. This inspired to model the driving of sheet pile with an analogous to the pumping of well. During the constant head loading due to the pumping, there is an increase in the head radially outward from the source. This resembles the phenomenon of pre-shearing in the field. The driving of the sheet pile was stimulated by the constant head loading.

The application of time series analysis (PRIFICT method) [8] provides the first estimation of the pore pressure response from the first of three days of field piezometric data of Kademmur damrak. The semi-empirical model was formulated influenced by the head response of the slug test. The response of the time series analysis helped to calibrate the semi-empirical model. The relationship evolved between the physical and modelling parameters established that the hydraulic conductivity is the key parameter in both the generation and the dissipation of the excess pore pressure [88], [20]. The analysis of the field data establishes the conservative assumption of 1m for the width of the liquefaction zone. The analysis of accelerometer data from the Amsterdam noord zuid metro line tunnel helps to establish the dependency of liquefaction on acceleration amplitude. This bolstered the threshold acceleration for liquefaction to be 0.1 - 0.3g.

The simple flow only Plaxis model helped to validate the proposed hypothesis. The hydraulic conductivity was established as the key parameter of the model. The integration of dynamic generation and transient groundwater flow model helped to analyse the evolution of excess pore pressure.

Contents

List of Figures

List of Tables

1
Introduction

With the advent of the vibrating technique to install steel sheet piles, it has been ever easier to build temporary and permanent steel retaining structures. It is the quickest and most economic way to build sheet pile walls around the world today. However, it comes with the drawback of excessive noise, settlement induced due to vibration [65] and vibration itself [24]. The idea of least social impact due construction techniques is gaining significant importance [38], [13]. Hence, the negative impacts that the vibratory method can create on the environment are leaving the design engineers apprehensive to maximize its use. These negative factors not only impact soil or the structure but also interferes with daily human activity in the neighbourhood limiting its application.

1.1. Problem Statement:

Vibration is the predominant factor that hinders geotechnical engineer from adopting vibratory installation of sheet piles. It has the potential to generate excess pore pressure, settlement, the interaction of generated pore pressure with the adjacent structures leading to the structural damages.

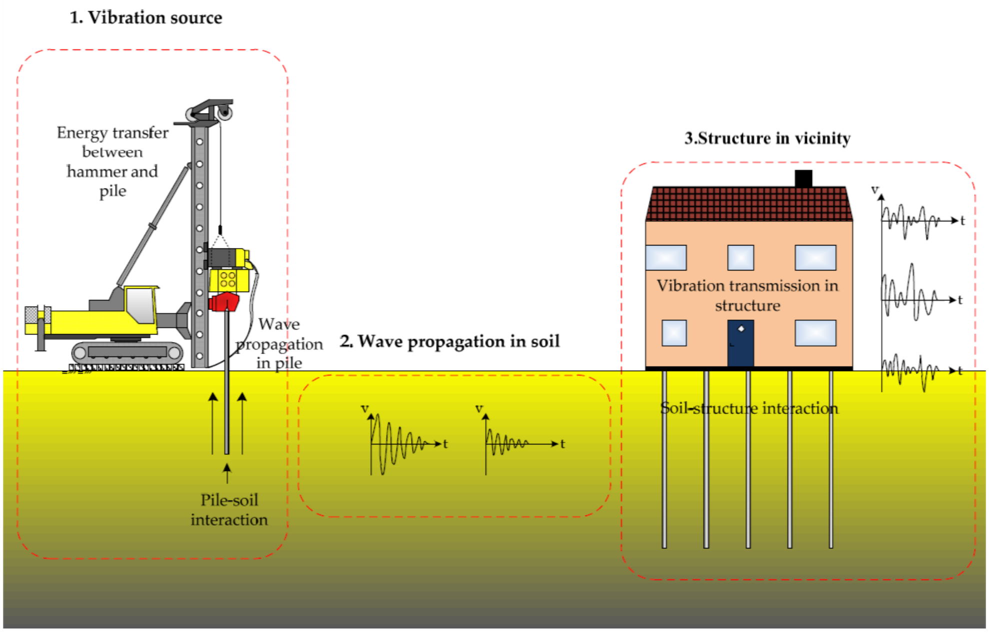

Figure 1.1: Vibration transfer during the pile driving in Urban areas [46]

The vibratory installation in the non-cohesive soil intervenes with the soil structures causing generation of excess pore pressure and settlement influencing the integrity of structures in the vicinity. The settlement may be caused due to densification of the granular soil leading to the volume loss affecting nearby structures.

It can be exemplified with changes in skin friction along the shaft of the piles impacting the bearing capacity of it [86]. Similarly, for the resistance of the tunnel walls and so on. In order to quantify the risk for adjoining structures, several models have been developed to estimate the impact of vibration on the buildings [25], excess pore pressure generation [57], [66], [41], densification [64],[59], post-liquefaction consolidations [4]. The excess pore pressure generated must undergo dissipation through the process of consolidation. It's crucial to interpret the behaviour of the soil for evaluating the risk adhered by the structures in the vicinity.

1.2. Aim and Objective

The objective of this research is to develop a practical tool for the estimation of generation and dissipation of excess pore pressures based on the integration of existing knowledge and validation on actual field data.

The study initially focuses on the literature investigation to better conceive the available knowledge on the physical process of generation of excess pore pressure due to the vibration of the sheet piles. Further, existing models to predict its magnitude and the extent of influence are reviewed. The second part of the literature aims to understand the process and soil parameters influencing the groundwater flow. The behaviour of pore pressure due to liquefaction and post liquefaction were expected to be modelled in terms of groundwater flow.

1.3. Extent and Limitation

The study is focused on the generation and dissipation of the excess pore pressure while driving the sheet-pile by vibratory methods. The stress-related investigation had been ignored in this study. The impacts of pore pressure generation on the adjacent structures are also not included as a part of the study. Upon numerical integration of necessary models and obtaining satisfactory results from it, adequately validated by the literature further attempts will be made to adapt the model for actual soil parameters from "Kademuur Damrak".

1.4. Research Question

The research question that is indicated below will act as a pivot for this work and also for the report. There are research works available that focuses on the magnitude of the excess pore pressure generated, settlement incurred due to the vibration activity and impact of vibration itself on the adjacent structures. However, very little has been done to get an integrated model for generation and dissipation of excess pore pressure. To cover this shortage, the research question is as follows:

1. *How can the existing knowledge on generation and evolution of porewater pressure during vibratory installation be effectively integrated into a model/tool, which verified by the postdiction of Kademuur Damrak measurements, can practically estimate the porewater over-pressure during vibratory installations?*
    (a) What are the parameters that influence the dissipation of the excess pore pressure?
    (b) How does the generation and dissipation of excess pore pressure and vary in the liquefied zone from non-liquefied?
    (c) How can the vibration attenuation affect the generation of excess pore pressure in sand?
2. *What are the limitations and controlling parameters of this model/tool?*
3. *What are the recommendations for future additional work on this model/tool?*

1.5. Research Approach and Strategy

The initial goal of the work was to understand the complete physical process of vibratory installation and groundwater flow. Later, a model was introduced to analyse and rebuild the field data. The analysis of field data also enabled to demarcate the soil continua into liquefied and non-liquefied zones. It established the rate of generation and dissipation of the excess pore pressure and relationship between various model parameters and physical parameters. Later, an attempt was made to model generation and dissipation of excess pore pressure during and post liquefaction using PLAXFLOW(the flow only module of PLAXIS). Further, a sensitivity analysis was carried out to create a better understanding of the process of dissipation and validation of the model using the available data from a case of "Kademuur Damrak".

1.6. Presentation of the Research Results

The project aimed to provide a model to predict the generation and dissipation behaviour of the pore pressure in the granular soil due to the vibratory installation of the sheet pile. The expected output from the project includes understanding the existing analytical models and numerically implement the finite element model. The research project was carried out in five stages and the chapters of the report were directly dependent on these stages. First, the literature investigation established suitable available models to be included in the different components of the proposed model. The existing theory of pore pressure generation and dissipation was reviewed and explained elaborately. Later, the process of formulation of the analytical model to rebuild the field piezometric data was elaborated. Later, the attempt to model the process in PLAXFLOW module is elaborated. Lastly, the discussions about the findings, inferences and conclusions made and recommendation for future work.

The outline of the report is as follows:

1. Introduction
2. Literature review
3. Data Analysis (Case of Kademmur Damrak)
4. Modelling implementation of the process
5. Discussions
6. Conclusions and recommendations for future work

2
Vibratory Installation of Sheet pile

In the Netherlands, the sheet piles are installed by three different technique: pressing, hammering and vibrating. The vibratory method accounts for 70% of installations due to its low cost, high productivity rate and less impact to the pile itself in Dutch conditions. Here the layer of saturated loose to medium compacted sand is confined between soft clay and peat. In case of very soft soil pressing technique is applied and in sand with high relative density, hammering is applied [83]. The objective of this work was to model the generation and dissipation of the excess pore pressure due to the vibratory installation of the sheet pile. This chapter provides the theoretical background for the proposed work.

The vibratory hammer is a complex mechanical device run on hydraulic or electrical power. The energy from the hammer is transmitted to the soil through the pile generating waves. These waves interact with the soil media and cause cyclic loading. The complexity of the cyclic loading leads to the degradation of the shear modulus of the sand. The degradation of the modulus is caused due to the generation of excess pore pressure which is dependent on the amplitude of vibration. The amplitude undergoes attenuation as a function of distance. Further, the cyclic behaviour of the sand can also be understood in the laboratory and relative field parameters can be computed by laboratory tests. The course of this chapter is represented in the flowchart (fig: 2.1).

2.1. Vibratory Hammer

The vibration from the hammer can be depicted as a sinusoidal wave. During the installation of the sheet piles, the vibration amplitude propagates to the adjacent soil medium as waves, transferring the energy. The oscillation of the particle around the state of equilibrium is similar to the vibratory motion and the propagation is characterized by displacement of particle or body in time due to the acceleration [47]. The action of wave allows transmission of energy through the material, without any material transport [86]. There are different types of vibro-drivers used in the field, but one of the most effective in reducing the vibration in the adjacent structures is the high-frequency vibrators with a frequency range of 30 - 40 Hz. [91]

The vibratory installation has 3 major components: **Vibratory hammer, Steel Sheet pile and Soil**.

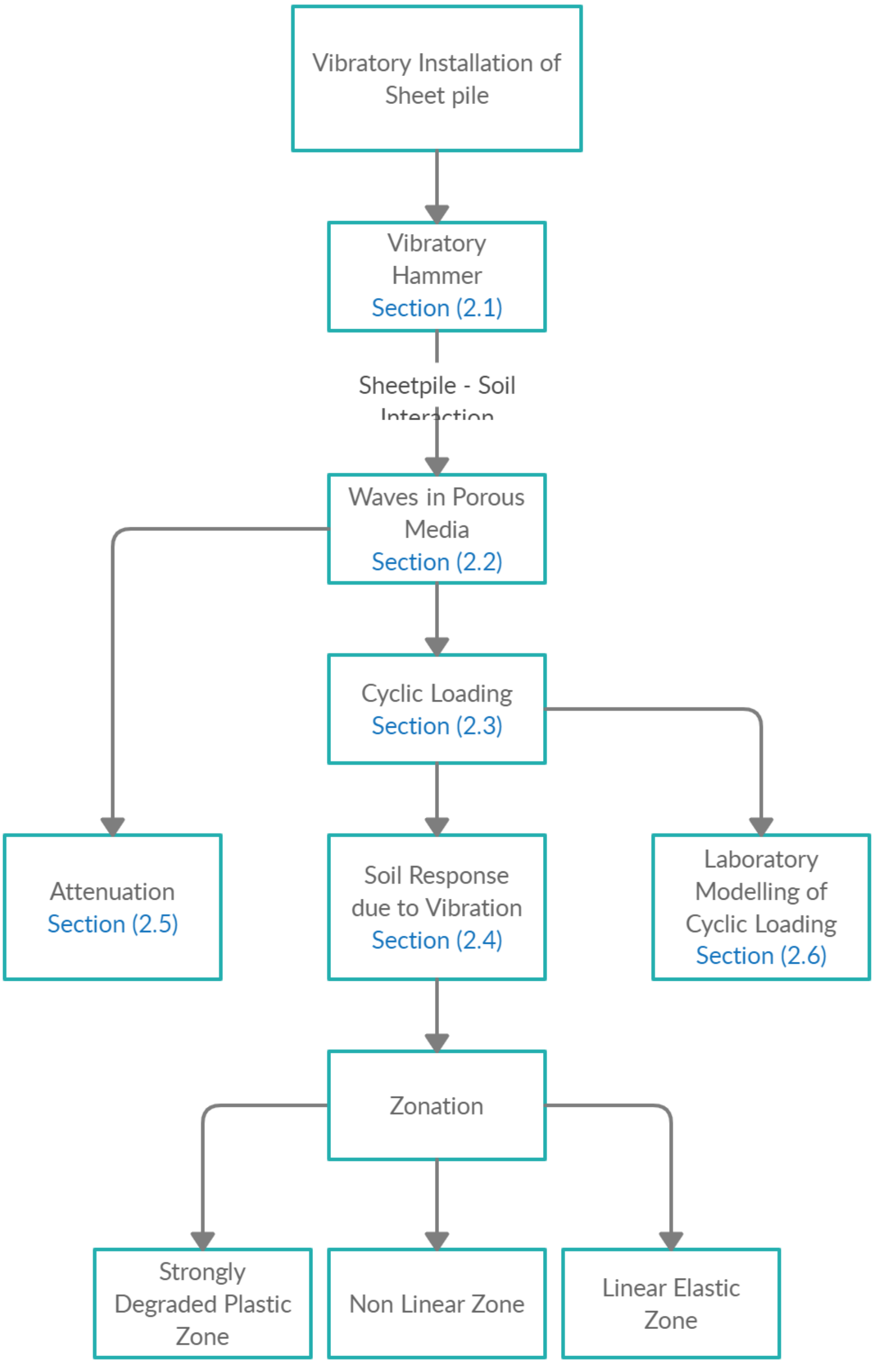

Figure 2.1: Flow of Chapter 1

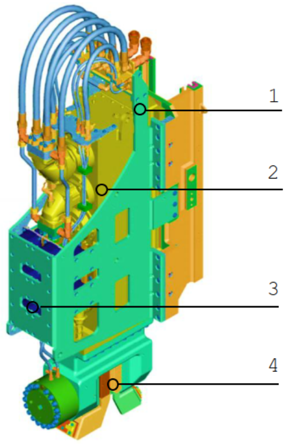

Figure 2.2: Vibratory Hammer (1.Suppressor housing, 2. Excitor block, 3.Elastomer pads, 4. Clamping device)

2.1.1. Components of vibratory hammer:

The modern hydraulic vibrator consist of 4 major parts:

- A suppressor housing
- Elastomer Pads
- An exciter block and
- Clamping device
- The exciter block is mounted to the **suppressor housing** with numerous elastomer pads. It's fitted with an eye in case of free-hanging type or to guide frame in case of leader mounted. The weight of the suppressor housing is called bias mass or static surcharge force.($G_{vibrator}$) [64].
- **Exciter(oscillator) block** of vibratory hammer houses a pair of eccentrically mounted masses in a frame. It's isolated from the hammer support by bias mass and between the bias mass and oscillator lies a very soft spring or **elastomer pads**. The bias mass adds as a static load to the pile while driving.

In the case of free-hanging system, the hanging force must be subtracted from the load of the bias mass. But in case of leader mounted it is possible to apply additional load by using the reaction force of the machine, hence it is not required to subtract the suspension force in this case [64].

for free hanging,

$$F_0 = G_{vibrator} * g - F_{pull} \tag{2.1}$$

Where,

- F_0 = Static Surcharge Force [N]
- $G_{vibrator}$ = Bias mass or Static surcharge force [kg]
- g = gravity [m/s^2]
- F_{pull} = Suspension force [N]

The leader mounted has a large range of applied static surcharge load during the installation whereas it is restricted in case of the free-hanging model. In contrary, the free-hanging method has a larger reach without altering the position of the crane and are more suited for the area with soft soils like Netherlands [87]. The vibration is generated by counter-rotating eccentric masses at a similar speed, therefore it cancels out the horizontal component of the centrifugal force that lead to harmonic vertical component over their time. However, horizontal vibration had been monitored in various studies [64],[25]. **Clamping device** holds the pile in position. It transmits the vibration from the hammer to the pile with least damage to the pile.

2.1.2. Working of Vibratory hammer

The vibratory hammer makes use of both vibratory and static surcharge to drive the sheet-pile into the ground. The crane is insulated from the vibration due to the elastomer pads provided that also adds to the static surcharge [93]. The vibration causes cyclic loading of sand which aids for the generation and buildup of excess pore pressure. This significantly reduces the static soil resistance and the pile penetrates into the ground. The vibration causes the soil mass to lose its shear strength by the reduction in the inter-granular forces due to the acceleration of the particle exceeding its initial overburden pressure[85].

The force components considered for the design of sheet-pile driving are as follows: [64]

1. Weight of the sheet-piles = $G_{sheet} = m * g$
2. Weight of the Vibrator = Bias Mass, Clamp, Exciter Block = $G_{vibrator}$

3. Line Pull = F_{pull}
4. Resultant of centrifugal force from the Vibrator = F_{dyn}
5. Tip Resistance = F_{tip}
6. Friction at Interface Wall - Soil = $F_{friction}$
7. Clutch Friction = F_{clutch}
8. Inertia of the sheet-piles = $m * a$

Item 1 to 4 are Driving force, and 5 to 8 are resisting forces.
The net downward force as a function of time during installation:

Downward movement:

$$F(t) = m * a = -F_{pull} + G_{vibrator} + G_{sheet} - (F_{clutch} + F_{friction}) - F_{tip} + F_{dyn} \tag{2.2}$$

Upward movement:

$$F(t) = m * a = F_{pull} - G_{vibrator} - G_{sheet} + (F_{clutch} + F_{friction}) - F_{dyn} \tag{2.3}$$

The significant machine parameters include the eccentric moment M_e, the driving frequency f, the resultant centrifugal force, static load, the driving force, free-hanging double displacement amplitude.

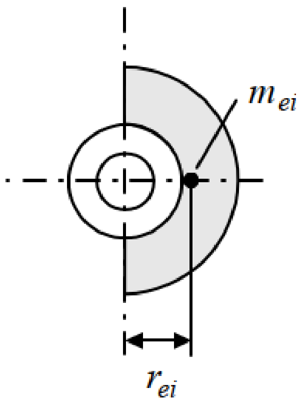

Figure 2.3: Eccentric Load and Radius [87]

Eccentric Moment: The eccentric masses in exciter block determines the eccentric moment. The center of gravity lies at a distance r_{ei} from the axis of rotation. In case of several eccentric loads the individual loads are summed up.

$$M_{ei} = m_{ei} * r_{ei} \tag{2.4}$$

Where:

- M_{ei} = eccentric moment [kg.m]
- m_{ei} = eccentric mass [kg]
- r_{ei} = eccentricity radius [m]

Driving Frequency (f_d): It's the number of revolution of the eccentric weights. The unit is Hertz(Hz).

$$f_d = \frac{\omega}{2\pi} \tag{2.5}$$

Where: ω = Angular Frequency

Vertical component (F_0): The amplitude of the vertical vibration force due to an eccentric mass is given by [83]:

$$F_0 = M_{ei} * (2\pi f_d)^2 \tag{2.6}$$

Vertical force (F_v): The dynamic vertical vibration force from the top of the sheet pile applied by the vibrator shall be given by [83]

$$F_v(t) = M_{ei}\omega^2 * sin(\omega t) \tag{2.7}$$

The horizontal component of the dynamic load gets cancelled out as eccentric loads rotate in opposite direction. Further in absence of the soil and the interlocking resistance, the amplitude of the vibration(d_0) shall be given as [83]:

$$d_0 = \frac{M_{ei}}{m_{dyn}} \tag{2.8}$$

Where,

- d_0 = Vibration amplitude [mm]
- m_{dyn} = Dynamic Mass (Dynamical Part vibrator, clamp, pile) [kg]

The vertical force generated by an individual eccentric load is summed up to achieve the total dynamic load (F_v). The total driving force is given by the sum of the dynamic load of F_v and static load of F_0. Thus, this vibratory motion is transmitted to the sheet pile and further to the soil. During the process, there is pile-soil interaction which needs to be intricately understood to design sheet pile installation close to the existing structures.

2.1.3. Design Equation for the vibratory piling

Even though the discussion on the design of vibratory piling is not relevant for the current work for the sake of completeness, a simple model utilized in the Dutch construction industry shall be discussed.

One of the most applied model in the Netherlands from CUR166 given by Dutch Civil Engineering and centre for Construction Research and Design rules(CUR)

$$m_r = \frac{m_{dyn} * d_0}{1000} * 9.81 \tag{2.9}$$

where m_r is total eccentric moment [Nm]. This equation can be rewritten as 2.8. It is accepted that once the free vibration amplitude(d_0) exceeds 5mm, the pile will be able to penetrate the soil media. It is important to note that there are no soil parameters available in the model.

2.2. Waves in Porous Media:

From, fig:1.1 it can be noted that the second part illustrates the propagation of waves in the soil which is of at-most importance in our study. The vibration may originate from various source but currently, we are considering the one due to the vibratory sheet-pile installation. The impact of any other sources was ignored. The Installation of the sheet-pile propagates its vibratory motion to the surrounding soil in form of waves. Both primary (P-waves) and shear waves (S-waves) are generated at the toe of the piles. Along the shaft, due to the friction, only S-waves are generated. However, it was later proposed that P- waves are also propagated as an attribute to the horizontal motion of the sheet-piles (fig: 2.5) [23]. Further, when the P & S wave reaches the free surface of the ground it forms Rayleigh waves. The generation and the propagation of the waves are well described in fig:2.5 [23].

2.2.1. P-waves:

P-waves can lead to the volume change in the medium as they cause compression and rare-fraction. These waves doesn't cause any shearing in the medium that it propagates through but oscillates the particle parallel to the direction of the wave propagation. It can propagate through both the solids and fluids [71], [56]. Propagation velocity c_P of p-wave is given by [56]:

$$c_P = \sqrt{\frac{M}{\rho}} = \sqrt{\frac{G(2-2\nu)}{\rho(1-2\nu)}} = \sqrt{\frac{E(1-\nu)}{\rho(1-2\nu)(1+\nu)}} [m/s] \tag{2.10}$$

- c_p = velocity of compression waves [m/s]
- M = Deformation modulus or Odometer modulus [Pa]
- G = Shear Modulus [Pa]
- E = Elasticity Modulus [Pa]
- ρ = material density [kg/m^3]
- ν = Poisson's ratio [-]

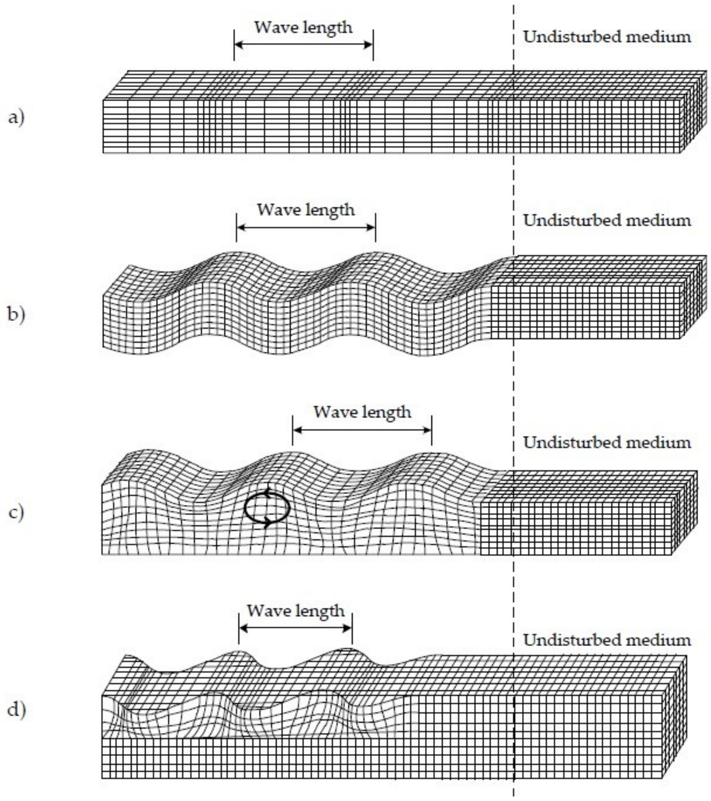

Figure 2.4: Visualization of different waves a) P-wave, b) S-wave, c) R-wave and d) Love-wave, [24]

2.2.2. S-waves:

The S-waves are transverse waves that cause shear deformation in the medium that it propagates. However, it cannot pass through fluids as they don't possess any shearing stiffness. The velocity of the shear wave (c_S) can be computed from [56].

$$c_S = \sqrt{\frac{G}{\rho}} = \sqrt{\frac{E}{2\rho(1-\nu)}}\,[m/s] \tag{2.11}$$

- G = Shear Modulus [Pa]
- E = Elasticity Modulus [Pa]
- ρ = material density [kg/m^3]
- ν = Poisson's ratio [-]

The S wave causes oscillation in the particle perpendicular to its propagation. The direction of the oscillation helps to breakdown the S-wave into two components SV(Vertical plane movement) and SH(Horizontal plane movement).

2.2.3. R - waves:

The R-waves or Rayleigh waves propagate along the surface of the ground having both horizontal and vertical components of motion. It's a product of the interaction of P-wave and SV-wave with the surface[56].The motion of the wave is in form of a retrograde ellipse as represented in fig: 2.4. The velocity of the R-wave (c_R) can be given by: [47][86].

$$c_R \approx \frac{c_s(0.87 + 1.12\nu)}{1+\nu} \tag{2.12}$$

Where

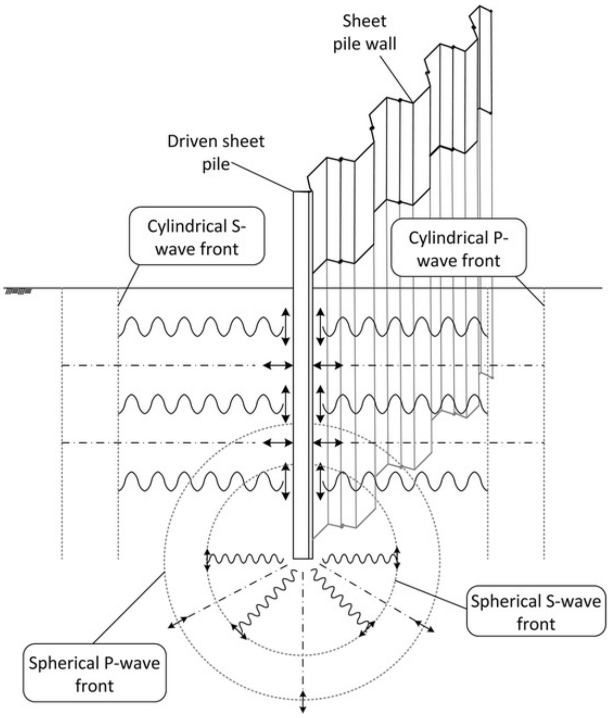

Figure 2.5: The propagation of the waves from sheet-pile to soil during vibratory driving of sheet-piles [23]

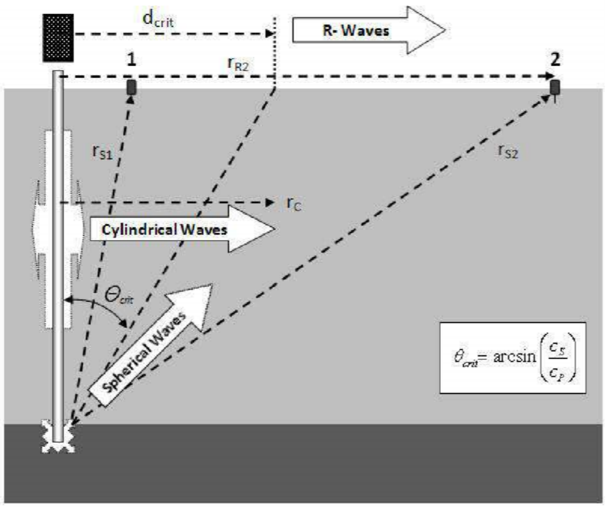

Figure 2.6: Illustration of the wave generation at the pile toe, Representation of Critical Angle [60]

- c_S = Shear wave velocity [m/s]
- ν = Poisson's ratio [-]

The propagation velocity of the R -wave are independent of the vibration frequency that makes it non-dispersible in the homogeneous half-space. [60] described critical distance as the extent at which P-waves reaches the surface of the ground from the toe of the pile(point of origin). It is represented as

$$\theta_{Critical} = arcsin\left(\frac{c_S}{c_P}\right) \tag{2.13}$$

Where

- c_S = S - wave velocity [m/s]
- c_P = P - wave velocity [m/s]

The critical distance $r_{critical}$ from the pile, where refraction will occur on the ground surface:

$$r_{critical} = tan\theta_{Critical} * d \tag{2.14}$$

Where d = Pile Penetration depth.

Soil	P - Wave Velocity [m/s]	S - Wave Velocity [m/s]
Clay	1450 - 1900	80 - 500
Sand	1400 - 1800	100 - 400

Table 2.1: Velocity of P - wave and S - wave [45]

The relationship to approximate the shear stress amplitude from the above computed parameters can be given as [60]:

$$\Delta v = \frac{\Delta a}{2\pi f} \tag{2.15}$$

$$\Delta\gamma = \frac{\Delta v}{C_s} \tag{2.16}$$

$$\Delta\tau = G * \Delta\gamma \tag{2.17}$$

Where

- Δa = amplitude acceleration
- Δv = amplitude velocity
- f = frequency
- $\Delta\gamma$ = amplitude shear strain
- C_s = shear wave velocity, where Cs = $\sqrt{\frac{G}{\rho}}$
- G = shear modulus
- ρ = unit mass of the soil
- $\Delta\tau$ = shear stress amplitude.

2.3. Cyclic Loading:

The vibration due to installation of sheet pile interacts with the soil along the interface of the pile. The interaction between the pile and soil leads to the energy transmission in form of waves 2.2. The relevant waves act upon the soil media and cause cyclic loading that leads to the building up of excess pore pressure, densification and settlement in loose - medium sand. The three aspects to be considered while installation of sheet-pile by the vibratory method include:

- Duration of loading
- Number of Load Cycles
- Loading amplitudes

.

During certain unfavourable ground conditions, the loading period to install sheet-piles may go up to 30 minutes instead of the usual 2 - 10 minutes. Also during unfavourable conditions because of availability of time, the system is expected to act as neither drained nor undrained, it undergoes partial drainage [32].

2.3.1. Cyclic Behaviour of Sand

Sand is treated as a continuum in geotechnical engineering. The cyclic loading due to the vibrating sheet piles are usually parametrized based on the duration of driving, a number of cycles and amplitude of loading. During driving of sheet pile, there is a movement of sand particles and in saturated conditions, the movement leads the generation of excess pore pressure. In the conditions of rapid loading, the pore pressure accumulates. There will also be simultaneous dissipation of excess pore pressure making it evident to understand the process of pre-shearing [64].

The cyclic behaviour of the sand can be explained in two distinct ways,

- Micro Level Behavior
- Macro Level Behavior

The micro-level particle interaction due to the cyclic shearing has been presented in the work of [99] fig: 2.7.The sand skeleton due to shear loading attempts to take denser form. In the unloading phase, the gap between the particles is regained. On reversal of strains, the gap collapses back and these repeated cycles lead to a condition where not all the strains are recovered during unloading. In case, if the initial state was denser, then soil matrix is expected to achieve relative density which will be less dense. But in case of loosely packed sand, the final state is denser than the initial state. The illustration of the interaction of the sand particle at the micro-level, i.e., two-particle in contact is explained by [27] using Hertz theory. The plastic shear occurs when the displacement is greater than the diameter of the particle. But this doesn't happen in the real world as the usual soil packing is extremely complex and shapes of the grains are irregular. There is also a possible presence of *local shear stress* even at zero average shear stress condition that may contribute to the failure. Further, the description of the total quantitative behaviour of sand can be depicted by Discrete Element Models.

The cyclic shear loading aids to the building up of excess pore pressure. In case of non-cohesive soil in saturated conditions, effects are subdivided as (a)highly degraded zone, (b) Near field, (c) Far-field [26]. The slip surface is highly degraded due to very high shear stress. In the near field condition, shear strain amplitude is higher and subsequent damping ratio is greater as well but in the far-field, both are greatly reduced due to the impact of attenuation [53]. The shear strain amplitude is a function of stress level which causes an increase in threshold amplitude. The magnitude of pore pressure generated is a function of shear strain amplitude [77].

The amount of pore pressure generated due to cyclic loading applied on the ground material due to sheet-pile installation can be computed using several models. The densification models usually have acceleration as their main loading parameter [64]. For the plane that falls perpendicular to the direction of propagation in case of a compression wave, it leads to the alternating rise and fall of normal stress in that assumed plane. This directly implies that it increases or decreases the resistance against sliding. Cyclic shear loading in the porous media is induced due to the shear waves [25].

Change in normal stress due to P-Wave can be computed by:

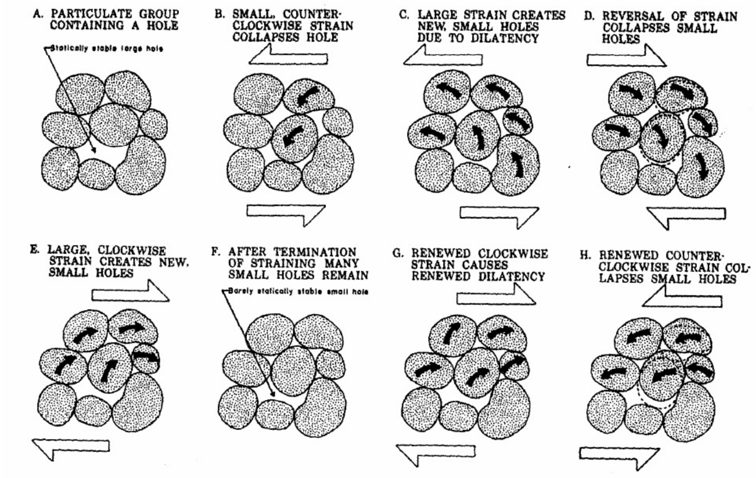

Figure 2.7: The group of soil particle illustrating packing due to cyclic loading [99]

$$\Delta\sigma_n = \frac{E\Delta v}{C_p} \tag{2.18}$$

Where

- $\Delta\sigma_n$ = stress amplitude [Pa]
- Δv = velocity amplitude [m/s]
- E = Young's modulus [kg/m^2]
- C_P = P-wave velocity [m/s]

The change in the normal stresses due to the P-wave loading is negligible on the surface and increases with depth. When the speed of deformation is low, the system gets enough time to drain but when loading is quicker, there is no sufficient time for dissipation to occur. This restricts any volumetric strain, but due to increased pore pressure the re-arrangement of grains within the fixed volume is carried out leading to the reduction of inter-particle stress and liquefaction happens in certain cases.

2.3.2. Pre-shearing effect

Pre-shearing: Generation and dissipation of the excess pore pressure may occur simultaneously. Also, the interim drainage significantly reduces the generation of pore pressure.

Pre-shearing examples: Wind and vibratory loading, isotropically loading and unloading of the sample (over consolidation), deviatoric loading and unloading of the sample and preloading with a large number of small amplitude cycles.

The excess pore pressure generation due to wave loading on a sandy seabed and also by placing a wave tank in a centrifuge, [73], also by [82]. In the test, wave loading is constant but the generation and dissipation of the excess pore pressure occur simultaneously. The excess pore pressure increases first and at this stage, the generation is in excess to the dissipation, after some time the generation reach saturation and excess pore pressure decreases as dissipation becomes dominant. The aspect of pre-shearing has been intensively investigated using modified triaxial test where simultaneous dissipation of the excess pore pressure is simulated. The two main mechanisms responsible for densification of the sand include :

1. Densification due to dissipating water.
2. Change in soil fabric.

2.4. Soil response due to the vibration:

The vibratory hammers work on the principle that the vibration applied to the soil reduces the shear strength of the soil allowing the penetration of the pile with lesser loads. The vibration induced by the pile applies cyclic displacement instead of cyclic loading on the soil due to a large number of cycles compared to the penetration speed. A typical soil response on harmonic cyclic loading is represented in fig: 2.8 [26].

The nature of the soil response is dependent on the magnitude of the shear amplitude exercised on it, modifying the moduli[26]. The vibration amplitude vary radially given by Bronitz equation[71] which is also attributed to Barkan [9] causing varying soil response 2.5.

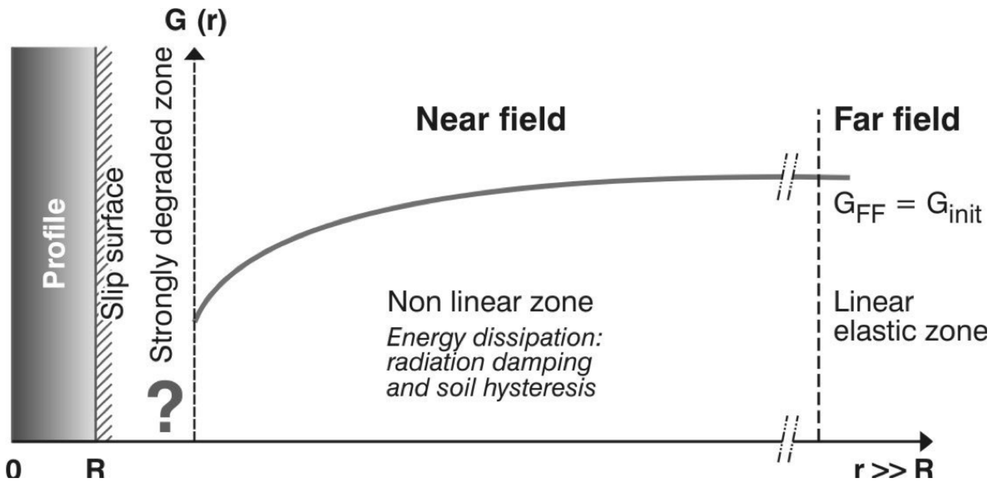

Figure 2.8: Influence on the mechanical properties described in zones during sheet-pile driving [26]

The response of the soil when vibration is applied to it is determined by the amplitude of the shear strain that determines the stiffness. This is usually related to the modulus reduction curve. Under small strains, the elastic waves are assumed to be generated but in the case of the large strains, the stiffness decreases and leads to the increase in damping ratio of the soil [56].

Attempts have been made to classify the soil behaviour based on the magnitude of the shear strains (fig:2.9). Further, in a dynamic situation, the acceleration also determines the behaviour of the soil (fig:2.10).

Shear strain	**10^{-6}**	**10^{-5}**	**10^{-4}**	**10^{-3}**	**10^{-2}**	**10^{-1}**
	Small strain	Medium strain		Large strain		Failure strain
Elastic						
Elasto-plastic						
Failure						
Effect of load repetition						
Effect of loading rate						
Model	Linear elastic		Visco-elastic		Load history tracing	

Figure 2.9: Soil response to the different shear strain levels [93] from [51]

Particle acceleration	**0.6g**	**1.5g**
Elastic state		
Shear strength reduction		
Fluidized state		

Figure 2.10: Soil response to the varying acceleration levels based on the shaft resistance [93]

Based on the above degradation behaviour of the soil, the soil can be radially distinguished into three prominent zones (a) Elastic zone, (b) Viscous-elastic zone, (c) Plastic zone.

2.4.1. Elastic Zone:

During the vibratory installation, far from the source, the soil strain falls below 10^{-5} and are expected to generate the elastic wave. This is ideally considered as far-field and the parameters are determined by parameters from the theory of elasticity as in 2.2.

Parameters	Expression	Unit	Definition
G	$G = \tau/\gamma$	[Pa]	Shear modulus - stress strain behaviour for elastic deformations
ν	$\nu = \epsilon_{yy}/\epsilon_{xx}$	[-]	Poission's ratio - ratio of transversal and axial strain
ρ	$\rho = m/V$	[kg/m^3]	Bulk density

Table 2.2: Parameters for Elastic State [93]

2.4.2. Viscous-elastic Zone:

For the medium strain levels, there is a rise in the relative motion between the grains leading to abrasion, degradation of the aggregates, energy lost due to the friction. These losses in turn attenuate the amplitude of the propagating vibration. This effect is termed as internal damping of the soil and can be explained by the hysteric effect or the viscous damping ratio(ξ). The internal damping is dependent on the soil characteristics and amplitude of the cyclic strain(γ_C) [45] and independent of the loading rate [93].

$$\xi = \frac{\Delta W_C}{2\pi\gamma_C\tau_C} \tag{2.19}$$

- ΔW_C = energy lost at each cycle $[J/m^3]$

- γ_C = cyclic Strain [-]

- τ_C = cyclic stress[Pa]

The shear modulus (G_{max}) decreases with the increase in the number of the cycles. The stress-strain degradation in the sand depends on the inter-particulate force which can be described by their relative density(D_r) and confining stresses. The sand is more susceptible to the vibration due to its ability to rearrange the particle upon vibration.

There are several experimental evaluations carried out by [84], [64],[26],[25] to understand the behaviour of the sand that vary due to the relative density and degree of saturation. The cyclic shearing of the saturated sand leads to the building up of the excess pore pressure causing reduction of the effective stress impacting shear strength and modulus [89]. The modulus degradation of the dry sand due to the acceleration has also been studied extensively [26].

When large strain is applied on the dense and medium sand, initially dilation occurs resulting in a reduction of pore pressure causing concave shape in the hysteresis loop. Further, on the continued application of strain contraction occurs driving up the pore pressure forming the convex shape in the hysteresis loop (fig:2.11) [84].

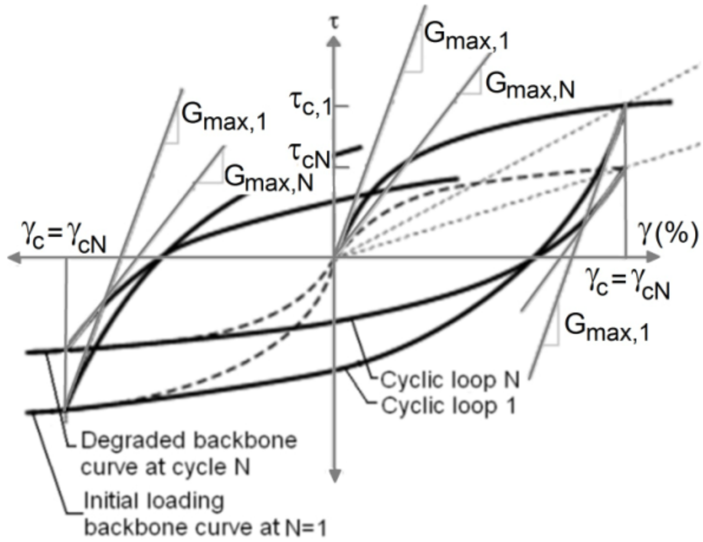

Figure 2.11: Soil Stiffness degradation due to cyclic shear [89]

2.4.3. Plastic Zone

The zone closest to the sheet pile is slip surface. It is strongly remoulded and expected to undertake convective motion of the remoulded soil. It is difficult to define a tangent shear modulus of this zone. It was also expected that slippage of the pile can occur [26]. This **multiscale computational framework** of the soil behaviour is advantageous as **continuum modelling of the highly degraded zone under large cyclic strains becomes non-viable**. It will also form the basis of the excess pore pressure modelling in this thesis.

2.5. Attenuation

The magnitude of pore pressure generated in the porous media is proportional to the amplitude of waves acting at the point leading to cyclic loading. As the distance from the source of the wave increases the amplitude gets attenuated due to the damping effect of the soil. Hence, it is important to derive a relationship between these variables. Further, these variables act as an input to the generation model which computes the magnitude of pore pressures. The attenuation of the ground vibration with distance due to the pile driving can be attributed to the following [6]:

- Radiation damping / Geometric damping
- Material damping / Hysteretic damping (friction of the system)

The ground vibration measurements due vibratory installation of the sheetpile are reported from the literature in fig:2.12 [6]. The simple attenuation model frequently used is linear log-log relationship [6],i.e.,

$$v = kr^{-m}$$

Where

- v = peak particle velocity at ground surface (vertical direction)
- r = radial distance from the source
- m = slope / attenuation rate
- k = constant

The attenuation of the ground vibration shall be given by Bornitz equation [71]

$$w_2 = w_1 \left(\frac{r_1}{r_2}\right)^n e^{-a(r_2-r_1)} \tag{2.20}$$

where,

- w_1, w_2 = vibration amplitudes at r_1 & r_2 from the source of vibration.
- n = coefficient of geometric damping
- a = coefficient of material damping

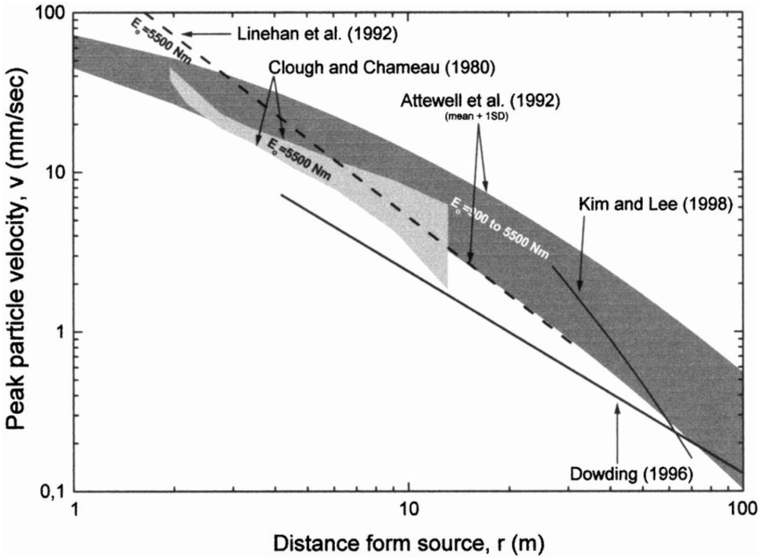

Figure 2.12: Attenuation of vibration with distance for vibratory sheet-pile driving [6]

2.5.1. Hysteretic Damping

It is internal damping caused by the dissipation of energy due to friction in soil elements. The energy is used up by storing in form of elastic energy and to destroy the edges and structure of the soil grains. Further, the energy also gets converted into sound and heat. Hysteretic damping is measured in terms of the damping ratio. It is a ratio between the amount of dissipated energy in the soil element per cycle(ΔW) of loading to the elastic energy stored per cycle (W). The coefficient of the material damping "a" is described as a function of the soil type and frequency of vibration [95]. Later, the coefficient was redetermined independent of the frequency, given as $a_0 = a/f$ [96]. The values of both the coefficients are included in the appendix.

Determination of Damping Ratio

The damping ratio can be obtained from the laboratory tests depending on the strain amplitudes. It is because shear modulus diminishes to the increasing shear strain. The **Resonant column** can be used to determine the shear moduli for the strains smaller than 10^{-4}. For the strain range larger than 10^{-4} the soil behaves plastic and the damping level is much larger. Cyclic loading test must be deployed for better understanding.

2.5.2. Radiation Damping

The waves are generated at the interface of the pile-soil. The energy gets distributed over the larger volume in the soil environment and this phenomenon is called radiation damping or geometric damping. The rate of the radiation damping depends on type of source (tab:2.3) or on the type of wave(Appendix: A).

Source	Attenuation Amplitude as a function of distance(R) from source
Cylindrical Source	$\frac{1}{\sqrt{R}}$
Spherical Source	$\frac{1}{R}$

Table 2.3: Radiation Damping based on varying source [48]

2.5.3. Shear Stress Attenuation

The main factor affecting the amplitude is distance,

$$\tau(r) = \tau(r = r_0) * (r/r_0)^n \tag{2.21}$$

Where

- $\tau(r)$ = shear stress amplitude at distance r
- $\tau(r = r_0)$ = shear stress amplitude at distance r_0
- r = considered distance
- r_0 = reference distance
- n = attenuation parameter, negative for decreasing shear stress amplitude

The value of n = -0.5 without any material damping and it can increase up to -1.0 to include material damping.

2.5.4. Velocity amplitude attenuation

To understand the velocity amplitude, simple empirical relation from CUR(Barkan's formula) [9] can be used.

$$v(r) = v_0\sqrt{\frac{r_0}{r}} * exp(-\alpha(r - r_0)) \tag{2.22}$$

Where

- v(r) = amplitude of the velocity at the distance r
- v_0 = amplitude of the velocity at the distance r_0
- α = A parameter accounting for material damping.

The centrifugal force also plays a part in determining the velocity amplitude.

2.6. Laboratory simulation of cyclic loading:

Various methods can be adopted to understand the effect of cyclic stress ratio in the laboratory. But most apt ones to easily correlate our work is by cyclic triaxial and simple shear test. First, we will understand the differences in triaxial and Simple shear before getting to the cyclic effects.

2.6.1. Triaxial Test:

The triaxial test is most widely used to understand the mechanical properties of the soil. The optimal height to diameter ratio is provided as 2, as end platens restrict the radial displacement leading to in-homogeneity in the test [50]. Also, it was recommended if the sample height to diameter is 1, the platens must be lubricated.

The rotation of the stress path is not possible in case of triaxial testing, the major principal stress is either vertical/radial stress. The stress path can either be triaxial compression or triaxial extension and deviatoric loading. In the case of triaxial compression or extension, the cell pressure is kept constant. But in the case of deviatoric loading, the cell pressure varies with the axial stress. The maximum shear stress occur at (45ř $+ \phi$)

Stress Components:

- Deviatoric Stress = $\frac{(\sigma_1 - \sigma_3)}{2}$
- Mean Stress = $\frac{(\sigma_1 + \sigma_3)}{2}$

2.6.2. Simple Shear Test:

The simple Shear test is a plain strain test, the principal axis of stress and strain rotates. The sample in this test is loaded horizontally with a vertical(static) load. Simple shear is more accurate in practical situations. In this test, complementary shear stress (Stress contributed by Poisson's ratio) are prohibited in the vertical boundaries along the plane of deformation and thus the sample is subjected to non- uniform distribution of stresses leading to the difficulties in interpretation of the results. There is also an in-homogeneity on the boundary of vertical ends of the sample and due to this constrained boundary, there is near zero shear stress. Further, the elongation of the membrane in the axial direction during shearing may also induce some shear stress. The results are assumed to be purely shear that remains highly questionable. The horizontal stress remains unmeasured in this case.

2.6.3. Comparison of Triaxial and Simple shear test:

Before work by [15], results from Simple Shear test were dismissed as the values were lower from the triaxial test. When comparing the stress state in triaxial and simple shear, the simple shear cannot achieve true shearing condition because the vertical sides of the apparatus do not allow for the complementary shear stress to develop. To overcome this the core part of the sample is considered and monitored by the instrumentation.

Also, past work did not account for the following:

- effects due to the rotations of the principal axes,
- full impact of the lateral stresses σx and $\sigma 2$
- difference in the stress path in both the devices

Later it was proved that the horizontal axes are not the plane of maximum shear stress. The slope of stress path in the simple shear test was found to be near unity using Cambridge Simple Shear Test apparatus Mk7 whereas the conventional triaxial test has a stress path slope of 3. The observed stress path for dense sand in simple shear curves initially and raises to the slope of 1.5. The initial curvature may be due to the effect of σ_2.

It is also observed that the major change in the σ_2 occurs during the initial 5% of shear strain and similarly, the majority rotation of the principal stress occurs during this phase. It concludes that often ignored intermediate principal stress plays a significant role in the response of soil in simple shear apparatus. The complete state of stress and strain in both the apparatus must be considered for developing a rational basis for comparing both the results [15].

2.6.4. Comparison of Cyclic triaxial and Simple shear test for pore pressure generation:

Several investigations were carried out and the relationship of excess pore pressure generated in various tests was equated with a correction factor. The relationship provided by [79] has been reviewed by further works.

The relationship between the field, simple shear and the triaxial test is as follows:

$$\left(\frac{\tau}{\sigma'_{v0}}\right)_{field} \approx 0.9\left(\frac{\tau}{\sigma'_{v0}}\right)_{simpleshear} \approx C_R\left(\frac{\sigma'_d}{2\sigma'_0}\right)_{triaxial} \tag{2.23}$$

Here $C_R = 0.57$ for K_0=0.4 and $C_R = 0.9$ for K_0=1

Later, based on the work by [79], the stress-controlled relationship was provided by [97].

$$\left(\frac{\tau}{\sigma'_{v0}}\right)_{field} \approx 0.9\left(\frac{1+2K_0}{3}\right)\left(\frac{\sigma_d}{2\sigma'_c}\right)_{triaxial} \tag{2.24}$$

where

- τ = Shear stress on the sample
- σ_{v0} = Effective vertical stress
- K_0 = Ratio between horizontal and vertical stress.
- σ_d = Deviatoric stress
- σ'_c = Effective confined stress

2.7. Summary

This chapter attempts to explain the modulus degradation of sand due to the cyclic loading of vibratory installation. Further, the rate and magnitude of degradation are based on the amplitude of the vibration applicable at the given point in porous media. The amplitude of vibration dictates the shear strain. The attenuation factor of the soil determines the dampening of vibration amplitude from the source. The modulus reduction curve determines the stiffness based on the shear strain. As the vibration attenuates with the increase in distance, the degree of degradation reduces. Based on the degree of degradation the porous media is classified into three zones. This technique is called a multiscale computational framework. This technique is particularly necessary to model the large deformations especially in case of slip surface formed due to the impact of vibratory installation on the saturated sand. However, the magnitude of degradation is also linked to the excess pore pressure, crushing of grains at the interface and decrease in friction angle [64]. But in our study, the emphasis is laid on the excess pore pressure. There are several models to describe the generation of excess pore pressure. The dissipation shall be described based on the groundwater flow model. Both shall form the subject of the following chapter.

3
Pore Pressure

Modulus degradation is a unique property contributed due to various factors including generation of excess pore pressure. The generation of excess pore pressure results in the reduction of effective stress. The phenomenon of liquefaction occurs when the magnitude of the excess pore pressure generated gets equivalent to the total effective stress. In other words, the effective stress gets to zero at an assumed point. There are different ways to compute the liquefaction potential of the soil. The generation of the excess pore pressure due to the vibratory loading can be computed using analytical models based on the shear stress or strain, number of cycles etc. The different available models relevant to our study shall be revisited in this chapter. The excess pore pressure generated must be dissipated for the system to return to a steady-state. In field conditions usually, simultaneous generation and dissipation occur as described as pre-shearing in the previous chapter. The groundwater flows through the geological formation called an aquifer. The generated excess pore pressure can be considered analogous to the groundwater with increase in head. The porous media flow can be well understood from the concept of pumping wells. This chapter lays a foundation for the available analytical models for generation and dissipation of excess pore pressure. The analogy between the vibratory piling of the sheet pile and pumping of the well shall be discussed and will serve as the base for the proposed model.

3.1. Pore pressure

The total stress is the sum of the effective stress and excess pore pressure.

$$\sigma = \sigma' + u \tag{3.1}$$

where,

- σ = Total Stress
- σ' = Effective Stress
- u = Pore pressure

In dense sand, due to the dynamic shear loading, sand will undergo dilation leading to the increase in the porosity of the soil. At this instance, there is insufficient time for the water to flow in. This leads to the generation of the suction pressure preventing further dilation and increase in the effective stress.

$$\sigma' = \sigma - (u - \Delta u_{suction}) \tag{3.2}$$

In loose sand, dynamic shear loading causes contraction due to the decrease in the porosity, but water cannot flow out. This leads to excess pore pressure decreasing the effective stress.

$$\sigma' = \sigma - (u + \Delta u_{excess}) \tag{3.3}$$

In Saturated conditions: Due to impact of vibration "soil will undergo continued deformation at constant low residual stress or with low residual resistance, due to build up and maintenance of high pore pressure is **liquefaction**" [57]. The liquefaction is distinguished into two types([93]):

1. Flow liquefaction
2. Cyclic mobility

In Dry State: Due to the impact of vibration, there will be shear strength reduction in granular material due to high acceleration [9]. The shear strength of the cohesion-less soil is dependent on the inter-granular contact which gets impacted due to acceleration [72].

- elastic state (a > 0.6g)
- trans-threshold state (0.7g < a <1.5g)
- fluidized response state (a > 1.5g)

As the current work focuses on saturated soil behaviour, we will restrict our discussions to saturated soil.

3.2. Liquefaction:

The liquefaction triggering may be assessed by different means. Here the two approaches are discussed:

- Critical State Approach - Effective stress-based analysis
- Cyclic stress-based approach

3.2.1. Critical State Approach

The critical state soil mechanics(CSSM) offers an excellent pathway for the liquefaction analysis for both static [17][10] and cyclic analysis [12][49][52][7].

The critical state soil mechanics (CSSM) offers an assuring direction for the analysis of liquefaction. The state parameter ψ is the difference between the current void ratio to the void ratio at the critical state line at similar effective stress [69]. The state parameter shall be computed by the in-situ test [63] which has edge over the semi-empirical estimations.

The liquefaction potential of the given soil in critical state approach is defined based on the in-situ void ratio of the soil and the critical void ratio at similar effective mean stress. [93].

3.2.2. Stress Based Approach:

During seismic action, two types of excess pore pressures are generated: transient and residual. Under the saturated condition, due to the changes in the applied mean normal stress transient pore pressures are generated and have insignificant influence on the effective stresses. However, residual pore pressure is generated due to the plastic deformation of the soil matrix and can have a drastic influence on the strength and the stiffness of the soil. Pore pressure is generated once the deviator stress crosses zero marks, all the contributing excess pore pressure accounts to the residual pore pressure.

The assessment of the liquefaction potential can be carried out by the stress-based approach of the cyclic shear stress (CSR) compared with cyclic resistance of the soil. Liquefaction is induced where shear stresses exceed the cyclic resistance.

Cyclic Stress Ratio (CSR) is the seismic demand on a soil layer. It can be attributed to the occurrence of earthquake, piling works etc. The capacity to resist liquefaction offered by the soil shall be expressed as CRR [98].

The reference stress level chosen for the computation of CSR is 0.65 [76]:

$$CSR = \frac{(\tau_h)_{avg}}{\sigma'_o} \simeq 0.65 \frac{a_{max}}{g} . \frac{\sigma_o}{\sigma'_o} . r_d \tag{3.4}$$

where,

- $(\tau_h)_{avg}$ = average shear stress [kPa]
- σ'_o = effective vertical stress [kPa]
- a_{max} = peak acceleration horizontal acceleration [m/s^2]
- g = acceleration due to gravity = 9.81 m/s^2

- σ_o = Vertical total stress [kPa]
- r_d = shear stress reduction factor accounting for the dynamic response of the soil.

$Factor of Safety = \frac{CRR}{CSR} \leq 1$

3.3. Pore Pressure Generation Models

The cyclic loading of the clean sand can be modelled using different approaches. The most frequently applied method is the stress based approach of Seed et al [78] and Polito et al [68]. There are models developed based on strain applied [58], [31], [16]. Considering the complexities in conversion of the vibration into equivalent stress/strain cycle, there are energy based models [39].

3.3.1. Acceleration based model

Barkan's Model

This work has served as the starting point for the work of several authors. Barkan's model was principally a settlement prediction model based on the changes in the void ratio(Δe) due to the effective acceleration magnitude. In this work, the unique non-linear relationship between void ratio and acceleration amplitude was pointed out.

$$e = e_{min} + C.e^{(-\alpha_B \eta)} \tag{3.5}$$

where,

- e = final void ratio
- $e_m in$ = minimum void ratio
- α_B = coefficient of vibratory compaction
- η = acceleration amplitude
- C = constant

$$e = e_{min} + (e_{max} - e_{min}).e^{(-\alpha_B \eta)} \tag{3.6}$$

$$e = e_{min} + (e_{max} - e_{min}).e^{(-\alpha_B (\eta + \eta_0))} \tag{3.7}$$

where,

- e_{min} = minimum void ratio [-]
- e_{max} = maximum void ratio [-]
- η_0 = acceleration amplitude below which no densification occurs

$$\eta_0 = \frac{-ln(1 - I_D)}{\alpha_B} \tag{3.8}$$

where,

- η_0 = threshold acceleration below which no densification occurs
- I_D = Relative density α_B = coefficient of vibratory compaction

The value of α_B highly depends on the water content 'w' [9]. At w = 0, α_B = 0.8 and at w = 4%, α_B = 0.2 and again increases at w = 17% as α_B = 0.85. The value of the fully saturated sand is not assessed.

3.3.2. Stress based model

Seed and Rahman:

Based on the comparisons made in the doctoral work of Piet Meijers [64], it is evident that Seed and Rahman's model [57] is the best suited to simulate the generation of excess pore pressure under completely saturated condition. The model is dependent on the empirical relationships derived from stress-controlled cyclic testing. Further, the model also accounts for pre-shearing. Unlike other models, this model focuses on the generation of excess pore pressure.

The development of the pore pressure can be described by the ratio between excess pore pressure and initial effective stress (r_u).

$$r_u = \frac{2}{\pi} arcsin\left(\frac{N}{N_{liq}}\right)^{\frac{1}{2\theta}} \tag{3.9}$$

Where,

- r_u = relative excess pore pressure (ratio between excess pore pressure and initial effective vertical stress) [-]
- N = applied number of cycles [-]
- θ = empirical parameter[-], a reasonable estimate is θ = 0.7
- N_{liq} = number of cycles to liquefaction in an undrained situation [-].

The value of N_{liq} can be adopted following empirical relationship [70]:

$$\frac{\frac{\Delta\tau}{\sigma'_{v0}}}{I_D} = a.N_{liq}^{-b} \tag{3.10}$$

- I_D = relative density
- $\Delta\tau$ = shear stress amplitude
- σ'_{v0} = initial effective vertical stress
- a, b = empirical parameters, reasonable estimates are a = 0.48, b = 0.2 [64]

In order to derive the value of N_liq, there is need for adjustment of the soil skeleton due to continuous generation and dissipation of excess pore pressure which is not feasible as it ignores soil fabric from consideration. However, the following empirical relationships may be applied [81].

$$N_{liq} = N_{liq,0} * 10^{-X\Delta n} \tag{3.11}$$

where,

- N_{liq} = number of cycles to liquefaction after change in porosity of Δn
- N_{liq},0 = number of cycles to liquefaction without pre-shearing [-]
- X = history parameter
- Δn = change in porosity (in unity) [-]

Developing on the work by Seed and Rahman as discussed earlier, Meijers proposed simplification for the number of cycles resulting in the soil liquefaction based on the experimental observations made in his case of Raamsdonksveer sheet pile test [64]:

$$N_{cycles} = \left(\frac{0.48 * I_D * \sigma'_{v0}}{\Delta\tau}\right) \tag{3.12}$$

The number of cycles to achieve liquefaction is dictated by initial relative soil density (I_D), effective stress(σ'_{v0}) and the amplitude of the shear stress ($\Delta\tau$).

The statistical reevaluation of the Seed's method demonstrated that the θ value is the function of cyclic stress ratio (CSR), fine content (FC) and relative density (RD) [68].

The relationship was given as:

$$\theta = 0.01166.FC + 0.007397.RD + 0.01034.CSR + 0.5058 \tag{3.13}$$

The equation: 3.13 is applicable only with the fine content lesser than 35%. In case of clean sand with no fines (FC = 0), the equation remains insensitive to the CSR and hence RD remains as the predominant controlling parameter. For this condition, the value of θ is expected to fluctuate between 0.73 to 1.14.

Even though Seed et al.'s actual and modified approach remains widely applied it comes with certain drawbacks [18].

- The evaluation of N_{liq} remains a challenge.
- The contribution due to cyclic liquefaction and mobility response is not widely differentiated.
- Inaccurate conversion of transient earthquake /vibration into equivalent harmonic cycles.

3.3.3. Strain based model:

A semi-empirical model was developed based on the strain-controlled cyclic test performed on dry sand. A relationship was established between volumetric straining and excess pore pressure in both dry and saturated condition [58].

$$\Delta u = E_r.\Delta\epsilon_{vd} \tag{3.14}$$

where,

- Δu = Increment of excess pore pressure
- E_r = tangent modulus of one-dimensional unloading curve corresponding to the initial effective vertical stress.
- $\Delta\epsilon_{vd}$ = Volumetric straining contributed from the cyclic loading.

Martin et al.(1975)

$$\bar{E}_r = \frac{(\sigma'_v)^{1-m}}{m.k_2.(\sigma'_{v0})^n - m} \tag{3.15}$$

$$\Delta\epsilon_{vd} = c_1\left(\gamma - c_2.\epsilon_{vd} + \frac{c_3.\epsilon_{vd}^2}{\gamma + c_4 + .\epsilon_{vd}}\right) \tag{3.16}$$

where,

- σ'_v, σ_{v0} = vertical and initial vertical effective stresses
- γ = induced cyclic shear strain
- ϵ_{vd} = accumulated volumetric strain
- c_i, m, n, k_2 = model coefficients

The recommended values for c_1, c_2,c_3,c_4 = 0.80, 0.79, 0.45 and 0.73 respectively. In case of different relative density other than 45%, there is a need to introduce a correction factor:

$$(\Delta\epsilon_{vd})D_{R1} = R.(\Delta\epsilon_{vd})_{RD=45} \tag{3.17}$$

Further, R is a function of RD for crystal silica sands, given by following[80]:

$$R = 0.00031.(100 - RD)^2 + 0.062 for 45 < RD < 80\% \tag{3.18}$$

In this work the cyclic shear strain (γ) response was formulated:

$$\gamma = \frac{\tau.a}{\sqrt{\sigma'_v} - \tau.b} \tag{3.19}$$

$$a = A_1 - \frac{\epsilon_{vd}}{A_2 + A_3.\epsilon_{vd}} \tag{3.20}$$

$$b = B_1 - \frac{\epsilon_{vd}}{B_2 + B_3.\epsilon_{vd}} \tag{3.21}$$

where,

- τ = cyclic shear stress
- $A_1, A_2, A_3, B_1, B_2, B_3$ = model coefficients

Based on the outcome of this work, further investigations were carried out to develop effective stress based constitutive model[35] [55].

Finn et al.

The volumetric strain is the summation of elastic and plastic components. The plastic volumetric strain with one complete cycle was given by 3.23

$$\Delta\epsilon_{vol} = \Delta\epsilon^{el}_{vol} + \Delta\epsilon^{pl}_{vol} \tag{3.22}$$

$$\Delta\epsilon^{pl}_{vol} = C_1 \left[\Delta\gamma - C_2\epsilon^{pl}_{vol} + \frac{C_3(\epsilon^{pl}_{vol})^2}{\Delta\gamma + C_4\epsilon^{pl}_{vol}} \right] \tag{3.23}$$

Where,

- $C_1, C_2, C_3,$ = Empirical parameters
- $\Delta\gamma$ = shear strain amplitude
- ϵ^{pl}_{vol} = plastic volumetric strain

Using a combination of strain history and strain amplitude the parameter κ (damage parameter), can be utilized to assess the magnitude of excess pore pressure. This is a damage parameter approach. For a particular type of soil, the magnitude of the pore pressure is directly proportional to the amplitude of the shear strain and the number of cycles.

$$\frac{du}{d\sigma} = \frac{\lambda}{4}\ln(1 + \frac{\kappa}{2}) \tag{3.24}$$

- $\kappa = \xi.e^{\Sigma\gamma}$
- $\Sigma = 5$
- ξ = 4N.γ_C (for constant amplitude cycles)

Byrne et al. The work by Martin et al. was further simplified by introducing incremental volumetric strain [16]

$$\Delta\epsilon_{vd}/\gamma = c_1.exp(-c_2.\frac{\epsilon_{vd}}{\gamma}) \tag{3.25}$$

where c_1 & c_2 are derived using the following equation:

$$c_1 = 7600.(RD)^2.5 \tag{3.26}$$

$$c_2 = \frac{0.4}{c_1} \tag{3.27}$$

The large application of the works by Finn & Byrne was due to the implementation in commercial software such as FLAC (Fast Lagrangian Analysis of Continua).

Dobry et al.

In their work they attempted to link cyclic shear strain amplitude and the number of cycles based on the strain controlled cyclic triaxial test. They also attempted to establish the minimum shear strain to initiate the excess pore pressure as 10^{-2}%. Based on modified version of Dobry et al [31] which was actually based on the work of Dobry et al [30] & Martin et al [58], a closed form model was introduced:

$$r_{u,N} = \frac{p.f.N_c.F.(\gamma_c - \gamma_{tvp})^b}{1 + f.N_c.F.(\gamma_c - \gamma_{tvp})^b} \tag{3.28}$$

where,

- γ_c = cyclic shear strain amplitude
- γ_{tvp} = volumetric threshold shear strain under-which no generation of the excess pore pressure is anticipated usually between 0.01 - 0.02% for the sand.
- f = Depends on the directions of shaking. Choose value 1 if its unidirectional and 2 if its bidirectional.

The other coefficients F, p and b are chosen from the laboratory data based fitting attempts. This technique has been widely applied by other authors in the nonlinear ground response modelling software such as D-Mod[62], D-Mod−2[61], Deepsoil[43]. Further, strain-based approaches were also revisited in the doctoral work of Hazirbaba to investigate the effects the non-plastic fines in the generation of the excess pore pressure [44].

Vucetic & Matasovic:

The factor of internal damping is considered as the driving parameter for this model and the effect of hysteresis allows to accumulate the modulus degradation due to the increase in the residual pore pressure r_u [89].

$$G^*_{mt} = G^*_{m0}\sqrt{\frac{\sigma'_{vc} - r_u}{\sigma'_{vc}}} = G^*_{m0}\sqrt{1 - r^*_u} \tag{3.29}$$

$$\tau^*_{mt} = \tau^*_{m0}\left(\frac{\sigma'_{vc} - r_u}{\sigma'_{vc}}\right) = \tau^*_{m0}(1 - r^*_u) \tag{3.30}$$

where,

- G^*_{mt} = bulk modulus at time "t"
- G^*_{m0} = initial bulk modulus of the sample
- σ'_{vc} = effective vertical stress[kPa]
- r^*_u = normalised residual excess pore pressure
- ${\tau'_{m0}}^*$ = effective initial shear stress[kPa]
- v = curve fitting parameter

3.3.4. Energy based model

Initially, the study of a generation of excess pore pressure due to vibration was mainly concerned with the effect of seismic loading [77] [51] or wave loading [73]. The accurate conversion of the non-uniform seismic action into a harmonic loading in order to implement the stress-based models was challenging. This allowed for the development of energy-based models [39].

The energy is lost due to frictional sliding at inter-granular contacts and viscous drag due to the movement of the generated pore pressure along with the soil matrix. The contribution of the latter in energy dissipation is small [40]. The dissipated energy, in general, is given by:

$$\Delta W_s = \int \sigma d\epsilon_p \tag{3.31}$$

Further, in case of simple shear test:

$$\Delta W_s = \int \tau(t)\gamma(t).dt \tag{3.32}$$

where

- ΔW_s = Energy Dissipated
- σ = Stress [kPa]
- ϵ_p = Plastic Strain [-]
- τ = Shear Stress [kPa]
- γ = Shear Strain [-]

Energy based GMP Model

It was named after the three contributors viz., **G**reen, **M**itchell and **P**olito. In this model, an attempt was made to empirically relate the generated residual excess pore pressure to the amount of the energy dissipated during to the vibratory loading [39].

$$r_u = \sqrt{\frac{W_s}{PEC}} \tag{3.33}$$

Where

- r_u = Ratio of excess pore pressure and initial effective stress
- W_s = Dissipated Energy per unit volume of soil divided by initial effective confining stress
- PEC = Pseudo Energy Capacity (Calibration Parameter)

The increment of the energy dissipated dW_s is a relationship related to stress conditions and increment in strain.

$$dW_s = (\sigma'_v d\epsilon_v + 2\sigma'_h d\epsilon_h + \tau_{vh} d\gamma_v h) * \frac{1}{\sigma_{mo}} \tag{3.34}$$

where,

- dWs = incremental dissipated shear energy normalized by the initial effective mean stress
- σ'_v = effective vertical stress
- $d\epsilon_h$= incremental vertical strain
- σ'_h = effective horizontal stress
- dϵ_h = incremental radial strain
- τ_{vh} = horizontal shear stress acting on a plane having a vertical normal vector
- $d\gamma_{vh}$ = incremental shear strain resulting from τ_{vh}
- τ_{hv} = vertical shear stress acting on a plane having a horizontal normal vector
- dγ_{hv} = incremental shear strain resulting from τ_{hv}
- σ'_{mo} = Initial mean effective stress

The 3.34 can be solved numerically. Pseudo Energy Capacity(PEC) is a calibration parameter that can be determined from the cyclic test data by plotting r_u versus $\sqrt{W_s}$. It is a function of cyclic stress ratio (ratio of shear stress amplitude and Initial Vertical Stress) and initial relative density. Using data from the literature, the correlation of PEC to the relative density was achieved as in equation:3.35 [64].

$$\frac{PEC}{\sigma'_{v0}} = 0.07 I_D^{1.7} \tag{3.35}$$

3.4. Hypothesis

Analogy between groundwater pumping and sheet pile driving:

The vibratory driving of the sheet pile shall be pictured analogous to groundwater pumping. The pumping of well leads to the increase or decrease in the head due to the rise or fall of the water level. The fluctuation in the head is compensated by the dissipation of pressure to bring the system to steady-state condition. The similar condition arises while vibratory driving of sheet pile in the aquifer. The driving of sheet pile by Vibro-hammer leads to the accumulation of excess pore pressure leading to the instantaneous increase in the head in a very short span of time due to liquefaction. The reason for generation is explained in the earlier sections of this chapter. The system must dive back to the stable state and that is achieved by the dissipation.

The penetration of the sheet pile in vibratory driving is attributed to the localized liquefaction. This can act as an direct source of constant pore pressure causing to increase the groundwater head of the aquifer in the radial direction. At the same time, there will also be pore pressure generation due to mobilization of particles in the densification zone. Once the driving of the sheet pile stops the groundwater head tries to return to the hydrostatic condition allowing settlement to occur [64]. During the driving of the pile, due to liquefaction the groundwater head is expected to be represented by the curve t_0 in the figure: 3.1 and at the end of vibratory driving the groundwater, the head is represented by t_n. It is analogous to the response of groundwater head when the water in the pumping well is maintained at a higher level, represented by recovery part in the figure: 3.3.

It is also important to understand that the transient groundwater flow models are based on a series of assumptions and the shortcomings due to these assumptions will be added to the possible outputs. The current thesis builds in line to represent a response of the geotechnical process in terms of the groundwater flow model.

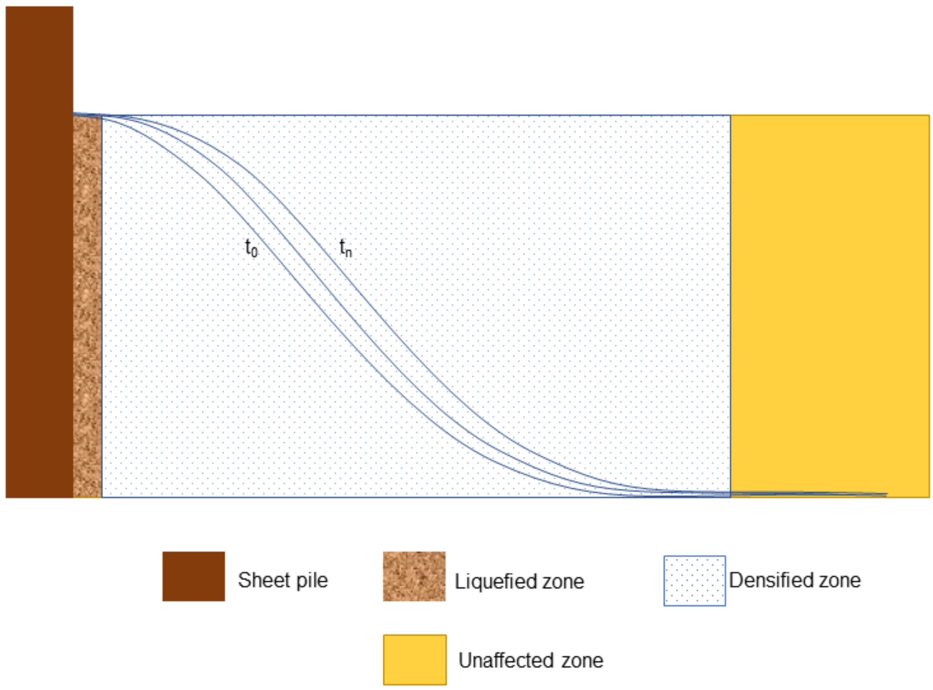

Figure 3.1: Illustration for the accumulation of the excess pore pressure due to vibratory piling

3.5. Groundwater

As the proposed model applies groundwater modelling approach, it is significant to establish an understanding of the groundwater and its modelling in a transient manner.

The occurrence of the groundwater is in pores and fractures of the subsoil and rocks. The spatial distribution of the groundwater depends on the porosity or permeability and head in the porous media. This is also dictated by the thickness and the structure of the hydrostratigraphic units. The movement of the fluid is dependent on the present-day hydrological cycle (i.e, precipitation, transpiration, evaporation etc.) for the upper regions of the groundwater zones but doesn't impact the deeper zones. The deeper zones usually get impacted only by the pressure gradient caused due to the large-scale (Paleo)-topography and tectonic forces and by thermo-chemical process [22].

3.5.1. Groundwater response due to pumping

Groundwater is usually stored in the geohydrological units called an aquifer. These usually possess high hydraulic conductivity values. The properties of the aquifer and its transient response to the perturbation (pumping) can be understood by carrying out transient hydraulic tests. The most prevalent one includes:

1. Pumping test
2. Slug test

The pumping test was introduced to measure the hydrogeological parameters of the aquifer based on the magnitude of discharge and the rate at which the head drops in the monitoring piezometer. Further, the slug test allows us to understand the rate of the recovery in the aquifer by varying the head at the source well [34].

The slug test is usually preferred over the pumping test as it requires lesser time and money to carry out. It also provides the properties of the short volume of the aquifer or immediately next to the good screen. There are several methods to analyse the data from the pumping and slug test and it is continuously evolving with increasing requirement in accuracy and improvement in the technology [36].

Pumping test

In a confined aquifer, the pumping of the fully penetrating well causes draw-down radially outward that also varies with time. When the main well is pumped, the discharge from the pumping well and draw-down in the monitoring well is measured, these can be aptly substituted into the good flow equation to compute the hydraulic characteristic of the aquifer.

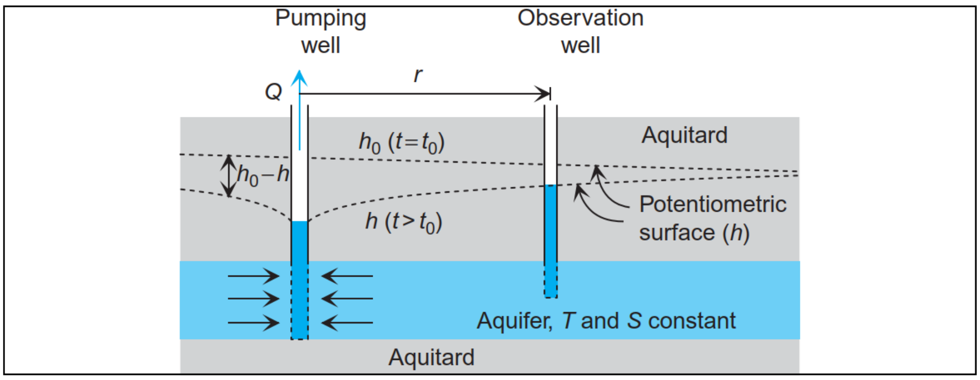

Figure 3.2: The head response near the well during pumping test in confined aquifer[36]

Slug test

The experiment starts with perturbation in the non-pumping well. It can be by both raising or dropping the head and then allowing the system to return to the steady-state. The rate of return depends on the permeability of the material. This process can help to compute hydraulic conductivity and specific storage. The downside of this test is that only a limited volume of water is considered for the study which restricts the analysis for the volume of aquifer close to the screen of the well.

An impulse to start the experiment is by instantaneously varying the level of the water column in the well either by inserting or withdrawing a "slug". This is usually done by bringing down a cylindrical solid. Alternatively, this can also be done by adding or removing the water from the well but where water quality is the cause of concern this method can make the water more susceptible to contamination. [36]

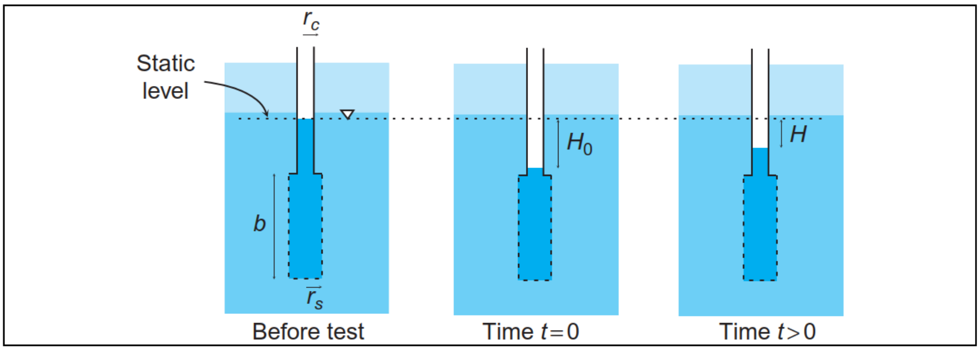

Figure 3.3: The head response near the well screen during slug test[36]

Let's assume that the well in which slug is entered as main well and the well in which the response is taken is the monitoring well. When the head in the main well is brought up from the steady-state and maintained at that level by insertion of slug, the head of the aquifer tries to achieve an equilibrium state. And when it is released by removing the slug, the head tries to bounces back to its initial steady-state condition. The transient head response due to the alteration is depicted in the 3.4. From 3.4 it can also be inferred that response on both increasing or decreasing side is exponential. This aspect shall be wisely implied in our proposed model.

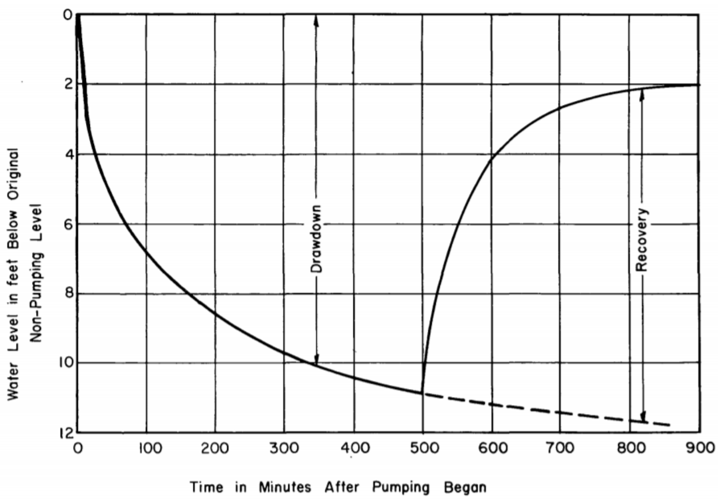

Figure 3.4: The head response due to pumping and recovery of the well [14]

3.5.2. Analysis of the pumping

Over the years, there are several methods that have evolved to carry out the analysis of pumping test data. Theis developed a mathematical model for unsteady-state flow based on time factor and storativity. This was derived based on the analogy between the movement of the groundwater due to pumping and conduction of heat [54].

Theis Equation

Theis equation [19] defines the groundwater flow in a radial confined, uniformly thick horizontal, homogeneous, the isotropic aquifer of the infinite areal extent with uniform thickness [19]. Further assumptions also include that the water is immediately discharged after removal from the storage.

$$s = \frac{Q}{4\pi T}\int_{u}^{\infty}\frac{e^{-u}}{u}du \tag{3.36}$$

Where,

- s = Drawdown [m] measured at observation well at distance r [m]

- u = Dimensionless time

$$u = \frac{r^2 S}{4Tt} \tag{3.37}$$

- h = Hydraulic head [L]
- Q = Discharge/ Pumping rate $[L^3/T]$
- T = Transmissivity $[L^2/T]$
- t = Time [T]
- S = Dimensionless Storage Coefficient / Storativity [-],

$$S = \frac{4Ttu}{r^2} \tag{3.38}$$

- r = Radial Observation distance from the pumped well [L]

W(u), the "well function" or "Theis well function" is referred to as dimensionless drawdown and u as dimensionless time. From the equation,

$$W(u) = \int_u^{\infty} \frac{e^{-u}}{u} du \tag{3.39}$$

Referring to 3.36, it can be observed that if s can be measured for different distances of r for varying time(t) and Q are known then S and T can be determined. The possibility of 2 unknowns and exponential integral make non-viable to achieve explicit solution [54]. By applying 3.36, 3.37 the curve fitting method was devised by Theis was to determine S & T.

The following assumption as made in order to model the groundwater flow. It is also necessary to understand that these not completely applicable to the pore pressure generated due to the installation of the sheet piles.

- aquifer has infinite areal extent;
- aquifer is homogeneous, isotropic, and of uniform thickness, item control well is fully penetrating;
- flow to control well is horizontal;
- aquifer is confined
- flow is unsteady;
- water is released instantaneously from storage with the decline of the hydraulic head;
- diameter of pumping well is very small so that storage in the control well can be neglected, values of u are small that is to say r is small and t is large.

Copper & Jacob's Method

Considering the infeasibility to derive the explicit solution for the Theis Well function, Copper and Jacob proposed an approximation using Taylor series [21]. Taylor Series of a real or complex function that can be infinitely differentiable at real or complex number is a power series.

$$f(x) = \sum_{n=0}^{\infty} \frac{f^{(n)}(a)}{n!}(x-a)^n \tag{3.40}$$

$$W(u) = -0.5772 - ln(u) + \sum_{n=0}^{\infty} \frac{(-1)^{(n+1)}(u^n)}{n.n!} \tag{3.41}$$

On expanding the Theis Equation by application of the Taylor series,
We have,

$$s = \left(\frac{Q}{4\pi T}\right)\left(-0.5772 - \ln u + u - \frac{u^2}{2.2!} + \frac{u^3}{3.3!} - ...\right) \tag{3.42}$$

For small values of r^2/t on comparison of 4T/S, u shall be so small that the terms after first 2 in the series 3.42 shall be ignored to achieve the approximate value. Following which the following equation was provided [21].

By approximation, [21]

$$s = \frac{Q}{4\pi T} \ln\left(\frac{2.25Tt}{r^2 S}\right) \tag{3.43}$$

3.43 is referred to as the Copper and Jacob equation [5]. The data from the pumping test is used to fit the Theis equation for approximate estimation of S and T values[29]. The radius of the well is considered negligible also the storage in the well will be ignored but the drawdown computation will be carried out from the edge of the well because at the centre of well (r = 0) the drawdown computation will become undefined.

Ferris & Knowles' Method

Theis equation presented the transient response due to constant discharge carried out in the well but in case of instantaneous introduction/removal of a volume, it becomes cumbersome to model it by applying the Theis equation. The work by Ferris & Knowles [34] described the response of the head due to the instantaneous line source in the infinite region.

$$s = \frac{Ve^{\frac{-r^2 S}{4Tt}}}{4\pi Tt} \tag{3.44}$$

where,

- s = residual head following injection of slug of water
- r = distance from injection well to observation well
- t = time form the injection of slug
- V = Volume of slug
- T = Coefficient of transmissibility
- S = Coefficient of storage

3.6. Summary:

The liquefaction is achieved when the effective stress is completely substituted by excess pore pressure. However, the soil behaves as liquefied media even when the excess pore pressure gets greater than 60% [75]. In the current work, the excess pore pressure is modelled analogical to the pumping of groundwater. The liquefied zone or plastic zone is assumed to be of width lesser than 1m [66]. This was expected to act as the major source of excess pore pressure to the radial aquifer.

4

Data from Kademuur Damrak

The analysis of the field piezometric data plays a critical role in the validation of the hypothesis assumed in the section:3.4. This chapter introduces the stratigraphy of Kademmur Damrak (Damrak), monitoring and installation of the sheet piles, understanding and preparation of the data for the analysis. Further, an attempt was made to rebuild the field responses on time series analysis. Followed by, application of the semi-empirical model to reconstruct the field response with its relation to involved physical parameters.

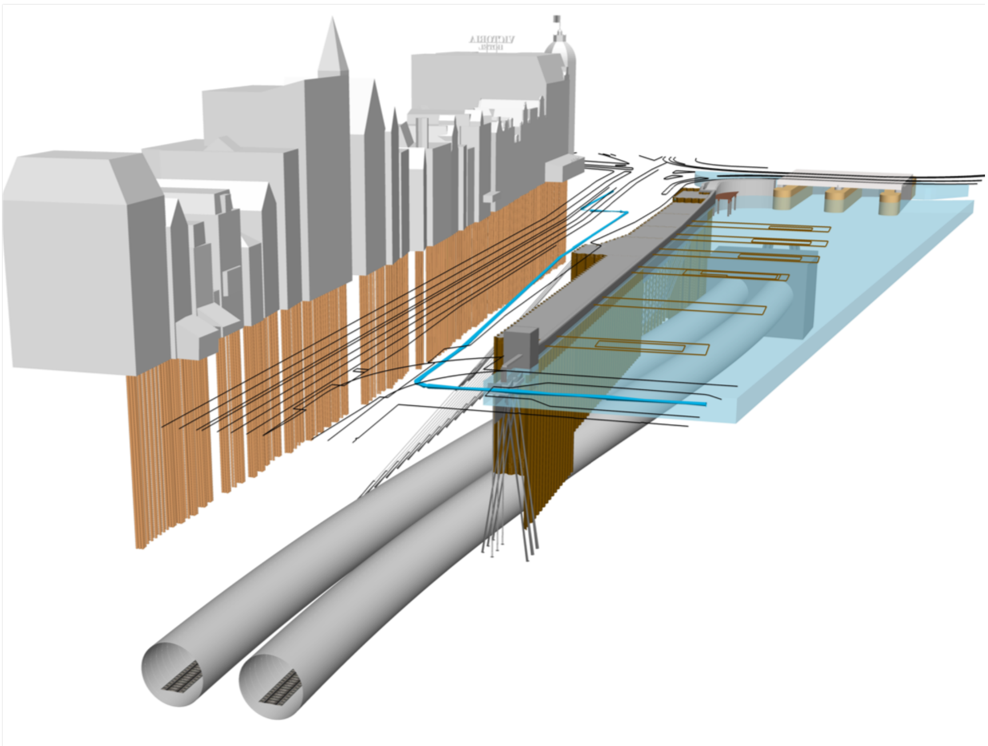

Figure 4.1: 3D rendering of Project

4.1. Kademmur Damrak

The data was obtained from the project site located at the waterfront of Damrak (near Amsterdam Central) over-crossing Noord Zuid metro tunnel (NZ Line). The project was undertaken to renovate the existing quay wall at Damrak waterfront. The sheet-piles were used as the foundation for the quay wall construction. The toe of the sheet pile was expected to get as closes as 1.4m from the lining of the NZ metro line. The installation was planned to carry out by vibratory hammer. It was expected that the vibratory method will induce excess pore pressure and requires monitoring. The high excess pore pressure in the vicinity of the tunnel lining was restricted and breaching the condition will render the tunnel warranty void. Hence, the monitoring of the excess pore pressure was made rigorous.

4.1.1. Stratigraphy:

The stratigraphy and geology of the subsoil at Damrak can be elaborated from the data obtained from the Dinoloket represented in the figure: 4.2] and investigation report by TNO [37]. The study by TNO, "De bodem onder Amsterdam: een geologische stadswandeling" [37] explains the geology beneath "Beurs van Berlage" as represented in the figure: 4.8 which is in close vicinity to the Damrak project. On correlation from the above, it was deciphered that the anthropogenic materials of late Holocene layer can be traced up to -1.5mNAP. This was followed by the tidal deposition of Naaldwijk formation of middle to late Holocene layer. Further to -6m NAP, the layer includes humic clay deposited from middle Holocene was located. Further, peat formation from early Holocene period (Nieuwkoop formation, basisveen bed) was located in the CPT data. The first aquifer layer constituted by late Pleistocene (Boxtel formation) comprising very fine to medium coarse sand with trace existence of sandy clay, humus and peat indicating the low permeability of the aquifer was noticed. Also, CPT [Appendix:B] report confirms the start of the first sand layer (aquifer) at around -13mNAP at Damrak. Every piezometer monitoring was carried out in the aforementioned aquifer and the data obtained from the piezometer was utilized in the analysis. The CPT report also reflects the presence of Pleistocene clay layer refereed as allerod [11] sandwiched between the Pleistocene sand deposition further lowering the transmissivity(T) of the aquifer. The fluvial deposit of the Kreftenheye formation follows the Pleistocene sand of Boxtel formation [74],(in figure: 4.2).

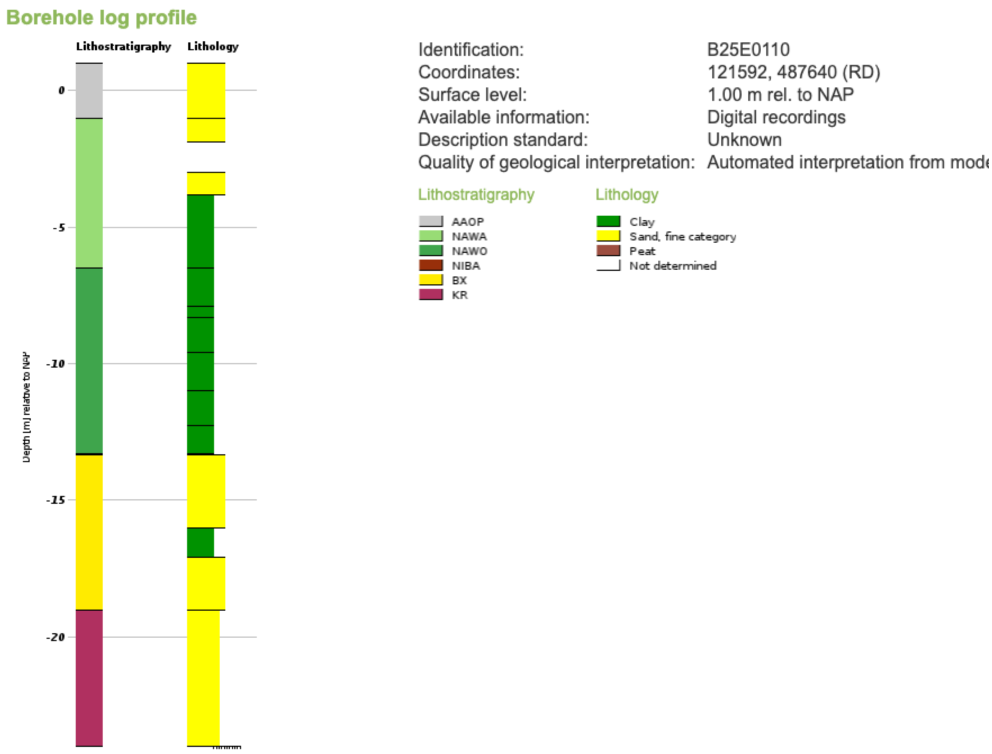

Figure 4.2: Description on the Geology of Amsterdam Damrak (Dinoloket)

4.1.2. Specification of the vibratory hammer:

Considering the stratigraphy and the penetration depth of the sheet pile, the installation was carried out by free-hanging high-frequency Vibro-hammer **ICE 36 RF**, a product of International Construction Equipment (ICE). The maximum operating frequency of the vibration is 2300rpm (38Hz) with a maximum displacement amplitude of 16mm. The maximum centrifugal force is 2030kN and the eccentric moment is 0 - 36kgm [2].

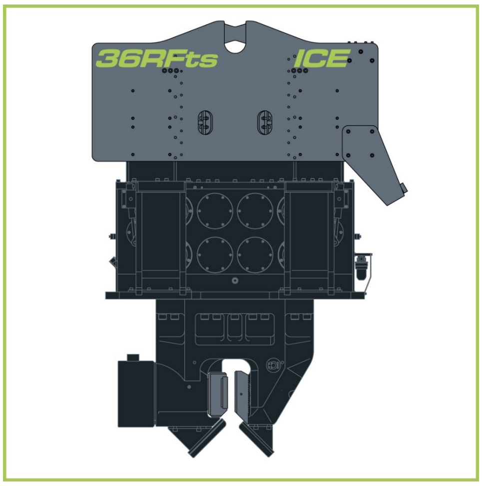

Figure 4.3: Vibrohammer - ICE 36 RF [2]

Figure 4.4: Free hanging vibro hammer(ICE 36 RF)

4.1.3. Geometry of the sheet pile

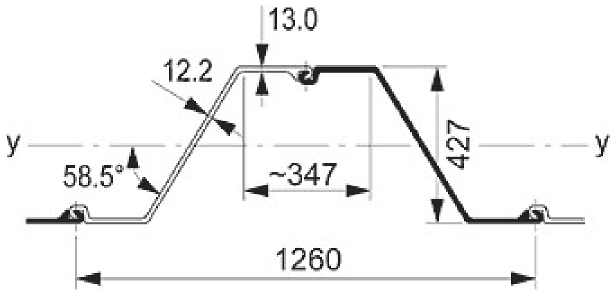

Figure 4.5: Typical geometry of AZ26 [All dimensions in mm] [1]

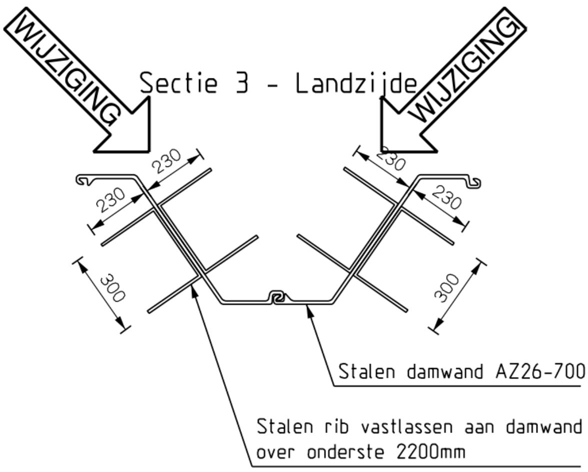

Figure 4.6: Geometry of AZ26 with wings utilized in Kademmur Damrak [All dimensions in mm]

The sheet piles are slender structures with a small cross-section compared to its length [25]. At Damrak, only AZ26-700 were utilized for the foundation. The typical cross-section of the sheet pile AZ26-700 is presented in the above figure:4.5. In Damrak, a special wing was welded to increase the frictional resistance as represented in the figure: 4.6. The attachment was only for 2.5m from the toe of the sheet pile.

4.1.4. Geotechnical monitoring & instrumentation:

The geotechnical monitoring is referred to as the marriage between capabilities of measuring instrument and the capabilities of the people [33]. The geotechnical design is based on the most probable chosen value of engineering properties approximated from the field and laboratory test. The engineering properties are expected to vary due to the due to the heterogeneity of the soil/rock. To overcome this drawback the monitoring of the field performances and geotechnical engineering properties plays an integral part in geotechnical construction. The monitoring shall be planned based on critical engineering properties, the boundary conditions, the magnitude of geotechnical risks and expected modes of failures. The geotechnical monitoring ensures safety, minimizes cost, control construction procedures and also provides legal protection to the stakeholders. The monitoring plan is aided by risk analysis and mitigation procedures that play a key role in managing geotechnical projects but this will not be discussed in the thesis as it is beyond the scope of work [33].

In Kademuur Damrak the key scope of work included the construction of a quay wall founded on the sheet pile. The closest encounter of the toe of the sheet pile to the tunnel lining was at a distance of 1.362m. In case of the vibratory installation, liquefaction was expected to allow the sheet pile to penetrate the ground 2.1.2. To ensure the structural integrity of the tunnel lining, it was mandated to monitor the excess pore water pressure in the vicinity to the tunnel. There were 5 numbers of piezometer(BAT Sensor) installed at varying distances. Further, an accelerometer was installed in the tunnel to monitor the magnitude of vibrations. The cone piezometer was installed in the first aquifer with varying depth depending on the stratigraphy (in the table: 4.1)

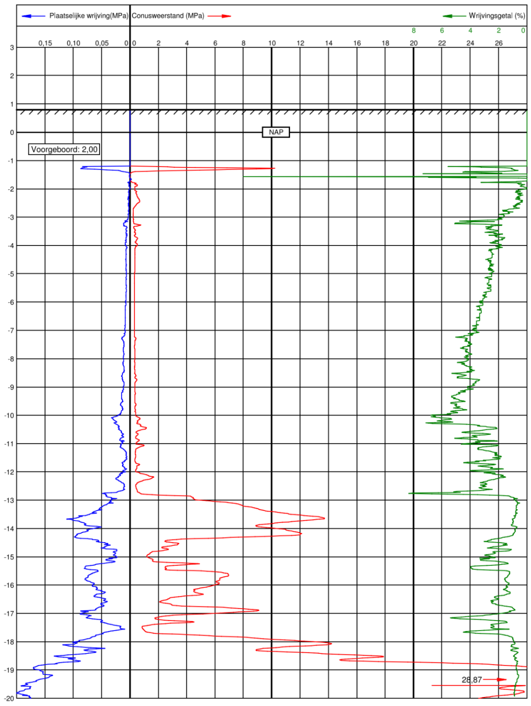

Figure 4.7: CPT (No:8)

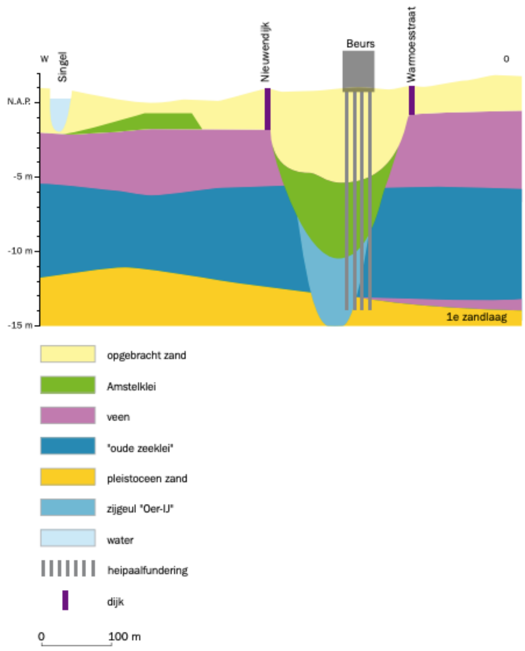

Figure 4.8: The Geology of the foundation Beurs van Berlage

Monitoring Sensors

The robustness of the data-driven models is dependent on the chosen parameters and the properties. But also the sophistication of the monitoring sensors and the quality of collected data plays a significant role in understanding the trend of the response to model them. The model built on high-quality data has a higher potentiality to validate the analytical model. As discussed in the previous section piezometer and accelerometer data were available at our disposal to understand and model the response of the soil due to vibratory installation of the sheet pile.

1. Cone Piezometer - BAT Sensor (3 Nos)
2. Accelerometer (Inside Tunnel)

BAT Sensors:

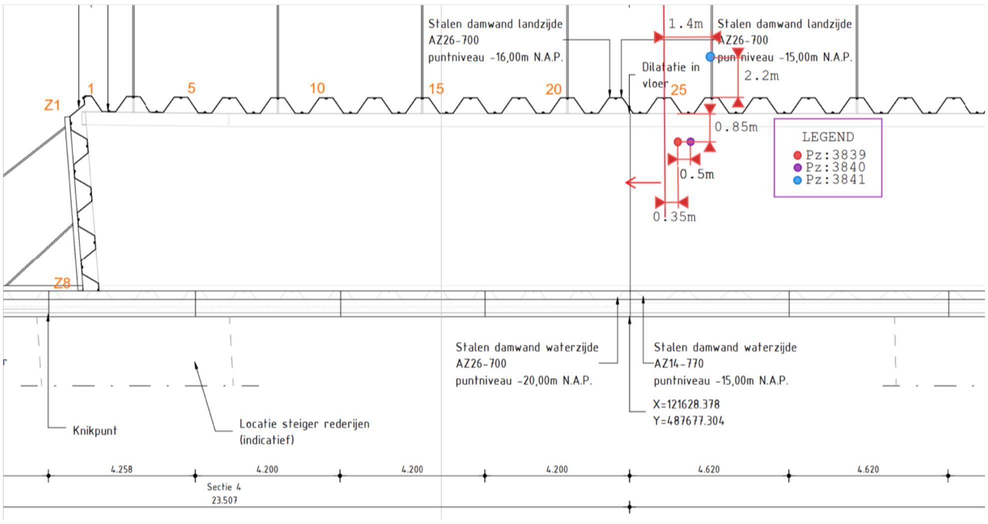

Figure 4.9: Layout of the proposed focus area for our study

The BAT Sensors have been found advantageous and are well established to measure pore pressure to determine the stability of dikes in the Netherlands [92]. The sensor used in Damrak was BAT filter tip MK 3 fabricated by Profound BV. The BAT-system consists of a filter tip and a sensor and doesn't have any sensitive element making it easy to handle. The logging of the pore pressure measurements was carried out at an interval of 13 seconds in this project.

By Darcy's law, the hydraulic conductivity describes the time taken for the water to travel from one point to another in the porous media. The response of the piezometers cannot be instantaneous with the onset of driving unless the monitoring is sufficiently close enough to the source. Thus developed excess pore pressure requires sufficient time to reach the sensor. As it is not feasible to detect the excess pore pressure immediately with the onset of the event, an alternative indication was required to meticulously ascertain the start and the end of the sheet pile installation. The frequency response of the accelerometer installed in the tunnel denoted the start and end of the events.

Accelerometer:

They are small instruments with large frequency and dynamic range [45]. The most common type of accelerometer uses piezo-electric properties of natural as well as artificial crystals. The shearing of crystal leads the current to flow in conductor opposite to it. The amount of current is equal to the magnitude of shear force. Infield crystals are positioned such that the seismic shear loading is applied on the crystal producing force equivalent to the acceleration [94]. Lately, the moving coil accelerometer has been developed to operate in the frequency range of 2-200Hz [45].

In Damrak, unfortunately, the detailed specification of the accelerometer and the exact location of the sensors remained unknown. These made it infeasible to draw clear conclusions from the available data of accelerometer. The available recorded data includes frequency, displacement, velocity and acceleration in all the three directions of the coordinate system (x,y & z). The frequency of accelerometer recording available for the analysis was $\frac{1}{13}$ Hz which was very unlikely the operating frequency range of the instrument. However, in the field due to non-scientific application, the frequency of data logging is much lower. It is also attributed to the cost of the storing devices.

The accelerometer was installed on the inner side of the tunnel lining. Hence, considering the dampening that tunnel could offer to the vibration it was cumbersome to assess and directly apply the accelerometer data in the model. The tunnel was expected to act as a monolithic structure and the energy of the vibratory hammer was anticipated to be insufficient such that the vibration reading could be directly associated with the generated excess pore pressure

Datalogger:

The data-logger is a commercial device connected to the sensors through cables installed on the site usually enclosed in the weatherproof housing. The datalogger communicates with the sensors to collect the input, stores and transmits it to the connected computer in case of online communication [28]. The communication between the sensors and the server is established by a 4G modem. It is also connected to alternative networks as a fallback option. The built-in internet connection supports to upload the data to the FTP server and can also be emailed at a preset time interval [3].

4.2. Construction of cofferdam

At Damrak, the sheet piles served as the foundation for the quay wall construction. The sequence of the cofferdam construction plays a vital role in understanding the evolution of the pore pressure. The sheet piles installed could form an obstruction or boundary to the excess pore pressure generated due to later installations. The sheet pile boundary could strongly influence the rate of dissipation of the excess pore pressure. The construction sequence is listed below:

1. Installation of the sheet pile on the waterfront side (No monitoring data available)
2. Day 1: Installation of two pairs of sheet pile (1a) from -9m to -15m.
3. Preparation: 12 pairs of sheet pile installed until a depth of -14m i.e., until the upper surface of the aquifer (No monitoring data available).
4. Day 2: Installation of 12 pairs of sheet piles from -14m to -15m (land side)
5. Day 2: Installation of 4 pairs sheet piles from -15m to -16m (landside).
6. Day 3: Installation of the remaining 8 pairs of sheet piles from -15m to -16m.

The sequence of installation for the sheet piles from depth -15m to -16m was altered from -14m to -15m. It was to better understand the variation in response of excess pore pressure when the source (liquefied zone) moves from farther to closer and vice versa. It was important to realise that the collected piezometric data was a cumulative response of several events and was necessary to isolate the individual response to build a model. This was accomplished by time series analysis and semi-empirical modelling in later sections.

4.3. Monitoring Data of Kademmur Damrak

4.3.1. Data acquisition:

Usually, written procedures are established to carry out data acquisition to maintain the coherence of data. The acquisition shall be carried out mindful of the application of the data. In Damrak, the data was collected to validate that the excess pore pressure did not exceed the tolerable limits set by the owner of the north-south metro tunnel.

As part of the research objective for this work, it was considered to understand the impact of the driving duration on the magnitude of generated excess pore pressure. Hence, it was indispensable to ascertain the actual start and duration of driving. The manual recording of the start and end time of installation was considered redundant as the event is said to be started when the vibrator achieves operating frequency. This was also to affirm that the penetration was only by dynamic loading and not by static loading. Its was also important as cyclic loading of the soil will occur only due to dynamic loading.

The mechanism of the propagation of vibration had been already discussed in the previous chapter. The frequency of the vibration propagation matches the operating frequency of the pile hammer. In Damrak, the vibration in the tunnel due to the sheet pile installation was monitored. The accelerometer data also provided us with the frequency response of the soil which indirectly indicated the start and the end of the event which provide us with the actual driving duration.

4.3.2. Data preprocessing

The analysis should be carried out only on the processed data to reduce inconsistencies, noise and redundant values [100]. The pre-processing of the piezometer data includes corrections for reference hydrostatic groundwater reference, correction to the piezometer's depth, atmospheric pressure correction, noise due to local fluctuations such as tidal variations, seasonal variations etc.

Non-synchronization of time stamps

The data points from the instrumentation recording has a timestamp associated with it. The raw piezometric and accelerometer readings responses for the closest event (0.92m) from the source was superimposed on the same time series and it was realized that the response of the piezometer sets in 40 seconds before the frequency response of the accelerometer(38Hz) which remains practically infeasible. Following which a correction of 40 seconds was made to align the time stamp of the piezometer and the accelerometer data.

Correction for the hydraulic head

The Dutch conditions are well known for the high water table. The piezometer readings should be corrected for reference groundwater table [h_{ref}] and average atmospheric pressure [$P_{avg-atm}$] [4.1]. The total pore pressure [$P_{tot-raw}$] at the tip of the sensor [Z_{sensor}] was corrected for average atmospheric pressure [$P_{atm-avg}$].

Description	Unit	Pr - 3839	Pr - 3840	Pr - 3841
$P_{tot-raw}$	kPa	212.87	220.23	221.81
$P_{atm-avg}$	kPa	100.8	100.8	100.8
P_{water}	kPa	112.07	119.43	121.01
h_{water}	m	11.4	12.2	12.3
h_{ref}	mNAP	-2.5	-2.5	-2.5
Z_{sensor}	mNAP	-13.9	-14.7	-14.8

Table 4.1: Correction for the Piezometer for Reference level

Local fluctuation

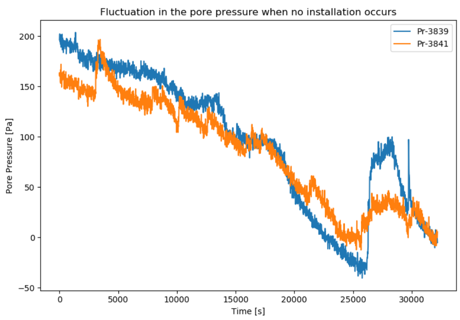

Figure 4.10: Illustration of the fluctuation in the pore pressure when no installation of sheet pile is undertaken

The response of the excess pore pressure was the focus of the study. It was crucial to understand the localized fluctuation in pore pressure due to other disturbances. It included tidal variations, movement of metro trains in the tunnel etc. The piezometric field data in absence of any installations of the sheet piles were analysed in an attempt to understand the variation due to other disturbances. These values were considered as baseline reading and the local fluctuations were ignored as the value are minimal (0 - 200 Pa) in order to simplify the analysis (figure: 4.10). Further, it was also complex to exactly understand the response of pore pressure due to the noises from the available data and hence it was ignored from modelling.

4.3.3. Data Classification:

The classification of the collected field data based on similarities allows in enhancing the data usability. In Damrak, the field piezometric data were classified based on the boundary conditions. It depended on the position of the piezometer concerning the cofferdam. The anticipated differences due to sheet pile obstructions or boundaries are elaborated in the table:4.3.3.

Before the installation of the sheet pile, five numbers of piezometers were installed in the field to monitor the excess pore pressure. Unfortunately, only part of them remained active during the course of installation of sheet piles. On day one Pr - 3841 was found active. On day two and three Pr - 3839, Pr - 3840 and Pr - 3841 were found active. The location of the piezometers with respect to the cofferdam is presented in the figure: 4.9. The scheme of data classification due to the boundary condition is presented in the flowchart in the figure: 4.11.

Piezometer's location	Response of the excess pore pressure
Outside cofferdam	The pore pressure was expected to dissipate at rate proportional to the transmissivity and storativity of the aquifer.
Inside cofferdam	The generated excess pore pressure was expected to reflect back from the boundary or dissipate at a lower rate due to a smaller value of transmissivity due to obstructing sheet pile.

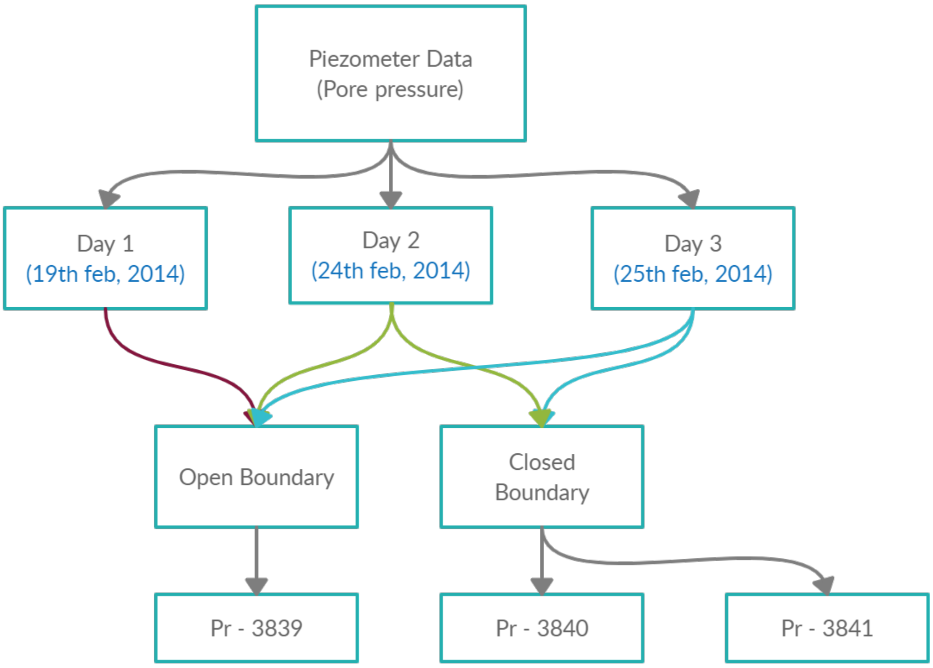

Figure 4.11: Schematisation of piezometric data classification

4.3.4. Data Understanding:

In order to model the pore pressure response of the sand due to the vibratory piling, it is important to visualize and understand the field data. From initial visualization, the distinct differences were established due to variation in the boundary conditions. Further, for consistency in the thesis, two terms are introduced here and shall be followed here on.

Event: The installation of a pair of sheet pile at a given distance from monitoring point with a given driving duration.

Set: Successive installation of sheet-piles within an interval of 10minutes at a varying distance from the monitoring point is termed as set. This is introduced as the recorded data didn't include the individual response due to the installation of single sheet pile but cumulative response due to several sheet pile. Thus the sequence of multiple sheet pile installed in a short interval of time is termed as Set.

Day 1

Further, considering the sequence of cofferdam construction 4.2, the plotting of the data from **day one** revealed that the interval between the installation provides sufficient time to understand the trend of the pore pressure generation and dissipation. It helped to establish an initial idea of the dynamics of the system.

Prior to day 1, two pairs of sheet piles to be investigated were already penetrated to a depth of -9.8m. The aquifer was expected at -12.8m NAP. The sheet pile were installed from **-9.8m NAP to -15m NAP** . The response of day 1 was captured only on the Pr-3841 and other sensors were found non-functional. It is very important to know that only on day 1 sufficient interval were allowed between the events so that the response reaches the peak. Also, only on the day, one distance between the source and monitoring point remained within the bandwidth of around 2.03m - 3.08m.

Day 2 & 3

On plotting the data of day two and three, the impact of variation in the boundary condition was distinctively recognized. The response of the pore pressure for the monitoring inside closed boundary condition was noticed to be four to five folds compared to open boundary (monitoring outside the cofferdam).

On day two & three, the pore pressure response curve possesses the manifestation of multiple events occurring successively at varying distances making it cumbersome to isolate the responses of individual events.

4.4. Methodology

Considering the complexity in understanding the influence of parameters on the magnitude of the generated pore pressure, the data modelling was carried out in two stages. Initially, the time series analysis approach was applied based on the initial visualization of the pore pressure response. The time series analysis allowed to estimate the initial rate of generation and dissipation. Following the initial estimation of the parameter, a semi-empirical approach was used to establish the relationship between the physical parameters. The model is inspired by the response generated in the Theis equation.

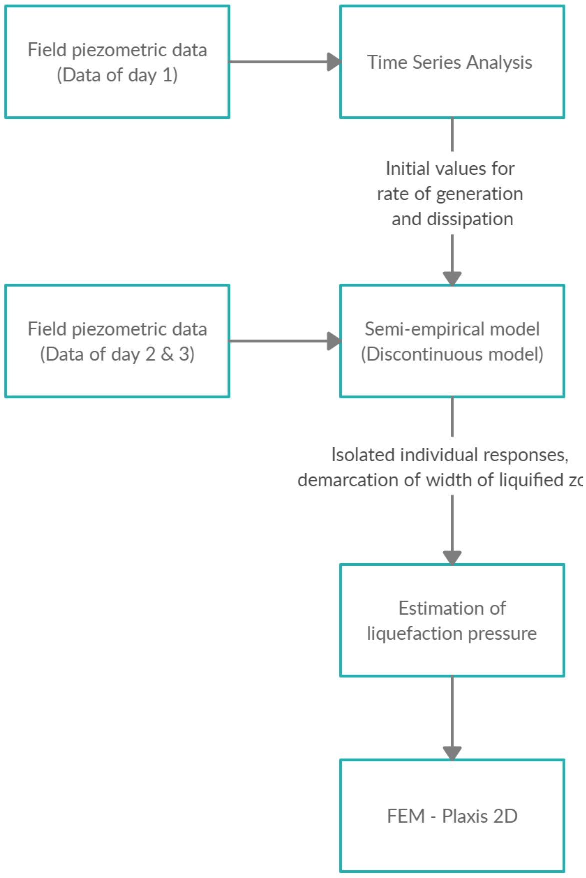

Figure 4.12: The Process of Data Analysis and Characterization

4.4.1. Modelling Strategy

The isolation of the individual responses from the cumulative graph of field data will aid to establish the relationship between the magnitude of pore pressure generated to various physical parameters. There are several techniques available to model and rebuild the data. During the initial phase of data analysis, attempts were made to apply machine learning technique to rebuild the data. However, it was soon realised that the data were insufficient to provide necessary constraints in the model. Later, the system identification module of MATLAB was applied to rebuild the data but both the spatial and temporal variation could not be successfully be modelled. However, system identification allowed to explore the various possibilities of mathematical modelling.

4.5. Stage 1 - Time series analysis

4.5.1. Convolution

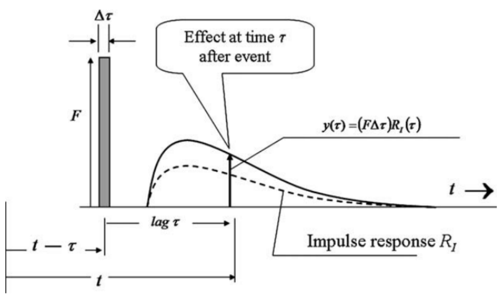

Figure 4.13: Response due to unit excitation [67]

The convolution can be applied advantageously in the groundwater modelling to solve complex problems. Convolution is a superposition technique that can handle input varying over space and time. It is more suitable for a linear system. The convolution technique is based on the unit step response generated by a unit impulse. The dynamic information about the unit response is mapped from the unit input. It is illustrated with an example [67]. For an infinitely small excitation of $lim_{\Delta\tau\to}(F\Delta\tau) = 1$, the unit response R_I shall be achieved as in figure: 4.13. With the variation in the input, the unit response curve shall be multiplied by $F\Delta\tau$ to achieve the actual responses. When the response R_I due to event (v_i) is known for a known time instance then excess pore pressure due to impulse shall be given by:

$$k(t) = \sum_{i=0}^{\infty} F(t-\tau_i)\Delta\tau_i.R_I(\tau_i) \tag{4.1}$$

Where,

- F(t-τ) = Function for the response curve due to previous event.
- t = time from infinite past.
- τ_i = the start of $i_t h$ event.
- R_I = Response cure due to the current corresponding event.

4.5.2. Time Series Analysis

As the objective was to innovatively model the dynamic geotechnical phenomenon using groundwater modelling, possibilities were explored within the groundwater regime to adapt a suitable technique to rebuild the data. To understand the dynamics of the hydraulic head of groundwater due to varying stresses such as rainfall, evapotranspiration, pumping of water were investigated by the application of time series analysis were found to be helpful [8]. In the proposed study, the groundwater head variation due to stress of vibratory piling needs to be investigated. Usually, in time series analysis a series of observation is simulated with explanatory series through a mathematical technique. In here, the observations were piezometric monitoring data and explanatory series were installation events.

In time series analysis it is necessary to develop an impulse response function of the stresses. After achieving the impulse response function F(t) for the stresses of varying time($R_I(t)$) is known, head [k(t)] as a function of time can be computed by applying convolution technique [67]. Impulse response functions represent the time response. As continuous time interval is taken, the convolution integral plays the part:

$$k(t) = \int_{\tau=0}^{\infty} F(t-\tau)R_I(\tau)d\tau \tag{4.2}$$

The function k(t) will include the response of the current event through R_I and the history of past through $F(t-\tau)$. Further as illustrated in the figure: 4.14, individual events can be superimposed to achieve the time series of multiple event responses.

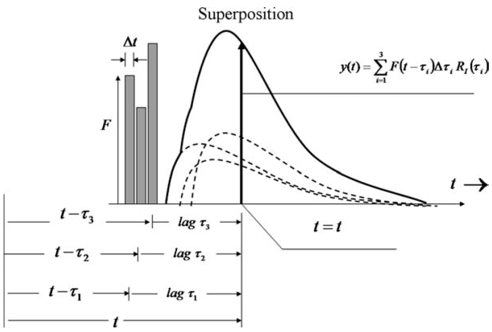

Figure 4.14: Response due to multiple impulses [67]

Usually, the dimension of the input and the output varies with the case. In the proposed study the input is in terms of driving duration and the inverse of the distance from the source and the output is in terms of the head. In practical cases usually, the response of several impulses are superimposed. This superimposition was carried out based on the start time of the event. The response curve depends on the individual input impulses are represented in the figure: 4.14.

4.5.3. Application of time series analysis in Kademuur Damrak case:

In the section:4.3.4, the characteristics of the data of day one was explained. It was also identified that the application of the time series analysis for the data of day one was suitable because of the following reasons:

- Between the events, there was a sufficient time interval to visualize the peak pressure of the events. This allowed to estimate the time delay to achieve the peak pressure and also to trace the start of dissipation tail from the response graph.
- The source of all the events on the day one were approximately at similar distances (within the bandwidth of 2.03 to 3.08m). Hence, it was expected to have a similar delay to achieve the peak pressure and was realistic to apply a continuous function to model them.

The time series analysis was used to model the responses generated with the impulse or excitation. In this work, the excess pore pressure is measured in terms of Pa generated by excitation of the driving sheet piles. The monitored pore pressure may be assumed to be a combination of the three elements:

$$p(t) = s + k(t) + o(t) \tag{4.3}$$

Where,

- p(t) = monitored pore pressure [Pa]
- s = pore pressure in absence of excitation [Pa]
- k(t) = pore pressure induced due to excitation [Pa]
- o(t) = other stresses (Noise) [Pa]

The understanding of the elements was carried out in the data processing section: 4.3.2. Here "s" is the contribution due to hydrostatic hydraulic head or when there are no stresses applied to the system. The induced pore pressure k(t) shall be the head response caused due to transient stress in the model. The parameter o(t) shall be considered as noise and could be a contribution due to several factors such as tidal & seasonal variations, movement of the train in the tunnel etc. The modelling of these variation remains complex. Further, there were limited data to validate them. Hence, the variable o(t) was ignored for the simplicity of the model.

The effect on the system *k(t)* due to vibration shall be computed through the impulse response function or transfer function 6.1. Then, this shall be summed up as convolution of stresses for multiple events. The transfer function for this case was adapted from PRIFICT method [8]. PRIFICT method makes use of a specific parametric function to represent the unit response of every stress. Usually, function with a maximum of four parameters is applicable [8]. In our case, one of the parameter from the exponential part was ignored as only one parameter was expected to influence the rate of dissipation. Thus, the chosen transfer function was:

$$k(t) = A * t^b * e^{-t/c} \tag{4.4}$$

where the parameters in the equation indirectly relates to,

- A - magnitude of peak pressure
- b - rate of generation
- c - rate of dissipation
- t - time

Transfer function 6.1 was expected to simulate the response of the excess pore pressure for the impulse due to the vibratory installation of the sheet pile at a distance (d) from the monitoring point driven for a time($\Delta\tau$). The parameter "A" relates the peak pore pressure. The initial analysis of the data showed that in the case of closer events, higher peak pressure was achieved. This representing the dependability of the pore pressure response on the distance. The second part of the transfer function dictates the rate at which generation of the excess pore pressure occurs. At the start of the event, the second term of the transfer function shall be dominating simulating the generation of the excess pore pressure. With the increase in time, the exponential part becomes predominant and simulates dissipation of pore pressure. It was expected that only transmissivity and storativity will play a role in determining the dissipation as the system remain undisturbed. At this juncture, it was important to be reminded that modelling of the noise was ignored.

4.5.4. Implementation of the model

As mentioned earlier, on the day one there was sufficient time interval available between the successive events such that the initial evolution of the pore pressure could be visualized. It was valid that the successive events sets in even before the pressure generated due to previous perturbation had returned to the ground state. Thus, the data obtained from the field includes only a cumulative response and isolation of the individual events was necessary. Tracing of the dissipation tail remains as the main task. It was achieved by calibration of the parameters and curve fitting using MS Excel and later in Pandas module of Python.

Calibration of parameters:

The objective of the time series analysis was to estimate the values of the parameters in the transfer function reconstruct the field data. In the monitored field data, the nature of the response was expected to vary between every event due to the following reasons:

- Anisotropic nature of the soil
- Variation in the depth of penetration
- Presence or absence of clutching force

As the installation of the piles progresses, the cofferdam was progressively built altering the boundary condition continuously. It possesses the capability to influence the dissipation of the generated excess pore pressure due to the obstruction created by the newly installed pile. However, it remains cumbersome to investigate the influence of this aspect from the available data and shall be ignored in the analysis.

The value of parameters was expected to vary for the events and was deduced by application of curve fit technique based on the least square approach. In other words the value of the objective function F is minimized [8]:

$$F = \sum_{i=1}^{N} (p_i - h_i)^2 \tag{4.5}$$

where,

- F = Objective function
- N = Number of observations
- p_i = field observations
- h_i = modelled value

Even though the model is more dependent on the curve fitting and also variables of the transfer function do not directly link to the physical parameters, it provides the first estimation to the trend of evolution of excess pore pressure. The discussions over the inferences from the model will be carried out in the following chapter. Regardless, the data of day one was more suitable for the convolution technique, it had certain limitations in order to validate our research objectives.

Limitations of the data of day one:

- The events on day one were at a distance of 2.03 - 3.08m from the source and hence extrapolating the response for the larger distance was unfeasible.
- The installation of the sheet pile did not start at the aquifer level which was anticipated at -12.8m NAP. The driving was started at -9m NAP which is expected to create an anomaly in the pore pressure reading.
- Unlike events on day two and three where the depth of penetration for each event remained constant (1m), the depth of penetration on the day one were varied.

Drawbacks of time series analysis
Further, when this technique was applied to rebuild the data of day two and three, there were severe setbacks:

- Developing a relationship between the physical parameters(duration of driving) to the excess pore pressure was the main aim of the proposed work. But there were no direct variables relating to these parameters.
- The time series analysis was based on a continuous function but the analysis of data showed that there was a need for a separate variable to independently control the rate of generation and dissipation for better analysis and understanding. The rate of generation was expected to be influenced by two factors: Hydraulic properties like transmissivity and storativity defining the delay to the peak pressure and distance from the source defining the magnitude of the peak pressure.
- Also when the source is within 1m of the monitoring point or the monitoring is within the liquefied zone (60% of vertical stress [75]) the rate of dissipation increases drastically and drops back to a normal rate after when the pressure dissipates. It becomes infeasible to model such drastic variation by application of a continuous function.

Unlike the data of the day one, the data of day two and three had variety i.e, the distance from the source to monitoring varied from 0.92 m to 18m. The duration of driving varied from 40 seconds to >10 minutes. These allowed us to better understand the variation in the response due to the "distance from the source" and "duration of driving" in addition to the variation in the boundary condition. Hence, it is a robust data to derive appreciable inferences from the analysis.

Considering the drawbacks of the data from day one and the limitations of the time series analysis. It was important to introduce a discontinuous model to cater to the shortcomings of time series analysis. The semi-empirical approach was followed due to the necessity to incorporate the physical parameters into the model.

4.6. Stage 2 - Characterization by semi-empirical approach

4.6.1. Modelling strategy:

The figure:3.4 represents the response of the aquifer close to the screen in the monitoring well. When the head in the pumping well is brought down instantly. There is a drop in the pressure head taking an exponential path dictated by the hydraulic properties of the soil such as hydraulic conductivity, storativity and distance from the well. This decay response was represented by the first part of the plot in the figure: 3.4. But when the well is left undisturbed after the drop, due to the groundwater inflow it will undergo a recovery process to achieve a steady-state condition. This recovery was represented by the second part of the plot in the figure:3.4. This inspired to develop a discontinuous semi-empirical model to simulate the pore pressure evolution due to vibratory installation of the pile. As the model includes the coefficient of the hydraulic conductivity in terms of generation and dissipation rates making it viable to relate the process to distance from the source (d), duration of driving (dt), depth of penetration. It should be noted that, during vibratory installation, the generation process would be stimulated by the recovery part and the dissipation would be replicated by the decay part of the slug test.

4.6.2. Generation model

This section introduces a semi-empirical model to analyse and validate the data of the excess pore pressure from day two and three. The model was inspired by the trend of transient head response in slug test [34], Theis equation [19] which is widely applied to investigate the hydraulic parameters of the aquifer in the groundwater modelling. This allowed for the assumption that transient generation response of the excess pore pressure could be modelled using an exponential function similar to the exponential part of Copper et al (1954) [21]. The constant(k) defining the rate of generation was expected to be a function of volume at the source(Q), transmissivity (T), distance from the source(r), storativity(S), and time (t) from the equation: 3.43. However, in our model, the soil is assumed to be isotropic and the value for Transmissivity, Storativity are assumed to be constant and the distance from the source (d) remains as the variable. Hence, a constant "k" was considered in the generation part of the model. Further, the dissipation part of the model was influenced by simple exponential modelling technique adopted in the work by Chian et al (2015) [20].

4.6.3. Dissipation model

The dissipation of the excess pore pressure is usually given by the classical one-dimensional consolidation equation:

$$\frac{\partial \bar{u}}{\partial t} = C_v \frac{\partial^2 \bar{u}}{\partial z^2} \tag{4.6}$$

where,

- $\bar{u}$ = excess pore pressure [Pa]
- t = time [s]
- z = depth of the soil
- C_v = Coefficient of consolidation
- $C_v = \frac{k}{m_v . \gamma_w}$

Further, the hydraulic conductivity of the soil (K) is given by:

$$K = k . \frac{\rho_w g}{\mu} \tag{4.7}$$

where,

- k = permeability of the soil
- ρ_w = density of the pore fluid
- μ = dynamic viscosity
- g = acceleration due to gravity

When there is no perturbation in the porous media the dissipation of the pore pressure occurs. The dissipation of the pore pressure could be idealized as self-weight consolidation due to the overburden. In the liquefied state, the overburden is carried by the pore pressure as the particles are not in contact have zero shear resistance. On dissipation of the pore pressure, the particles come in contact with each other and generate inter-granular forces providing shear resistance to the soil. It was confirmed that there is no influence of the depth during the dissipation of the excess pore pressure [20]. The dissipation process was simplified to an exponential decay function[20]:

$$\bar{u}(t) = e^{-\alpha^2 C_v t} = e^{(-At)} \tag{4.8}$$

where A is a constant. The constant A was linearly related to the hydraulic conductivity of the sand [20]. In the proposed model the decay is given by the constant "d*".

The rates of generation and dissipation from the time series analysis (stage 1) shall be applied to the data of day 2 & 3. It will help to estimate the evolution of excess pore pressure due to the individual events in stage 2. These resulting responses shall further allow us to derive the physical relationship between predominant factors inducing water overpressure in subsurface due to vibratory installation.

The response curve is first bifurcated into **generation** and **dissipation** part.

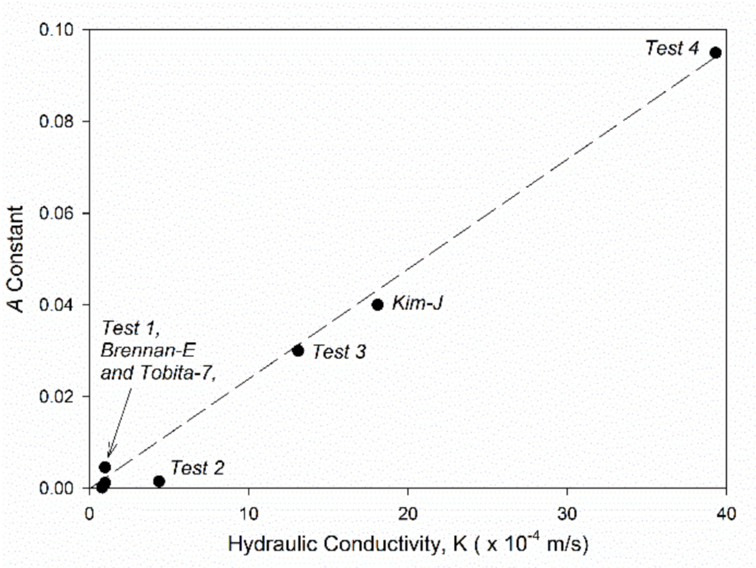

Figure 4.15: Linear relationship between A and hydraulic conductivity of the sand[20]

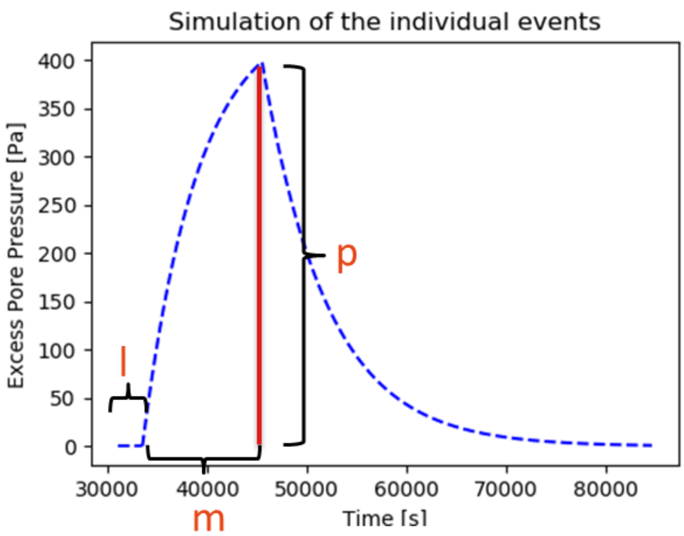

Figure 4.16: Breakdown of the curve for parametrization

4.6.4. Semi-empirical model

The proposed semi-empirical model is composed of 2 parts as discussed in the previous section,

- Generation
- Dissipation

$$p_G(t) = P(1 - e^{-k*t}) \tag{4.9}$$

$$p_D(t) = P(e^{-d^* * t}) \tag{4.10}$$

Where,

- $p_G(t)$ = Excess pore pressure during generation [Pa]

- $p_D(t)$ = Excess pore pressure during dissipation [Pa]
- P = Peak pressure [Pa]
- k = rate of generation
- d* = rate of dissipation

4.7. Analysis Strategy

4.7.1. Generation

The generation curve allowed to parametrize three factors,

- Time delay to initial response (l)
- Time delay to achieve the peak pressure(m)
- Magnitude of peak pressure (P)

The first two parameters (l & m) were a function of distance. The third parameter peak pressure (P) was also a function of distance. The property of the soil such as transmissivity, storativity plays a vital role in relation to the distance. Also, as the major source of the excess pore pressure was assumed to be the liquefied zone and transmitted groundwater flow in the non-liquefied zone. The time delay to initial response and the time delay to achieve the peak pressure should be representative of the hydraulic conductivity of the soil.

Attenuation was expected to define the width of the liquefied zones as in figure:3.1. The magnitude of the excess pore pressure in the liquefied zone in a given soil shall be defined by the attenuation. In the non-liquefied zone, it shall be dictated by geohydrological parameters as the contribution is from the groundwater flow. The relationship between the parameters l, m & P shall be established from the analysis of pore pressure response of the field data of "Kademuur Damrak" and shall be discussed in the next chapter.

Relationship between the parameters:

- A relationship between **"l"** parameter and the distance shall be derived from the data analysis. The parameter represents the time delay to the first response of pore pressure. This was expected to be directly proportional to the distance of the piling (or source) from the monitoring point.
- Similarly relationship between the parameter **"m"** and distance were deduced. This was expected to be the function of hydraulic conductivity and storativity.
- The parameter **"P"** was expected to be the function of the depth of penetration (dl), distance from the source(d) and the energy of the vibratory hammer.

  Depth of penetration(dl): The magnitude of the excess pore pressure is directly proportional to the depth of penetration. It can be understood from the fact that larger the penetration of the sheet pile, longer the soil column will be liquefied sourcing more excess pore pressure to the monitoring sensors unless the aquifer is assumed to be leaky. However, this variable has been taken as constant as the penetration depth per event was 1m only.

  Energy of Vibro-hammer: It is understood from the shear stress and strain based pore pressure models 3.3 that the magnitude of shear stress or strain acting on the pile-soil interface drives the excess pore pressure. This allows us to understand that driving energy plays an important role in the magnitude of pore pressure generated. As the same driving hammer was used for all the installations in the course of the project at "Damrak" this was assumed to be constant in order to simplify the modelling. However, it should be understood that the driving energy varies also on the operator's skills and mindset.

- The relationship derived from the data analysis,

  1. Distance vs Delay time of initial response (l)
  2. Distance vs Peak Pressure (P)
  3. Distance vs Delay time to Peak Pressure (m)
  4. Duration of driving vs Peak pore pressure (P)
  5. Duration of driving vs Delay time to Peak Pressure

4.7.2. Dissipation:

In a soil system after the driving event is stopped and once the pore pressure has reached a peak, the pressure will start dissipating. Due to the absence of any other external forcing the system is considered to be free. Under such circumstances, the soil properties that can influence the rate of discharge or dissipation shall be the hydraulic conductivity(K) 4.6.3. As discussed earlier, the rate of dissipation will be given by d*. This can be evaluated by fitting the exponential decay equation to the dissipation field data.

4.7.3. Python Implementation of the Data Analysis:

Python was utilized to clean, visualize and analyse the data. The knowledge from the time series analysis (Stage 1 model) on the data from outside the cofferdam (Pr -3841) was utilized to rebuild the response using the semi-empirical model (Stage 2 model). The knowledge includes the rate of generation and dissipation inferred from stage 1 model.

1. From the cumulative response curve of a day, the response curve of one set was isolated by extrapolating the dissipation trend of the previous set.

2. The response curves resembling the isolated R_I from the time series analysis were rebuilt using the semi-empirical model by estimating the values of its parameters.

3. The rebuilt response curve was applied to the cumulative curve from step 1. The events with known responses from time series analysis (2.03 to 3.08m) were deducted from the cumulative curve. The residual curve was the response due to other events for which the response was unknown. For instances, a set with 3 events originating at 2.1m, 8m, 2.8m. The response of event 1 & 3 was deducted and leftover was the response due to the event at 8m.

   This process was iterated several times and the knowledge developed from there was applied to a new set in order to validate the responses and residual is considered as error.

$$Error[E] = \frac{Area under the residual curve}{Area under the cumulative curve} * 100 \tag{4.11}$$

The process was repeated for the data monitored within the cofferdam (Pr-3839, Pr-3840) as well, to understand the variations in the responses with different boundary conditions. The variation of the rate of generation and dissipation between both the boundary condition were analysed using PLAXIS model and will be discussed in the later chapters.

4.8. Summary:

In this chapter, the stratigraphy of the Kademuur Damrak was introduced. The geological understanding was aided by the work by TNO [37]. The monitoring sensors were installed in the Holocence sand layer. The presence of the alternating layer of allerod and sand poses the threat of lower permeability of the aquifer. This was also observed in the data visualization, it took much longer than the driving duration for the pore pressure to reach the peak. The cofferdam enclosure formed by the sheet pile installed on the waterfront side and newly installed sheet pile on landside expected to hinder the normal dissipation affecting the transmissivity of the aquifer. To understand the impact of driving duration on the peak pore pressure, the start and end of the driving events were recognized from the frequency response of the accelerometer. The time series analysis provided the first estimates of the pore pressure response to calibrate the semi-empirical model.

5

Hydrogeological model for a dynamic phenomenon

In this chapter, the pore pressure response due to vibratory installation of the sheet pile was modelled with a hydro-geological viewpoint in Plaxis 2D. Being a hydro-geological model, PLAXFLOW module (or flow the only module) was utilized. The analysis of piezometric data from Kademuur Damrak plays a predominant role in validating this model.

Finite Element model was based on the hypothesis mentioned in the section: 3.4. Zone 1 was assumed to be the liquefied zone and zone 2 was non-liquefied zone. The driving of the sheet pile was simulated by applying a constant head at source or the edge of the sheet pile. The constant head drives up the pressure in the aquifer radially outward. The head response at a point "x" m radially away from the source progressively increases at rate dh due to the constant head loading at the source. The increment of the pore pressure radially in the aquifer due to constant head loading resembles the partial drainage of excess pore pressure during driving of the sheet pile also referred to as pre-shearing. As the event or installation of the sheet pile comes to halt dissipation should get dominant. Further, the possible contribution of excess pore pressure due to consolidation was ignored in the modelling.

5.1. Finite Element Model in PLAXFLOW

The transient and steady-state confined and unconfined well flow problems shall be modelled using PLAXFLOW. The dynamic problem of pore pressure generation and dissipation due to the vibratory installation of the sheet piling shall be modelled as transient response. The version used in the current work was Plaxis 2D 2019 - Plaxflow.

5.1.1. Geometry

The problem was modelled as axisymmetric. The dimension of the finite element model depends on the width of the radial stretch of aquifer and stratigraphy of the soil in the problem. The assumed width of the aquifer defines the right boundary of the model. The extent of the boundary must not allow for the ghosting of the excess pore pressure along the boundary. However, the extent of the boundary should also not be excessively large that model takes extremely large calculation time. A balance should be established between both the width of the boundary and the calculation time.

Width:

The model extends to a width of 100m in the radial direction and 26m in the vertical direction as represented in the figure:5.2. As it will be expected that pore pressure dissipation should be radial in nature in a confined aquifer, the boundary of the model should be kept sufficiently far so that boundary influence is kept negligible. The sensitivity was carried out to affirm the width of the model.

To carry out the sensitivity analysis for the optimum width of the geometry, the pore pressure response at a radial distance of 4.463m was computed for varying width (25m, 50m, 100m, 1000m). The computed excess pore pressure was noticed to be dissipating prematurely in case of 25m. Progressively, it was noticed to saturate at the width of 100m. There was negligible variation in the rate of excess pore pressure dissipation between 100m and 1000m as illustrated in the figure:5.1. Hence, the width of the model was adapted to be 100m. Further, the bottom and the right boundary were chosen as seepage boundary. This is again to avoid any boundary effects.

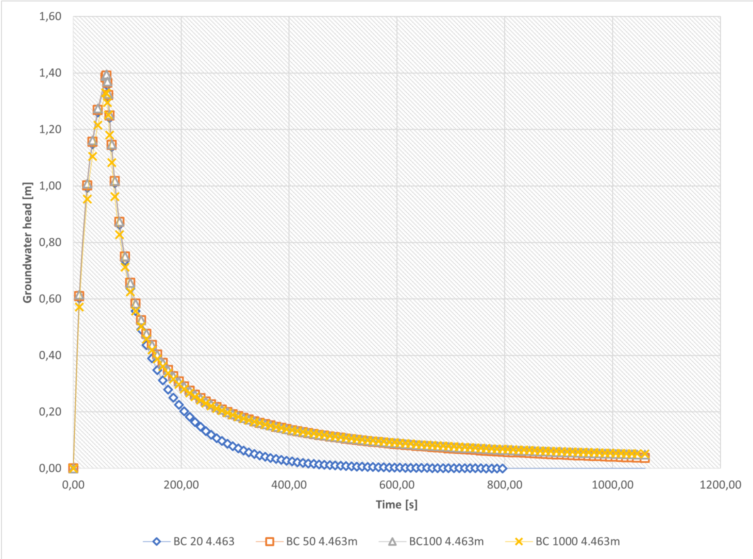

Figure 5.1: Illustration of the sensitivity of of model width on the pore pressure evolution at a radial distance of 4.463m

Soil profile of the model:

The soil profile of the model plays a predominant role simulating field like situation in the model. The significant contribution of the soil profile with respect to the current model is the presence of an alternating layer of allerod and sand at the monitoring depth. The presence of lesser permeable layer could delay the dissipation of the excess pore pressure and also contribute to the quicker accumulation of the pore pressure to achieve liquefaction. Hence, it was very important to accurately estimate the soil profile for the model. The nearest available CPT is represented in the appendix:B. It was applied to the model by using the borehole tool of Plaxis. Being a flow only model, hydraulic conductivity (K) was the only direct input parameter for the model in PLAXFLOW. The other factors that are expected to influence are based on geometry and boundary conditions and shall be discussed in later sections.

5.1.2. Source

The evolution of excess pore pressure generation due to the vibratory installation of the sheet pile was implemented in an axisymmetric model. The major source of the excess pore pressure shall be from the liquefied zone. The source was the centre of the axisymmetric model from where the pore pressure shall be introduced by the constant head loading equivalent to the driving duration of sheet pile. The Plaxis allows head as the input pressure for the model. Hence, the pressure contribution of 40kPa at 0.92m away from the source as observed in the field data was utilized for the modelling. The width of the liquefied zone was 1m and 4m of head per unit square area was applied. The modelling was carried out only for the representative penetration depth of 1m of sheet pile for efficient comparison of the field data.

5.1.3. Time step

The time taken to complete each simulation depends on the chosen geometry of the model and the time step in the computation. Based on the chosen time step, pore pressure is calculated at every stress point of the finite element model. The smaller time interval could provide greater accuracy to simulate dissipation of excess pore pressure. Hence, a balance is needed between the accuracy and the time step. It was important to understand that with a single large time step there was a possibility of the instantaneous vanishing of excess pore pressure due to higher hydraulic conductivity. Thus sudden disappearance of the excess pore pressure in a single time step hampers us from drawing a reasonable trend for dissipation. Hence, the sensitivity of the time step was carried out for the model.

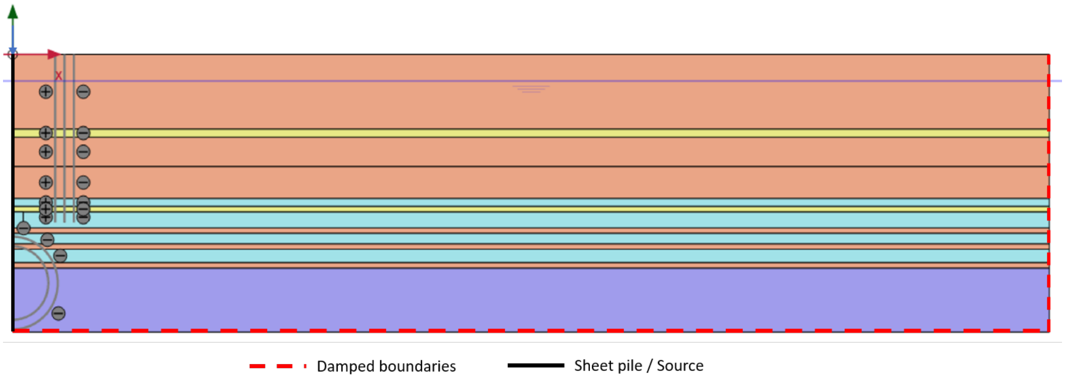

Figure 5.2: Finite Element Mesh for the pore pressure dissipation modelling

The sensitivity of the time step was carried out for 1s and 10s. The groundwater head response was calculated at 1.974m from the axisymmetric centre. The model response is represented in the figure: 5.3. The head response in both the time steps overlapped with each other. Hence in order to consider an optimized calculation time 10s was used in further modelling.

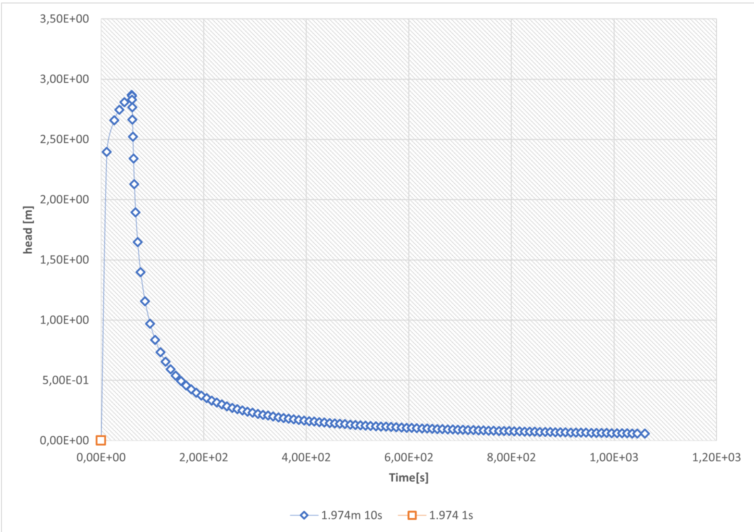

Figure 5.3: Illustration of the sensitivity of model time step on the head response at a radial distance of 1.974m

5.1.4. Hydraulic conductivity

The value applied for the sand is usually in the range of $10^{-4} m/s$. It was noticed from the CPT 8 & 9 [Appendix: B] that the first sand layer has an alternating layer of sand and allerod with an intermittent fluctuation in the cone resistance within 14 - 16m. Hence, the hydraulic conductivity of the sand layer was assumed to be $5 * 10^{-5} m/s$ to initiate the analysis. However, in later sand layer with higher cone resistance representing clean sand, hydraulic conductivity of $2 * 10^{-4} m/s$ was chosen. The hydraulic conductivity of all the soil layers is presented in the table: 5.1 and the configuration of the values are represented in the figure: 5.4.

5.2. Methodology

The analysis of data established the liquefied soil volume around the sheet pile. As described in the hypothesis in section: 3.4 the soil will be separated as zones, the constant head loading for the driving duration shall be applied to simulate the head generated due to the liquefied volume (Zone 1). The excess pore pressure from zone 1 in form of groundwater flow contributes the excess pore pressure to zone 2 of the PLAXFLOW model. The head response as a function of time and space is plotted in the Plaxis model to understand the sensitivity of the influencing parameters. From the data analysis, it was understood that boundary condition,

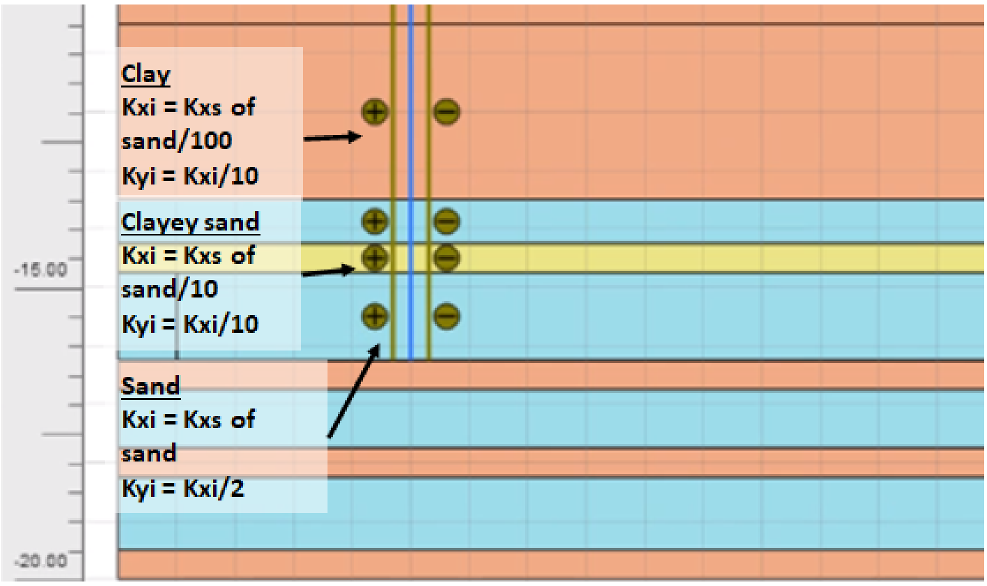

Figure 5.4: Schematisation of the choice of K values for different soil layers in Plaxis model

Soil description	K_x/K_y	Hydraulic conductivity (m/s)
Sand	K_x	$5*10^{-7}$
	K_y	$2.5*10^{-7}$
Clayey Sand	K_x	$2*10^{-8}$
	K_y	$2*10^{-9}$
Clay	K_x	$2*10^{-9}$
	K_y	$2*10^{-10}$
Clean Sand	K_x	$4*10^{-4}$
	K_y	$2*10^{-4}$

Table 5.1: Hydraulic conductivity of the soil types in the model

distance from the source drives the dissipation of accumulated pore pressure. Further, we also understand from the data modelling part that rate of dissipation is a factor of hydraulic conductivity. The impact of the parameter values shall be studied by the analysis of the finite element model.

From the hypothesis of the research work, the pumping well expected to generate a radial flow of the water in the aquifer and similar response shall be expected from the model. The literature suggested that the width of the liquefied zone will be lesser than 1m [66]. Also, the analysis of field data of Damrak allowed us to establish the width of zone 1 to be 0.92m. A conservative width of the zone 1 shall be 1m. Further, the width of the transition zone shall be elaborated later in the upcoming chapter to be from 1m to 2m. For simplicity, the modelling of the transition zone was ignored. The width of the zone 2 depends on the radial extent to which the groundwater can flow.

5.2.1. Staged construction

The staged construction of the model includes 3 phases. (a) Initial phase, (b) Phase 1 - Generation phase (c) Phase 2 - Dissipation phase.

Stage	Time	Zone 1	Zone 2
1	During Installation	Liquefaction pressure (Width of liquefaction zone(1m), liquefaction head(4m), thickness of the aquifer(1m))	-> Flow from liquefaction zone + Consolidation
2	Post installation	Consolidation - Post Liquefaction	-> Flow from zone 1

Table 5.2: Schematisation of the methodology for pore pressure contribution of the Plaxis model

Initial phase:

This phase represents the situation before the start of the sheet pile installation. In this phase, the values of soil properties are initialized. This phase is not significant in the presented analysis.

Phase 1:

This phase represents the vibration or driving period of the sheet pile. During liquefaction, the amount of pore pressure generated must be equivalent to the vertical effective stress. However, from the analysis of the field data, it was found that in our problem the maximum pore pressure achieved was 0.5-0.6 times of the expected maximum vertical effective stress at 0.92m. This can be attributed to several factors and shall be discussed in the later chapter. Hence, 4m of the head was applied for a width of 1m. To simulate the driving of the sheet pile a constant head (h) is maintained at the source for a duration equivalent to driving time (dt), there will increment in the head due to transmission of water head radially to the aquifer simulating the effect of pre-shearing. As the zone 1 is modelled to be liquefied in this phase, the value of hydraulic conductivity shall increase by 4 times from the initial value [90]. In reality, there is a gradual transition from the liquefied to non-liquefied zone, unlike the model. The hydraulic conductivity of the zone 2 remains unchanged from the initial value.

Phase 2:

Phase 2 represents dissipation phase, the excess pore pressure gets dissipated post liquefaction. The hydraulic conductivity of the liquefied zone returns instantly to the initial value at the end of phase 1. This is not true in reality, however, the modelling of gradual transition from liquefied to non - liquefied hydraulic conductivity post liquefaction is ignored for simplicity. The single value of hydraulic conductivity is maintained throughout all the zones.

5.3. Sensitivity

The model evolved gradually in steps. This section discusses the development of the model and the sensitivity of parameters. The sensitivity of the finite element model evaluates the impact of soil properties and boundary conditions on the evolution of pore pressure. The parameters anticipated to affect the model are verified and discussed in this section.

5.3.1. Non-leaky aquifer model

Non-steady flow in an infinite radial aquifer is a prevalent concept during the pumping of a well in groundwater flow model [42]. A similar approach is applied here with the PLAXFLOW module. In this initial model, the ideal condition of a non-leaky aquifer is considered. In a non-leaky aquifer, the vertical conductivity is restricted. Thus the dissipation or the transmission of the excess pore pressure occurs only in the radial direction. To simulate non-leaky aquifer, the K_y value of sand was chosen to be $4 * 10^{-9}$ m/s. This restricts the flow in the vertical direction.

Further, to understand the response of the peak excess pore pressure with the distance, the sensitivity of hydraulic conductivity. The excess pore pressure was expected to reach larger distances as the dissipation was only in the radial direction. The value of the hydraulic conductivity of the soil type assumed in the model is described in the table: 5.1. The result of the simulations is not discussed as it does not stand relevant to reality or field observations.

5.3.2. Leaky aquifer model

The non-leaky aquifer is an ideal condition applied by hydro-geologist to approximate the expected discharge from an aquifer. In case of Kademmur Damrak, there was alternating layer of discontinuous high and low permeable soil as represented in the CPT (Appendix: B). Hence, there was expected vertical conductivity of the soil. The value of the hydraulic conductivity was chosen based on the regime presented in the figure:5.4. The most adaptable value of the hydraulic conductivity is presented in the table: 5.1.

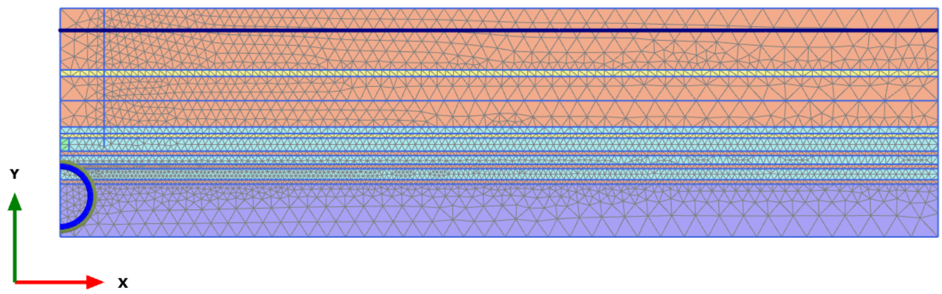

Figure 5.5

5.3.3. Leaky aquifer with underground structures

The sheet piles in Damrak were installed over the NZ tunnel line. Hence, an investigation of the effect of the introduction of the tunnel structure into the model was necessary. The tunnel was constructed by the tunnel wizard of the Plaxis modelling. As in the field, a tunnel of 6.44m diameter was adopted. The standard lining property from the Plaxis manual was adopted as presented in the table: C.1. The considered lining properties were expected not to influence the behaviour of the pore pressure as it was modelled with a closed boundary for water flow.

Based on the available knowledge about the field from the project information. An attempt was made to replicate a similar scenario using a simple Plaxis model. From the analysis of the field piezometric data, it was realised that the response of the excess pore pressure was significantly determined by the distance from the source. The property of the soil that immediately relates to distance with regard to the flow to the non-liquefied zone is hydraulic conductivity and transmissivity. There are other factors that could affect the process such as storativity, obstruction to the flow boundaries, the magnitude of the pore pressure itself. An attempt is made in the later sections to understand the impact of obstruction to the dissipation boundary by the introduction of sheet pile with closed water boundary into the domain replicating the field behaviour. The comparisons of the result shall be carried out in the following chapter.

5.3.4. Leaky aquifer with sheet pile boundary

In construction at Damrak, the sheet pile formed a closed cofferdam structure. The waterfront side had a deeper pile, penetrating up to 20m and this formed a closed boundary to the generated excess pore pressure while installing the landside sheet pile. A similar scenario was simulated with the source or the landside sheet pile at the axisymmetric centre and the waterfront sheet pile was introduced 6m apart as represented in the figure: 5.6 . In the model, the function of the sheet pile is only to form a boundary to the flow as no stress consideration as taken here. The higher peak pore pressure was expected within the boundary and the rate of dissipation was expected to get impacted.

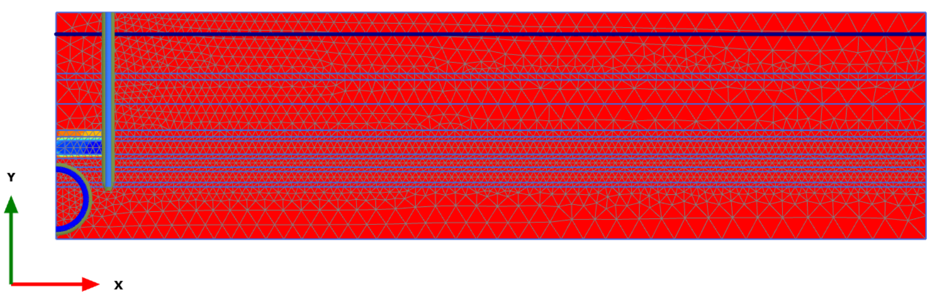

Figure 5.6: Schematisation of the Plaxis model with sheet pile as obstruction to the dissipation boundary

5.4. Summary:

Thus, the simple Plaxis model allowed us to investigate the magnitude of pore pressure achieved at a distance (d) from the source of the vibration. The sensitivity of the model parameters assures the absence of the dispensable errors in the model. The model was initiated from a simple form and more details were added once the theoretical behaviour was confirmed. For instance, the presence of vertical conductivity on providing reasonable K_y value. The modelling of an alternating layer of allerod and sand was a significant aspect. The presence of the sheet pile was to alter the dissipation boundary to simulate the effect of sheet pile on the waterfront side.

There was a certain limitation of the model: (a) The constant head is an input to the model which is difficult to estimate. (b) The hydraulic parameter such as storativity could not be provided as a parameter in the PLAXFLOW (c) There is a strong dependency of this model on the duration of driving. But there was no clear relationship established between the duration of driving and distance or with the pore pressure.

6

Result and Discussion

This chapter is dedicated to discuss the results of the analysis conducted and the validation of the models into consideration.

6.1. Analysis of the field data

6.1.1. Time series analysis

In this study, the analysis of the field piezometric data was carried out by applying a transfer function using time series analysis. It was followed by semi-empirical modelling. The time series analysis was carried out by optimizing the parameters in the model to fit the field piezometric data of day 1.

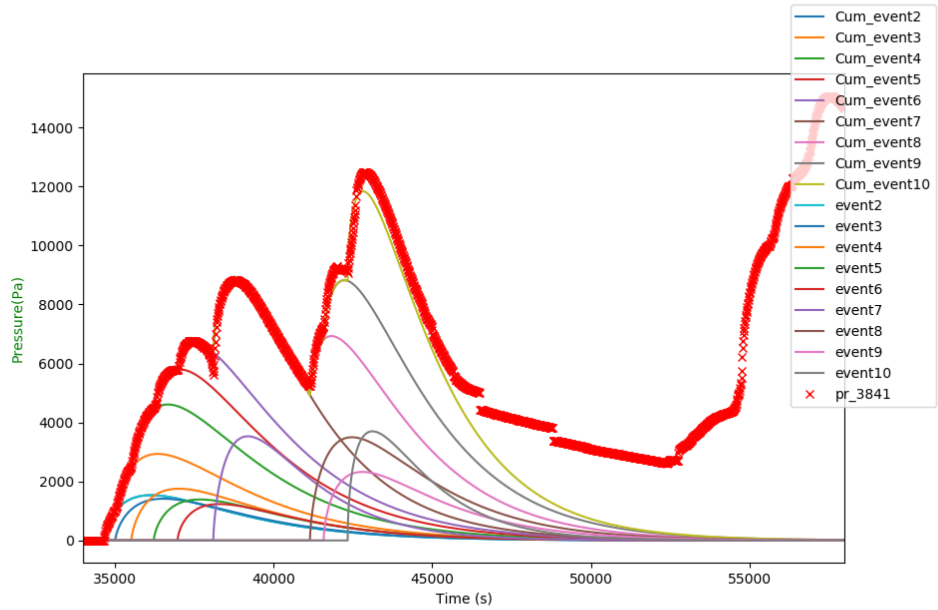

Figure 6.1: Illustration of the time series analysis on the piezometric data of day 1 (Pr - 3841)

The first event on this day was the installation of sheet pile up to -12.8m NAP. But the aquifer has anticipated this depth. Hence, this event was ignored by the analysis. In this section, the results from the modelling of time series analysis will be discussed.

Relationships between modelling parameters:

$$k(t) = A * t^b * e^{-t/c} \tag{6.1}$$

Parameter "A", indirectly represents the peak pore pressure of the event. However, its relationship with distance from the source (d) remains inconclusive (figure: 6.2). The reason for this could be the varying depth of penetration between the events of the day one as represented in the table: 6.1 and all the distances are around 2 to 3m. The parameter "b" is directly proportional to the distance i.e., the value increases with the distance as shown in the figure: 6.2. This also remained true for the parameter "c" illustrated in the figure: 6.3. As the sampling of day 1 was restricted to 2.03 to 3.08m, it was difficult to integrate the fitting parameters for varying distances as in day 2 & 3. Hence, the semi-empirical modelling approach was introduced. However, the relationship between peak pore pressure(P) and distance from the source(d), rate of generation and dissipation served to calibrate the semi-empirical models.

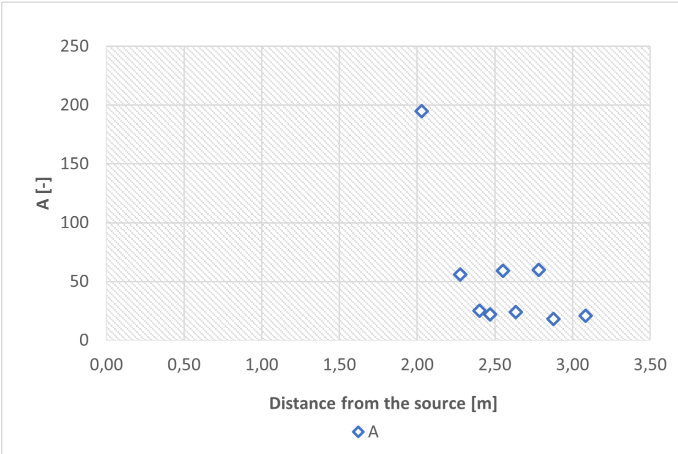

Figure 6.2: Relationship between parameter "A" vs distance from the source

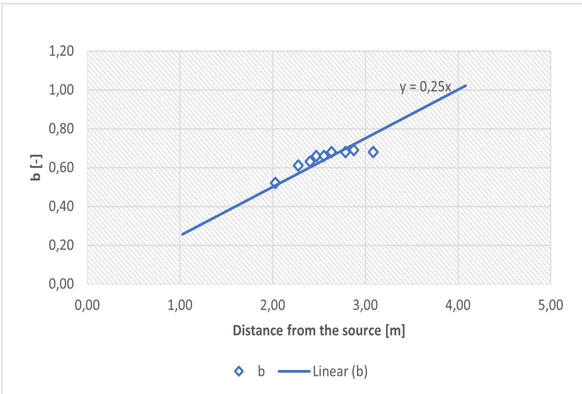

Figure 6.3: Relationship between generation parameter (b) vs distance from the source

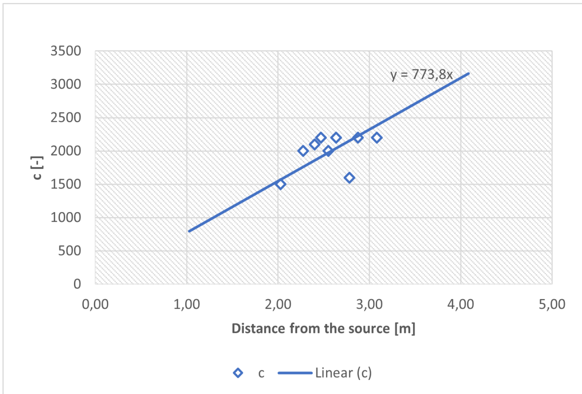

Figure 6.4: Relationship between dissipation parameter (c) vs distance from the source

The time series analysis provided the first estimates for the rate of generation, dissipation for the response curve of the events around 2m from the source. This prior knowledge provided us with the initial values of the parameters in the semi-empirical modelling. In order to understand the relationship between physical parameters from the response curves, regression graphs were plotted between these parameters.

Relationships between physical parameters:

The time series analysis allowed us to draw inferences that acted as the precursor to building the semi-empirical model. There was an inverse relationship between distance from the source (d) and the peak pressure (P) presented in the figure: 6.5. However, no clear distinction could be established on the impact of duration of driving on peak pore pressure (Duration of Driving - Labelled on the data points in the figure: 6.5). In the previous studies conducted to model the excess pore pressure and the settlement due to vibratory

Start depth [m NAP]	End depth [m NAP]	Depth of penetration(dl)[m]	Distance from source (d)[m]
-12.8	-13.0	0.2	3.08
-13.0	-13.5	0.5	2.88
-13.5	-14.0	0.5	2.63
-14.0	-14.5	0.5	2.47
-14.5	-15.0	0.5	2.40
-12.8	-13.0	0.2	2.78
-13.0	-13.5	0.5	2.55
-13.5	-14.0	0.5	2.28
-14.0	-15.0	1.0	2.28

Table 6.1: Penetration depth for the events on day 1

installation by [66], [64], [25] the maximum settlement occurred at 1m radius from the sheet pile. Based on this, we could also infer that the maximum excess pore pressure will be generated close to the source. This also validates the assumption of slip surface close to the sheet pile. From the relationship between distance vs time to peak pressure in the figure: 6.5 it was observed that for the larger distance the time to achieve the peak pressure was much greater than the duration of driving. This was also supported by the semi-empirical model as presented in the figure: 6.10. This phenomenon indicates that the main source of excess pore pressure may not be directly due to the cyclic loading of the soil at that point in the non-liquefied zone but rather due to the possible presence of alternative source i.e., groundwater flow. The presence of the liquefied zone could be validated due to instantaneous leap in the excess pore pressure in closer observations as presented in the figure: 6.9. However, the generation of the excess pore pressure due to the cyclic mobility and later due to consolidation of the sand was ignored. The delay to achieve the peak can be attributed to the hydraulic conductivity or the transmissivity of the sand.

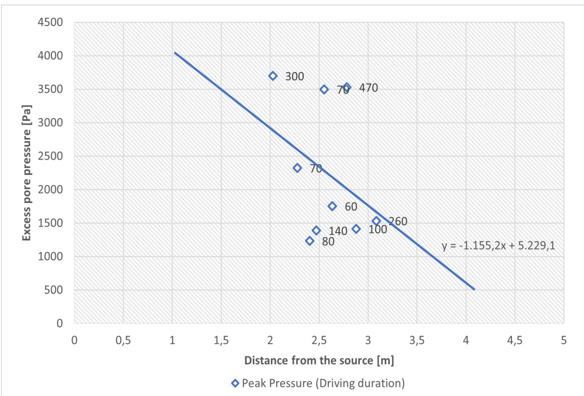

Figure 6.5: Relationship between peak excess pore pressure (P)
vs
distance from the source (d)

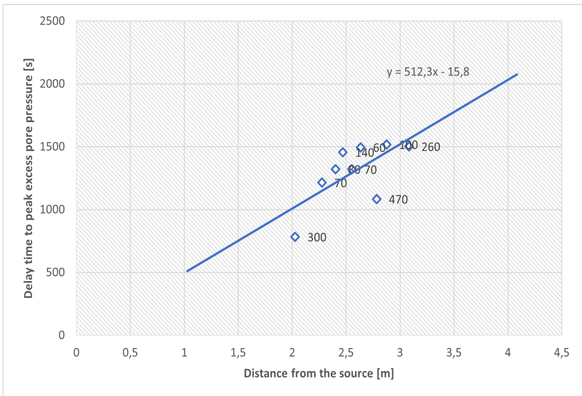

Figure 6.6: Relationship between delay time to peak excess pore pressure
vs
distance from the source (d)

6.1.2. Semi-empirical model

$$p_G(t) = P(1 - e^{-k*t}) \tag{6.2}$$

$$p_D(t) = P(e^{-d^* * t}) \tag{6.3}$$

Relationship between modelling parameters:

Unlike time series analysis, the proposed semi-empirical model uses parameters directly relating to the rate of generation and dissipation to rebuild the trends of excess pore pressure in a simple approach. The generation is driven by parameter "k" and possess an exponential relationship with the distance from the source (d) as illustrated in the figure: 6.7. As the sand is assumed to be isotropic and also the energy from the vibro-hammer is considered constant in subsection: 4.6.2, the volume of generation(V), transmissivity (T), storativity(S) are assumed as constants for modelling. If the mentioned parameters are assumed as a constant in the field, the rate of generation could vary only due to the influence of distance from the source (d). However, this is not true due to the heterogeneity of the soil. The figure: 6.7 represents that the rate of generation reduces exponentially with the distance (d). This indicates that the magnitude of accumulating pressure acts as the driving parameter for the generation rate (k). In the case of higher pore pressure closer to the source, the rate of generation was faster. Further, the rate of dissipation (d*) of the excess pore pressure fluctuated in within very small bandwidth presented in the figure: 6.8. The slight variation in the dissipation rate could be attributed to the heterogeneity of the soil.

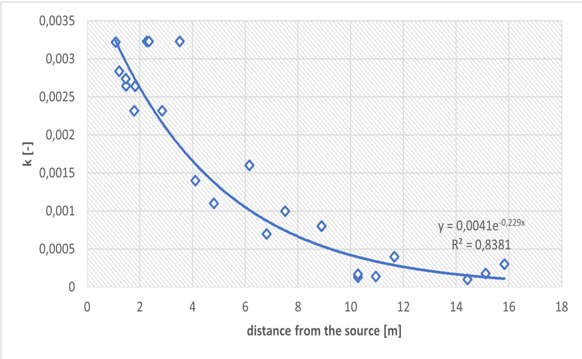

Figure 6.7: Relationship between rate of generation (k) vs Distance from the source (d)

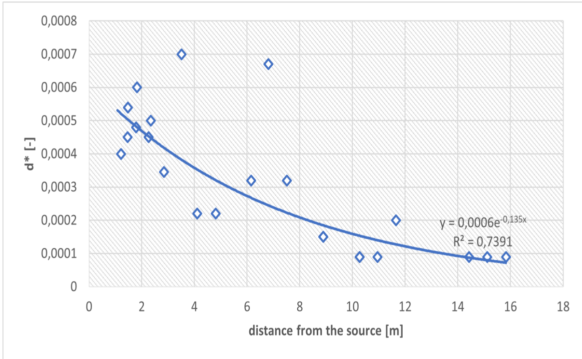

Figure 6.8: Relationship between rate of dissipation (d*) vs Distance from the source (d)

A linear relationship was observed between delay time to the initial excess pore pressure response (l) and the distance from the source (d) (figure:6.9). Further, there was also a linear relationship between delay time to achieve the peak pressure(m) and distance from the source presented in the figure: 6.10. As discussed in the previous subsection: 6.1.1 of time series analysis, the delay to peak pressure indicates the time taken for the groundwater to reach larger distances which will be a function of hydraulic conductivity of the soil.

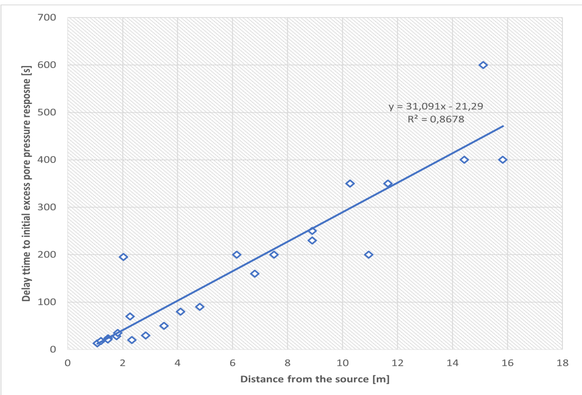

Figure 6.9: Relationship between delay to initial response of excess pore pressure(l) vs distance from the source (d)

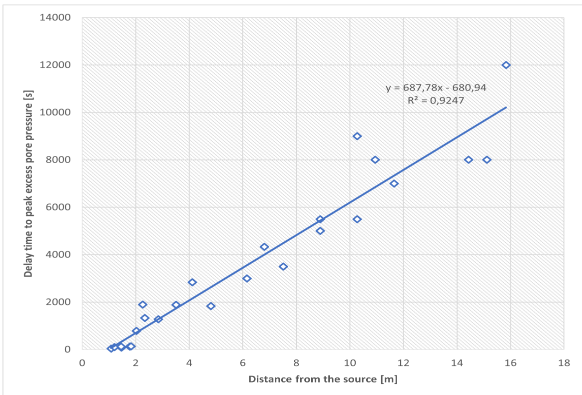

Figure 6.10: Relationship between time to peak excess pore pressure (m) vs Distance from the source (d)

The data analysis of day two and three by semi-empirical modelling resulted in the most important outcome for the proposed work. This was modelled as a graph between peak excess pore pressure vs distance from the source(d) with open boundary condition as illustrated in the figure: 6.11. The excessively high pore pressure closer to the source represents the formation of the liquefied zone. From the table: 6.2, the closest point monitored was at a distance of 1.08m from the toe of the sheet pile (center of the penetrating depth is taken) to the tip of the monitoring sensors (point to point distance) but at a radial distance of only 0.92m, this achieved a peak pressure of 40.416 kPa. However, in another event with a similar radial distance of 0.92m, the toe of sheet pile was at different depth resulting in point to point distance of 1.82m. In this instance, it achieved a peak pressure of mere 8.411kPa. This indicates that the major contribution of excess pore pressure during pile driving occurs at the tip of the pile [6].

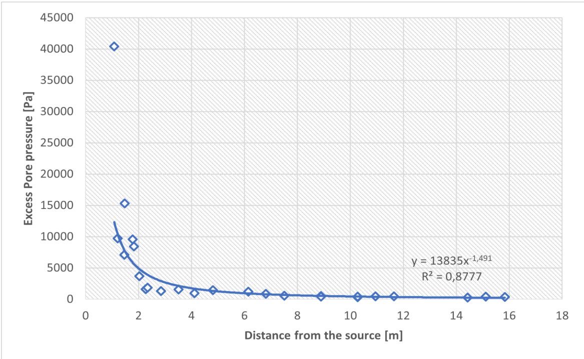

Figure 6.11: Relationship between peak excess pore pressure(P) vs distance from the source(d) [depth of penetration = 1m (all events)]

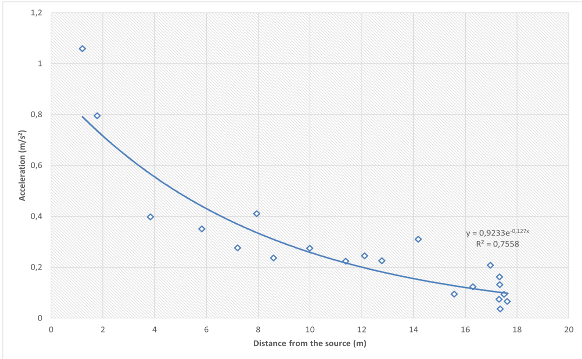

Figure 6.12: Relationship between peak acceleration (Z direction) vs Distance from the source

Varying dissipation rate of liquefied zone:

The dissipation rate of the excess pore pressure in the liquefied zone was noticed to be very large until 28kPa as represented by a solid red box in the figure: 6.13. This phenomenon can be attributed to the increase in hydraulic conductivity of liquefied sand by at least four times [90]. During liquefaction, the entire overburden load is taken by the excess pore pressure and there is no contact between the particles. The dissipation of the pore pressure brings the particles back in contact with each other allowing in the reduction of the hydraulic conductivity to return to the value which may be different from insitu value. An extensive research on the behaviour and properties of the soil post liquefaction is in progress [90], [4], [32]. The post liquefaction dissipation requires a dynamic dissipation rate which was not undertaken in this work. However, to pursue that there is need to establish the state at which the behaviour changes from liquefied to non - liquefied.

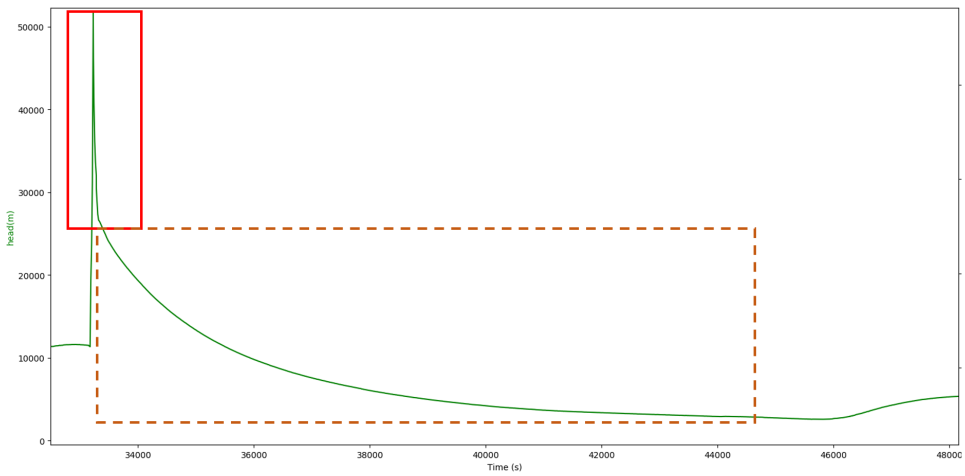

Figure 6.13: Illustration of dual dissipation rate in liquefied sand

Width of the liquefaction zone:

The results in the table: 6.2, signify that the liquefied zone has a width of only 1m that may be a function of several other factors such as soil parameters, the energy of the machine, etc. The liquefied zone is up to 1m and transition zone is noticed between 1 to 2m based on the peak pore pressure mentioned in the table: 6.2.

Point to point distance [m]	Radial distance [m]	Peak pore pressure [Pa]
1.08	0.92	40416
1.47	1.35	15335
1.21	1.20	9730.6
1.78	1.77	9580
1.82	0.92	8411
1.46	1.20	7074

Table 6.2: Comparisons of the peak pore pressure

However, to understand the width of this zone and the influence of other factors on it, further investigations are required.

Liquefaction pressure:

The peak pressure of the liquefaction observed in this data was 40.416kPa after isolating using the data model and 51.744kPa as a cumulative excess pore pressure. However, these values were noticed to be smaller than the computed effective stress of 80kPa. This could be attributed to the following reasons:

- The horizontal distribution of the load due to inter-granular forces between the sand particles allowing arching and load spreading of Holocene sand layer.
- The impact of storativity shall not be disregarded.
- The observation of 40.416kPa was at 0.92m radially away from the source. There can be a possible dampening of the excess pore pressure reaching 0.92m. It could be also argued that a higher pore pressure can be detected on monitoring closer to the source. However, it should not be disregarded that further close to the sheet piles undergoes a very high straining and could have an anomaly in monitoring the pore pressure by application of sensors. Further, the behaviour of the soil response resembling the liquefied medium at 0.92m could be attributed to the fact that sand tends to behave as a liquefied medium at an excess pore pressure of 60% of the effective stress [75].

Relationship between physical parameters

In the semi-empirical model physical parameters such as depth of penetration(1m), hydraulic conductivity is assumed to be constant. The factor **duration of driving** against peak pore pressure remained inconclusive.

Error:

The rebuilding of the data by semi empirical approach based on the available and gained knowledge undergo several iterations. After certain iteration the error converges. In here, the error in the four data set is represented below:

Day	Set	Error[%]
2	1	8
2	3	9
3	1	8
3	2	7

Table 6.3: Error in the semi empirical model

6.1.3. Relationship of pore pressure with acceleration

Based on the work by Barkan et al.(1962) [9], Seed and Idriss (1971)[77], Nijs et al(2003)[66] it was concluded that the liquefaction is possible with the acceleration magnitude of 0.1 - 0.3g [66]. In the case of Damrak, the accelerometer definitely aided to describe the start and end of the event due to the frequency response. As the instrumentation was inside the tunnel the impedance of the tunnel was extremely large and expected to act as a rigid structure. The tunnel dampens the acceleration amplitude to a greater extent. Unfortunately, the exact location of the accelerometer was not exactly traced from the project document. This restricted the quantitative assessment of the generation of the pore pressure with a dynamic model. Further, based on approximate information the peak acceleration data was analysed and was found to have an exponential relationship with distance as described in the section: 2.5. The relationship for data of day 2 is presented in the figure: 6.12. On comparison of figure: 6.11 & 6.12 and the excess pore pressure & acceleration data, it was noted that only in two occurrences the peak acceleration was close to $1 m/s^2$ (approximating to 0.1g). In both these occurrences, exceptionally high peak pore pressure was noticed representing the presence of a liquefaction zone in close vicinity. This allows us to affirm several assumptions made throughout the work:

- There must be a minimum threshold acceleration in order to achieve liquefaction.
- Even in the data points mentioned above, there was a delay in the initial response and time taken to achieve the peak pore pressure. This proves that the source is at a certain distance from the monitoring point. Additionally, it also proves that the pore pressure monitored is not a direct consequence of cyclic loading of the sand rather due to alternative phenomenon such as groundwater flow. Thus following the theory of zonation or the multiscale computation framework.
- From the figure: 6.12, the peak acceleration was noticed to attenuate exponentially with distance confirming Bornitz or Barkan's equation.

6.2. Plaxis model

The sensitivity of the hydraulic conductivity provides us with a comparison of the trends of the generation and dissipation. From the plot in the figure:6.14, it can be understood that the higher hydraulic conductivity leads to higher peak pressure at a distance from the source. However, the pressure is short-lived or dissipates faster due to higher hydraulic conductivity. Further, in the case of higher hydraulic conductivity, the effect of the source is felt at larger distances represented in the comparison in the figure: 6.18.

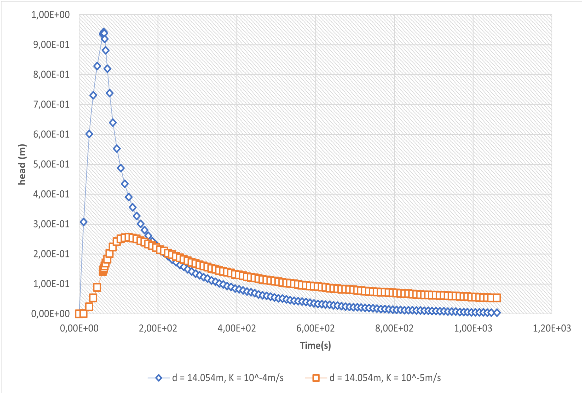

Figure 6.14: Illustration of peak pressure due to increasing Hydraulic conductivity

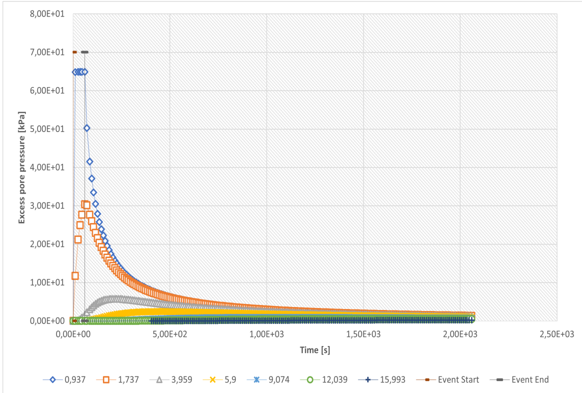

Figure 6.15: Evolution trend of excess pore pressure with $K_{sand_x} = 5 * 10^{-7}$ m/s for varying distances in [m]

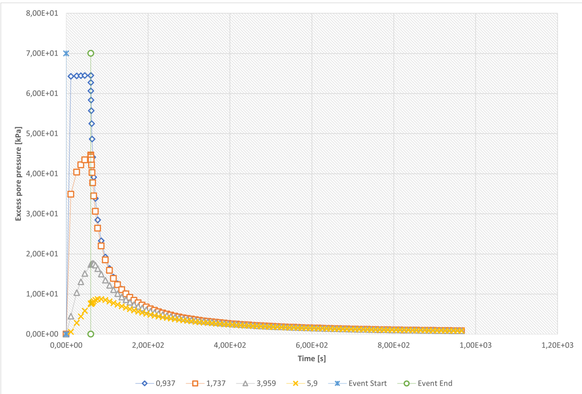

Figure 6.16: Evolution trend of excess pore pressure with $K_{sand_x} = 5 * 10^{-6}$ m/s for varying distances in [m]

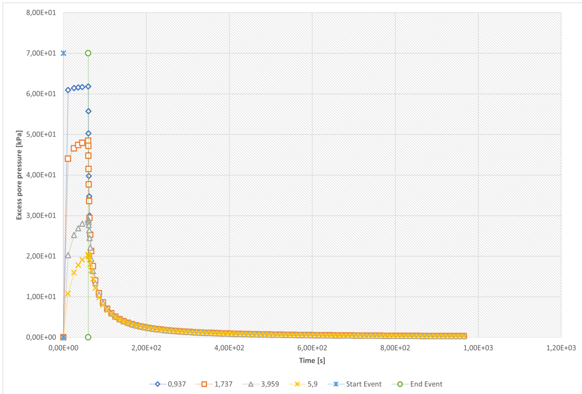

Figure 6.17: Evolution trend of excess pore pressure with $K_{sand_x} = 5 * 10^{-5}$ m/s for varying distances in [m]

Leaky aquifer with tunnel:

Significant inferences were made from the model with leaky aquifer with the tunnel. The field data represented an extremely large delay time to reach peak pressure. The delay time represents the soil with lesser permeability. This behaviour could only be simulated in the proposed model by providing lower permeability to the soil layer. In the figure: 6.17 it was realised that the peak pressure is achieved at the end of the event but that is not the case in the field observations. In figure: 6.16 a slight delay was observed at 5.9m from the source. An appreciable delay was noticed when the hydraulic conductivity of $5*10^{-7}$ m/s was set. The K value = $5*10^{-7}$ m/s was in the range of silty sand. But it was interesting to compare this response with the field data, In the field, it takes around 2000s to achieve the peak pressure at a distance of 3.95m whereas the model achieved the peak in 180s. Thus, it is important to note that there is a different property controlling this phenomenon apart from the hydraulic conductivity. The CPT data presented in the Appendix: B, clearly indicated towards lower permeability due to the presence of an alternating layer of allerod and sand.

From the analysis of the field data, it was demonstrated that the excess pore pressure is a very localized phenomenon and excess pore pressure at a distance greater than 5m falls around 1kPa. The similar phenomenon was simulated in the model with lesser permeable sand. However, care must be taken in presence

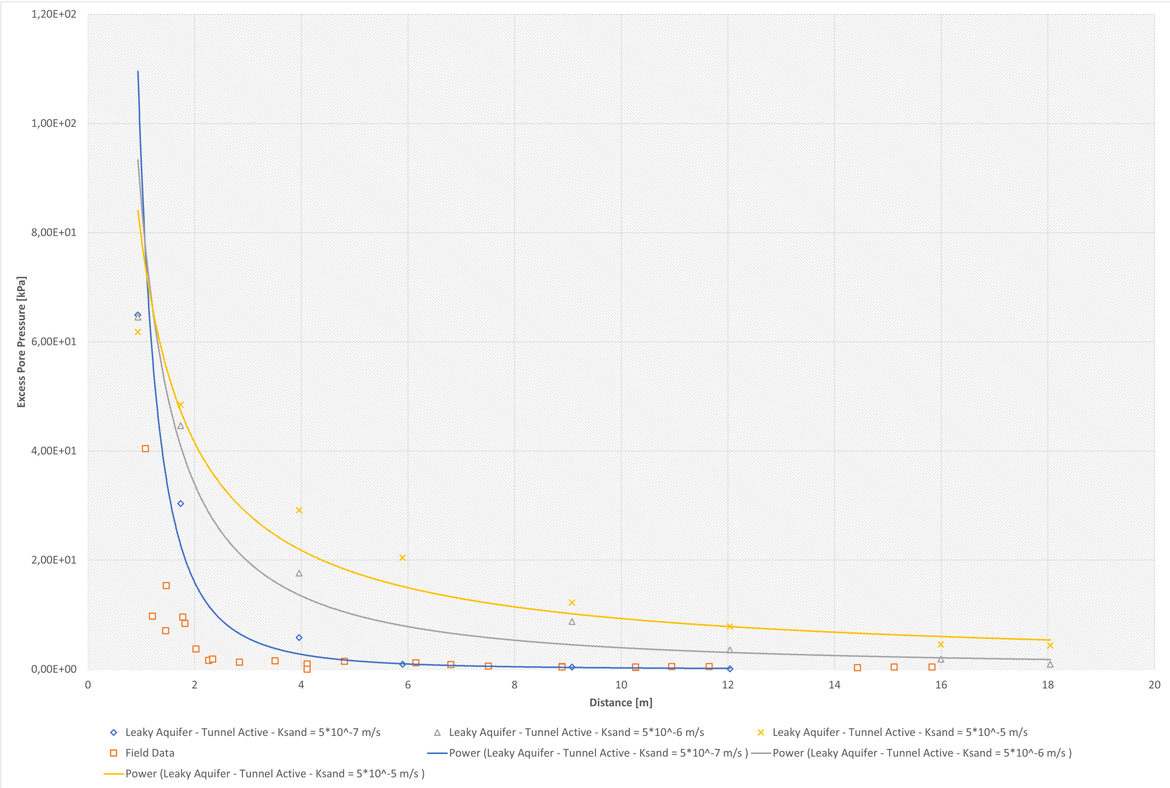

Figure 6.18: Relationship between modelled & field peak pore pressure vs distance from the source

of clean sand as it gets capable allowing excess pore pressure with higher magnitude reaching larger distances. However in that case it gets dissipated faster.

Monitoring in different layer:

The actual position of the tip of the piezometer with respect to the expected position always remains uncertain due to the possibility of bending of the driving pipes. The position of the different piezometer tip is mentioend in the table:4.1. The comparison of response in the different layer will help to understand the possibility of locating the piezometer tip in a different layer. This was carried out in the Plaxis model, the stress points with similar radial distances but with varying depth (for choosing differnt soil layer) were chosen for comparison as represented in the fig: 6.20. The peak pore pressure response is controlled by hydraulic conductivity, the layer with higher conductivity achieves higher peak as represented in the figure: 6.19.

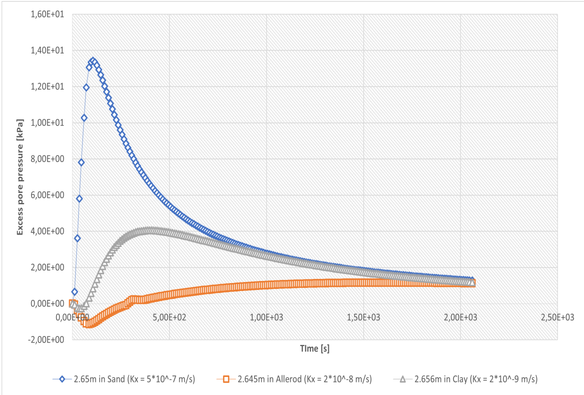

Figure 6.19: Comparison of excess pore pressure in different layers of the soil profile

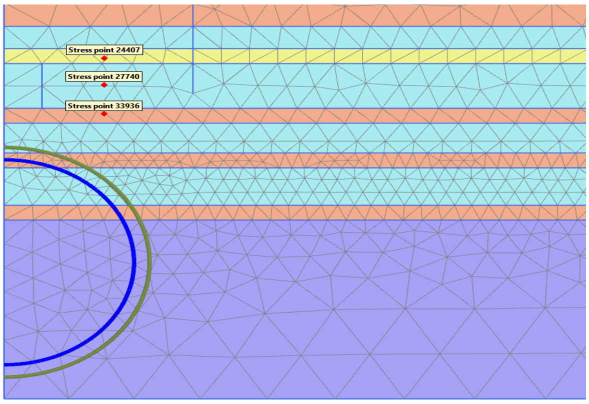

Figure 6.20: Stress points from different layers of the soil domain Stress point 24407 - In allerod, Stress point 27740 - In sand, Stress point 33936 - In clay

Leaky aquifer with sheet pile boundary

The introduction of the sheet pile in the Plaxis model simulating the waterfront side sheet pile at a distance of 5 -6 m in the field obstructs the dissipation boundary. The behaviour was understood using the Plaxis model. The pore pressure evolution was calculated at 1.681m from the source, it was noticed that the initial dissipation matched the result with no sheet pile however in the later part the rate of dissipation was slower in the case with sheet pile. This can be attributed to the boundary effect of the sheet pile.

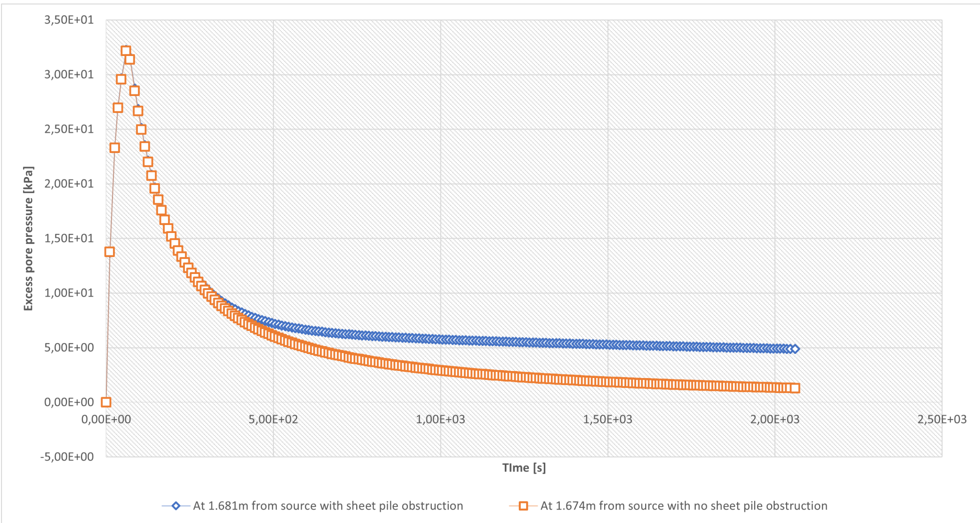

Figure 6.21: Illustration of the pore pressure evolution in presence and absence of sheet pile

7

Conclusion & Recommendations

The thesis presents the understanding of the generation and dissipation of the excess pore pressure in closer vicinity due to vibratory installation of the sheet pile in sand. The implementation of the model to rebuild the data using time series analysis and the semi-empirical approach and modelling the scenario using simple Plaxflow model allowed to answer the research questions framed during the formulation of the project. To answer the main question sub-question were formed.

7.1. Conclusion

The developed simple tool helps to integrate the dissipation mechanism of the excess pore pressure with a liquefied and non-liquefied zone. A conservative estimate of excess pore pressure equivalent to the effective stress shall be taken for modelling. The nible estimation of field hydraulic conductivity shall play a major role as it is the key parameter of the model. The liquefaction width of 1m shall be a conservative assumption. The hydraulic conductivity of the liquefied zone shall be at least 100 times of the non-liquefied zone. The integration of these could allow for practical estimation of the porewater overpressure due to vibratory loading of sheet pile.

7.1.1. Sub-question: 1

What are the parameters that influence the dissipation of the excess pore pressure?

The dissipation of excess pore pressure was the function of the hydraulic conductivity and was also anticipated to have a pressure dependency. Further, the hydraulic conductivity of the soil is dictated by the stratigraphy. The obstruction in the dissipation boundary has a significant impact on the rate of dissipation. It was proved by the presence of the sheet pile in the dissipation boundary. Lastly, only in the liquefied zone due to high pore pressure, there is an increase in the void ratio and henceforth the increase in hydraulic conductivity, allowing a faster rate of dissipation.

7.1.2. Sub-question: 2

How does the generation and dissipation of excess pore pressure vary in the liquefied zone from non-liquefied?

The magnitude of pore pressure in the liquefied zone is dependent on the amplitude of the vibratory loading, overburden pressure or vertical effective stress, length of the penetration of sheet pile, properties of the soil. Surrounding the penetration zone of the sheet pile, the presence of lenses of low permeability soil promotes the accumulation of the excess pore pressure and lesser time to achieve liquefaction. Hence, transmissivity or the hydraulic conductivity also serves as a factor to the generation of the excess pore pressure. Due to liquefaction, the hydraulic conductivity increases allowing a faster rate of dissipation in the liquefied zone until the soil particles come back in contact. Hence, the rate of dissipation in the liquefied zone shall vary depending on the state of excess pore pressure with respect to the effective stress.

As the non-liquefied zone is fed by the groundwater flow, the rate of generation of excess pore pressure in this zone shall be dictated by the hydraulic conductivity of the path of the groundwater flow. This can be impacted by the stratigraphy of the soil. The rate of dissipation in the non-liquefied zone shall be dictated by the hydraulic conductivity and condition of the dissipation boundaries.

7.1.3. Sub-question: 3

How can the vibration attenuation affect the generation of excess pore pressure in the sand?

The amplitude of the vibration attenuates exponentially. There must be a threshold acceleration for the soil to undergo liquefaction. Based on the analysis it could be established that the minimum threshold of acceleration is between 0.1 - 0.3 g below which liquefaction doesn't occur. It is conservative to assume that the energy from the driving of the sheet pile could liquefy to a maximum of 1m radius of the soil.

7.1.4. Sub-question: 4

What are the limitations and controlling parameters of this model/tool?

Controlling parameters:

The main controlling parameters of the PLAXFLOW model includes hydraulic conductivity, the constant head applied in the liquefaction zone, the duration of the loading (application of constant head), length of penetration of sheet pile and the width of the liquefaction zone.

Limitations:

- The model is highly dependent on the hydraulic permeability of the soil. However, the precise estimation of the field hydraulic conductivity has always remained as a challenge for the engineers.
- The analysis showed that the peak excess pore pressure was estimated to be 40kPa which is almost 0.5 -0.6 times of the expected maximum liquefaction pressure. This could be due to various factors:
  - Storativity of the aquifer
  - Dampening of the actual source liquefaction pressure. The closest monitoring was only at a radial distance of 0.92m from the source.
  - Presence of lower vertical effective stress due to the horizontal distribution of inter-granular forces.
- The excess pore pressure estimation due to the volume addition of the sheet pile has not been computed.
- The contribution of the excess pore pressure due to cyclic mobility and also the consolidation of the sand in the non-liquefied zone has not been considered.

7.1.5. Other significant conclusion:

- The excess pore pressure generation due to the vibratory installation of the sheet pile is a localized effect. The non-liquefied zones are fed by the overpressure of the liquefied zone influenced by the hydraulic conductivity of the soil.
- The presence of the lesser permeable soil in the vicinity of the penetration zone shall allow a much longer time period for the excess pore pressure to achieve the peak.

7.2. Recommendation for future work:

What are the recommendations for future additional work on this model/tool?

- The semi-empirical model should be validated rigorously with a 3D Plaxis model with varying hydraulic conductivity to use it for prediction of excess pore pressure in the field.
- The current model takes an input of the liquefaction pressure. The integration of a dynamic generation model within the existing model could bring completeness to the developed tool.
- The excess pore pressure induced due to the cyclic mobility and the consolidation in the non-liquefied zone has been ignored in this study. Investigation on the ability of the soil to contribute for excess pore pressure other than liquefaction will help to enhance the model.
- The post liquefaction dissipation requires a dynamic dissipation rate. During liquefaction, the pore pressure keeps the sand particle away from each other increasing the void ratio. But after the event stops due to dissipation of the excess pore pressure, the sand particles try to return to normal state reducing the dissipation rate.

- The loss of vibration amplitude during the transfer of energy from the hammer to the pile and then to the soil can be integrated from the available knowledge. This could allow direct computation of the acceleration amplitude in the field from machine parameters to estimate the magnitude of the excess pore pressure.
- In this work, the width of the liquefied zone was established. The investigation of parameters that influences the width of the zone could help engineers to define the critical zone while piling very close to the adjacent structures.
- The excess pore pressure accumulated due to the vibratory installation is short-lived. The assessment of the impact of these excess pore pressure on underground structure such as deep and shallow foundation, tunnels and buried pipes could allow engineers to understand the risk of vibratory driving in a congested urban environment with extensive underground utility networks.

A

Appendix-A

Source location	Source type	Induced wave	n
Surface	Point	Body wave	2.0
		Surface wave	0.5
	Infinite line	Body wave	1
		Surface wave	0
In-depth	Point	Body wave	1.0
	Infinite line		0.5

Figure A.1: Geometric attenuation coefficients for various sources of vibration [from Kim and Lee] [6]

Class	Material damping coefficient a (1/m)		Description of material
	5 Hz	50 Hz	
I	0.01–0.03	0.1–0.3	Weak or soft soils ($N_{SPT} < 5$)
II	0.003–0.01	0.03–0.1	Competent soils ($5 < N_{SPT} < 15$)
III	0.0003–0.003	0.003–0.03	Hard soils ($15 < N_{SPT} < 50$)
IV	< 0.0003	< 0.003	Hard, competent rock ($N_{SPT} > 50$)

Figure A.2: Proposed classification of earth materials by material attenuation coefficient [Woods] [6]

Soil group		a_0 ($\times 10^{-3}$ s/m)
Rocks (covering layer within 1.5–2.0 m)	Shale, limestone	0.385–0.485
	Sandstone	0.580–0.775
Hard plastic clays		0.385–0.525
Broke stones of medium density cobbles		0.850–1.100
Plastic clays, coarse sands and gravels of medium density		0.965–1.200
Soft plastic clays, silts, slightly dense, medium or coarse sands		1.255–1.450
Silty clays, silts and saturated fine sands		1.200–1.300
Recently deposited clays and unsaturated loose sands		1.800–2.050

Figure A.3: Values of energy attenuation coefficient, a0, for various soil and rock types[Yang] [6]

B

Appendix-B

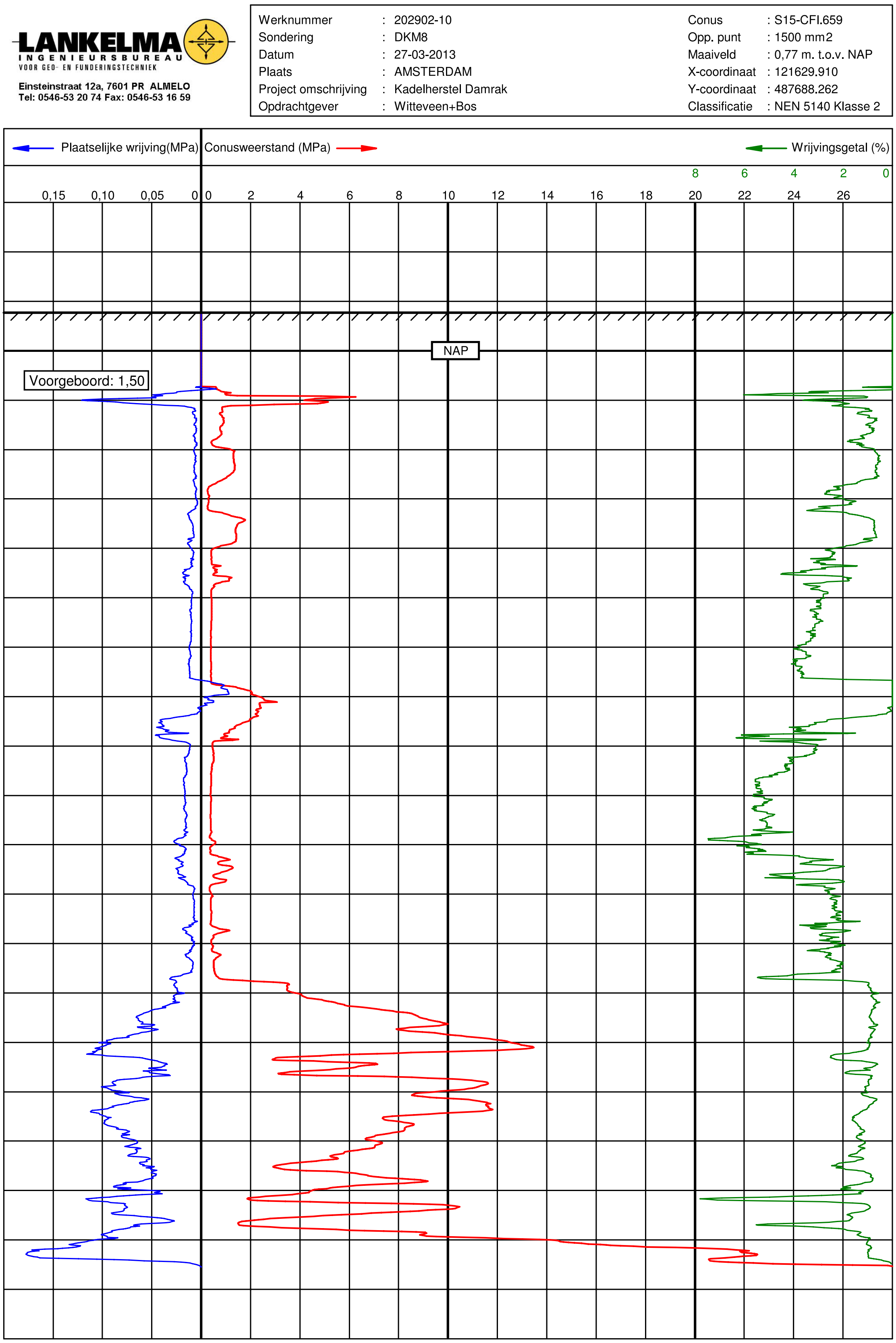
LANKELMA
INGENIEURSBUREAU
VOOR GEO- EN FUNDERINGSTECHNIEK
Einsteinstraat 12a, 7601 PR ALMELO
Tel: 0546-53 20 74 Fax: 0546-53 16 59
Werknummer : 202902-10
Sondering : DKM8
Datum : 27-03-2013
Plaats : AMSTERDAM
Project omschrijving : Kadelherstel Damrak
Opdrachtgever : Witteveen+Bos
Conus : S15-CFI.659
Opp. punt : 1500 mm2
Maaiveld : 0,77 m. t.o.v. NAP
X-coordinaat : 121629.910
Y-coordinaat : 487688.262
Classificatie : NEN 5140 Klasse 2
Plaatselijke wrijving(MPa)
Conusweerstand (MPa)
Wrijvingsgetal (%)
8 6 4 2 0
0,15 0,10 0,05 0
0 2 4 6 8 10 12 14 16 18 20 22 24 26
NAP
Voorgeboord: 1,50

LANKELMA
INGENIEURSBUREAU
VOOR GEO- EN FUNDERINGSTECHNIEK

Einsteinstraat 12a, 7601 PR ALMELO
Tel: 0546-53 20 74 Fax: 0546-53 16 59

Werknummer	: 202902-10	Conus	: S15-CFI.659
Sondering	: DKM9	Opp. punt	: 1500 mm2
Datum	: 26-03-2013	Maaiveld	: 0,79 m. t.o.v. NAP
Plaats	: AMSTERDAM	X-coordinaat	: 121620.037
Project omschrijving	: Kadelherstel Damrak	Y-coordinaat	: 487672.941
Opdrachtgever	: Witteveen+Bos	Classificatie	: NEN 5140 Klasse 2

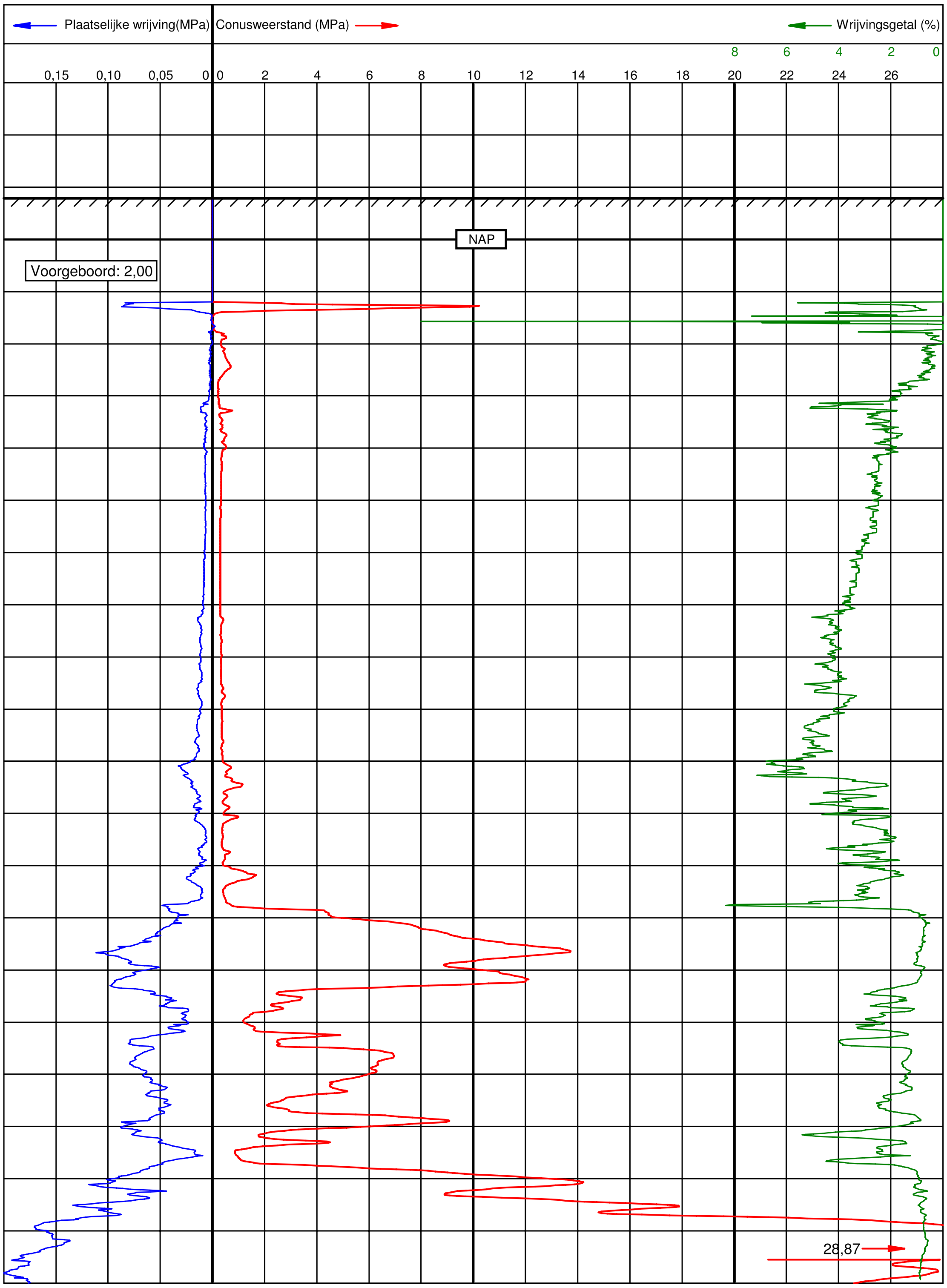

C

Appendix-C

Parameter	Name	Unit	Property
Material Type	Type	Elastic;Isotropic	-
Normal Stiffness	EA	$1.4.10^7$	kN/m
Flexural rigidity	EI	$1.43.10^5$	kNm^2/m
Weight	w	8.4	kN/m/m
Poisson's ratio	ν	0.15	-

Table C.1: Properties of the tunnel lining for Plaxis model

Bibliography

[1] Az 26. URL `https://projects.arcelormittal.com/foundationsolutions/products/product_range/steel_sheet_piles/z_sections/AZ_26/language/EN`.

[2] Related products. URL `https://www.ice-holland.com/producten/135/36616/ICE-36RFts/Trilblokken/`.

[3] Geomonitoring. URL `https://profound.nl/geotechnische-monitoring/?lang=nl`.

[4] Adamidis and GSP Madabhushi. Post-liquefaction reconsolidation of sand. *Proceedings of the Royal Society A: Mathematical, Physical and Engineering Sciences*, 472(2186):20150745, 2016.

[5] Abdon Atangana. Chapter 2 - principle of groundwater flow. In Abdon Atangana, editor, *Fractional Operators with Constant and Variable Order with Application to Geo-Hydrology*, pages 15 – 47. Academic Press, 2018. ISBN 978-0-12-809670-3. doi: https://doi.org/10.1016/B978-0-12-809670-3.00002-3. URL `http://www.sciencedirect.com/science/article/pii/B9780128096703000023`.

[6] George Athanasopoulos and Panagiotis Pelekis. Ground vibrations from sheetpile driving in urban environment: Measurements, analysis and effects on buildings and occupants. *Soil Dynamics and Earthquake Engineering*, 19:371–387, 07 2000. doi: 10.1016/S0267-7261(00)00008-7.

[7] MAL Baki, MM Rahman, and SR Lo. Predicting onset of cyclic instability of loose sand with fines using instability curves. *Soil Dynamics and Earthquake Engineering*, 61:140–151, 2014.

[8] Mark Bakker, Kees Maas, and Jos R Von Asmuth. Calibration of transient groundwater models using time series analysis and moment matching. *Water Resources Research*, 44(4), 2008.

[9] Dominik D Barkan. *Dynamics of bases and foundations*. McGraw-Hill Companies, 1962.

[10] J Bedin, F Schnaid, AV Da Fonseca, and L De M Costa Filho. Gold tailings liquefaction under critical state soil mechanics. *Géotechnique*, 62(3):263–267, 2012.

[11] Johan W Bosch and Wout Broere. Small incidents, big consequences. leakage of a building pit causes major settlement of adjacent historical houses. amsterdam north-south metro line project. In *Safe Tunnelling for the City and Environment: ITA-AITES World Tunnel Congress, 23-28 May 2009, Budapest, Hungary*. Citeseer, 2009.

[12] George D Bouckovalas, Konstantinos I Andrianopoulos, and Achilleas G Papadimitriou. A critical state interpretation for the cyclic liquefaction resistance of silty sands. *Soil Dynamics and Earthquake Engineering*, 23(2):115–125, 2003.

[13] Wout Broere. Urban underground space: Solving the problems of today's cities. *Tunnelling and Underground Space Technology*, 55:245–248, 2016.

[14] Jack Bruin, Herbert Edson Hudson, et al. Selected methods for pumping test analysis. Technical report, Illinois State Water Survey, 1955.

[15] Budhu.M. On Comparing Simple Shear and Triaxial Test. *Journal of Geo- technical Engineering*, 110 (12):1809–1814, 1984.

[16] Peter M Byrne. A cyclic shear-volume coupling and pore pressure model for sand. 1991.

[17] Alessandro Carrera, MR Coop, and Renato Lancellotta. Influence of grading on the mechanical behaviour of stava tailings. *Géotechnique*, 61(11):935–946, 2011.

[18] K Onder Cetin and H Tolga Bilge. Cyclic large strain and induced pore pressure models for saturated clean sands. *Journal of geotechnical and geoenvironmental engineering*, 138(3):309–323, 2012.

[19] Theis. Charles V. The relation between the lowering of the piezometeric surface and the rate and duration of discharge of a well using ground-water storage. 1935.

[20] SC Chian. Empirical excess pore pressure dissipation model for liquefiable sands. In *Proc., 6th Int. Conf. on Earthquake Geotechnical Engineering, New Zealand Geotechnical Society, Wellington, New Zealand*, 2015.

[21] H.H. Cooper and C.E. Jacob. A generalized graphical method for evaluating formation constants and summarizing well field history. *Am. Geophys. Union Trans.*, 27:526–534, 1946.

[22] JJ De Vries. Groundwater. *Geology of the Netherlands*, pages 295–315, 2007.

[23] F Deckner, K Viking, and S Hintze. Vibration Transfer During Sheet Pile Driving – A Full-Scale Field Test. Number November, Christchurch, 2015b.

[24] Fanny Deckner. *Licentiate Thesis*. Phd, KTH, Royal Institute of Technology, Stockholm, 2013. URL `https://www.bth.se/com/aje.nsf/bilagor/Lic{Å}seJevinger{_}1{_}pdf/{\protect\T1\textdollar}file/Lic{Å}seJevinger{_}1.pdf`.

[25] Fanny Deckner, Kenneth Viking, and Staffan Hintze. Wave Patterns in the Ground : Case Studies Related to Vibratory Sheet Pile Driving. *Geotechnical and Geological Engineering*, 35(6):2863–2878, 2017. ISSN 1573-1529. doi: 10.1007/s10706-017-0285-x.

[26] Nicolas Denies. *Dynamic behavior of vibrated dry sand: sphere penetration experiments and discrete element modeling of vibrofluidization*. PhD thesis, UCL-Université Catholique de Louvain, 2010.

[27] H. Deresiewicz. Mechanics of granular matter**this study was supported by the office of naval research under contract nonr-266(09) with columbia university. volume 5 of *Advances in Applied Mechanics*, pages 233 – 306. Elsevier, 1958. doi: https://doi.org/10.1016/S0065-2156(08)70021-8. URL `http://www.sciencedirect.com/science/article/pii/S0065215608700218`.

[28] Xiaoli Ding, Dayong Ren, Bruce Montgomery, and Chris Swindells. Automatic monitoring of slope deformations using geotechnical instruments. *Journal of surveying engineering*, 126(2):57–68, 2000.

[29] Carl D.McElwee. Theis parameter evaluation from pumping tests by sensitivity analysis. *Ground Water*, 18:56–60, Jan - Feb,1980.

[30] R Dobry. Liquefaction of soils during earthquakes, national research council (nrc), committee on earthquake engineering. Technical report, Report No. CETS-EE-001. Washington, DC, USA: National Academy Press, 1985.

[31] R Dobry, WG Pierce, R Dyvik, GE Thomas, and RS Ladd. Pore pressure model for cyclic straining of sand. *Rensselaer Polytechnic Institute, Troy, New York*, 1985.

[32] Saizhao Du, Siau Chen Chian, and Changbing Qin. Post-liquefaction pore pressure dissipation in sand under cyclic stress triaxial testing. *Géotechnique*, 70(2):95–107, 2020.

[33] John Dunnicliff. *Geotechnical instrumentation for monitoring field performance*. John Wiley & Sons, 1993.

[34] JG Ferris and DB Knowles. *The slug test for estimating transmissibility*. Number 20. US Department of the Interior, Geological Survey, Water Resources Division ..., 1954.

[35] WD Liam Finn, Peter Michael Byrne, and Graham R Martin. Seismic response and liquefaction of sands. *Journal of Geotechnical and Geoenvironmental Engineering*, 102(ASCE# 12323), 1976.

[36] Charles R Fitts. *Groundwater science*. Elsevier, 2002.

[37] W de Gans. *De bodem onder Amsterdam: een geologische stadswandeling*. TNO, 2011.

[38] Jean Paul Godard. Urban Underground Space And Benefits of Going Underground. *World Tunnel Congress 2004 and 30th ITA General Assembly - Singapore*, 2003(May 2004):22–27, 2007.

[39] RA Green, JK Mitchell, and CP Polito. An energy-based excess pore pressure generation model for cohesionless soils. In *Proc.: Developments in Theoretical Geomechanics–The John Booker Memorial Symposium*, pages 16–17. Sydney, New South Wales, Australia, Nov, 2000.

[40] Russell A Green. *Energy-Based Evaluation and Remediation of Liquefiable Soils*. PhD thesis, Virginia Tech, 2001.

[41] Russell A. Green and James K. Mitchell. *Energy-based evaluation and remediation of liquefiable soils*. PhD thesis, Virginia Polytechnic Institute and State University, 2004.

[42] Mahdi Salih Hantush and C Ei Jacob. Non-steady radial flow in an infinite leaky aquifer. *Eos, Transactions American Geophysical Union*, 36(1):95–100, 1955.

[43] YMA Hashash. Deepsoil. 1-d non linear and equivalent linear wave propagation analysis program for geotechnical seismic site response analysis for soil deposits user's manual. *University of Illinois*, 2009.

[44] Kenan Hazirbaba. *Pore pressure generation characteristics of sands and silty sands: a strain approach*. PhD thesis, 2005.

[45] JM Head and FM Jardine. *Ground-borne vibrations arising from piling*. Number 142. 1992.

[46] Staffan; S. Liedberg; R. Massarsch; M. Hanson; H. Elvhammar; B. Lundahl Hintze and S-E. Rehnman. Omgivningspåverkan vid pål- och spontslagning. Technical report, 1997.

[47] Arnberg P W Holmberg, R, D Bennerhult, L Forssblad, L Gereben, L Hellman, K Olsson, K Rundqvist, C Sjoeberg, Sjoekvist, and G Wallmark. VIBRATIONS GENERATED BY TRAFFIC AND BUILDING CONSTRUCTION ACTIVITIES. *VTT Technical Research Centre of Finland*, page 36, 1984.

[48] P Holscher. Msc course: Cie5340 soil dynamics – part a soil dynamics in urban areas. 2016.

[49] An-Bin Huang and Sin-Yu Chuang. Correlating cyclic strength with fines contents through state parameters. *Soils and foundations*, 51(6):991–1001, 2011.

[50] L B Ibsen. The stable state in cyclic triaxial testing on sand. 13:63–72, 1994.

[51] Kenji Ishihara. Soil behaviour in earthquake geotechnics. 1996.

[52] Mike Jefferies and Ken Been. *Soil liquefaction: a critical state approach*. CRC press, 2015.

[53] Dong Soo Kim and Jin Sun Lee. Propagation and attenuation characteristics of various ground vibrations. *Soil Dynamics and Earthquake Engineering*, 19(2):115–126, 2000. ISSN 02677261. doi: 10.1016/S0267-7261(00)00002-6.

[54] Gideon P Kruseman, Nicolaas Arie De Ridder, and Johanna Maria Verweij. *Analysis and evaluation of pumping test data*, volume 11. International institute for land reclamation and improvement The Netherlands, 1970.

[55] WD Liam Finn, Kwok W Lee, and GR Martin. An effective stress model for liquefaction. *Electronics Letter*, 103(ASCE 13008 Proceeding), 1977.

[56] Steven L.Kramer. *Geotechnical Earthquake Engineering*. 1996. ISBN 8131707180.

[57] H. Bolton Seed M. S. Rahman, John R. Booker. Pore pressure development under offshore gravity structures. *Journal of the Geotechnical Engineering Division*, 103:1419 – 1436, 1977.

[58] Geoffrey R Martin, WD Liam Finn, and H Bolton Seed. Fundementals of liquefaction under cyclic loading. *Journal of Geotechnical and Geoenvironmental Engineering*, 101(ASCE# 11231 Proceeding), 1975.

[59] K Rainer Massarsch and Bengt H Fellenius. Ground vibrations induced by impact pile driving. 2008.

[60] B.H; Massarsch, K Rainer; Fellenius. Ground vibrations induced by impact pile driving . Ground Vibrations Induced by Impact Pile Driving. In *The Sixth International Conference on Case Histories in Geotechnical Engineering*, number August, page 38, 2010.

[61] N Matasovic. D-mod_2–a computer program for seismic response analysis of horizontally layered soil deposits, earthfill dams, and solid waste landfills. *User's Manual*, 2006.

[62] N Matasovic and M Vucetic. Seismic response of horizontally layered soil deposits. *Report No. ENG 93*, 182, 1993.

[63] Paul W Mayne, MR Coop, Sarah Springman, An-Bin Huang, and J Zornberg. Soa-1: Geomaterial behavior and testing. In *Proceedings of the 17th International Conference on Soil Mechanics and Geotechnical Engineering: 5–9 October 2009, Alexandria, Egypt*, pages 2777–2872. Millpress, Rotterdam, the Netherlands, 2009.

[64] Piet Meijers. *Settlement during vibratory sheet piling*. PhD thesis, Technische Universiteit Delft, 2007.

[65] A. M. J. Mens, M. Korff, and A. F. van Tol. Validating and improving models for vibratory installation of steel sheet piles with field observations. *SpringerLink*, Jul 2012. URL `https://link.springer.com/article/10.1007/s10706-012-9506-5`.

[66] R.E.P. de Nijs. Het trillen van damwanden in granulaire bodem. *Geotechniek*, (56-64), 2003.

[67] Theo N Olsthoorn. Do a bit more with convolution. *Groundwater*, 46(1):13–22, 2008.

[68] Carmine P Polito, Russell A Green, and Jongwon Lee. Pore pressure generation models for sands and silty soils subjected to cyclic loading. *Journal of Geotechnical and Geoenvironmental Engineering*, 134 (10):1490–1500, 2008.

[69] Md Mizanur Rahman and TG Sitharam. Cyclic liquefaction screening of sand with non-plastic fines: Critical state approach. *Geoscience Frontiers*, 11(2):429–438, 2020.

[70] Jaber.W.Y; Rahman.M.S. A simplified drained analysis for wave-induced liquefaction in ocean floor sands. *Soils and Foundations*, 26(3):57–68, 1986. doi: https://doi.org/10.3208/sandf1972.26.3_57.

[71] F. E. Richart, John R. Hall, and Richard D. Woods. *Vibrations of soils and foundations / F.E. Richart, Jr., R.D. Woods, J.R. Hall, Jr.* Prentice-Hall, 1970.

[72] AA Rodger and GS Littlejohn. A study of vibratory driving in granular soils. *Geotechnique*, 30(3):269–293, 1980.

[73] S. Sassa and H. Sekiguchi. Wave-induced liquefaction of beds of sand in a centrifuge. *Geotechnique*, 49 (5):621–638, 1999. ISSN 00168505. doi: 10.1680/geot.1999.49.5.621.

[74] J. Schokker, M.A.J. Bakker, C.W. Dubelaar, R.M. Dambrink, and R. Harting. 3d subsurface modelling reveals the shallow geology of amsterdam. *Netherlands Journal of Geosciences - Geologie en Mijnbouw*, 94(4):399–417, 2015. doi: 10.1017/njg.2015.22.

[75] H Bolton Seed. Design problems in soil liquefaction. *Journal of Geotechnical Engineering*, 113(8):827–845, 1987.

[76] H Bolton Seed and Izzat M Idriss. Analysis of soil liquefaction: Niigata earthquake. *Journal of the Soil Mechanics and Foundations Division*, 93(3):83–108, 1967.

[77] Harry Bolton Seed and Izzat M Idriss. Simplified procedure for evaluating soil liquefaction potential. *Journal of Soil Mechanics & Foundations Div*, 1971.

[78] Harry Bolton Seed, Robert Pyke, and Geoffrey R Martin. *Effect of multi-directional shaking on liquefaction of sands*. Earthquake Engineering Research Center, University of California, 1975.

[79] Bolton Seed.H. Soil Liquefaction and Cyclic Mobility Evaluation for Level Ground during Earthquakes. 105:201–255, 1979.

[80] Marshall L Silver and H Bolton Seed. Volume changes in sands during cyclic loading. *Journal of Soil Mechanics & Foundations Div*, 1971.

[81] FP Smits, K H Andersen, and G Gudehus. Pore pressure generation. In *Proceedings Int. Symposium on Soil Mechanics Research and Foundation Design for the Oosterschelde Storm surge Barrier, Foundation aspects of Coastal Structures*. The Netherlands, October 9-12, 1978, 1978.

[82] B. M. Sumer, J. Fredsøe, S. Christensen, and M. T. Lind. Sinking/floatation of pipelines and other objects in liquefied soil under waves. *Coastal Engineering*, 38(2):53–90, 1999. ISSN 03783839. doi: 10.1016/S0378-3839(99)00024-1.

[83] Stefan van Baars Baars. Design of sheet pile installation by vibration. *Geotechnical & Geological Engineering*, 22(3):391–400, 2004.

[84] JF Vanden Berghe. *Sand strength degradation within the framework of pile vibratory driving."*. PhD thesis, Doctoral Thesis, Université Catholique de Louvain, Belgium, 2001.

[85] K Viking. The vibratory pile installation technique. Proceedings of TRANSVIB, Paris, France, page 65-82, 2006.

[86] K Viking and A Bodare. *Laboratory studies of dynamic shaft resistance of a vibro-driven model pile in granular soil by varying the relative density*, volume 2, page 863–869. 1999.

[87] Kenneth Viking. *V IBRO - DRIVEABILITY*. PhD thesis, Royal Institute of Technology, Stockholm, Sweden, 2002.

[88] George Z Voyiadjis and Chung R Song. Determination of hydraulic conductivity using piezocone penetration test. *International Journal of Geomechanics*, 3(2):217–224, 2003.

[89] Mladen Vucetic. *Cyclic threshold shear strains of sands and clays*. Department of Civil Engineering, University of California, Los Angeles, 1993.

[90] B Wang, K Zen, GQ Chen, YB Zhang, and Kiyonobu Kasama. Excess pore pressure dissipation and solidification after liquefaction of saturated sand deposits. *Soil Dynamics and Earthquake Engineering*, 49:157–164, 2013.

[91] Don Warrington. Vibratory and Impact-Vibration Pile Driving Equipment. (March 1989), 1992. doi: 10.13140/RG.2.2.15745.51044.

[92] J Weijers, GT Elbersen, AR Koelewijn, and N Pals. Macrostabiliteit ijkdijk: Sensor-en meettechnologie. 2008.

[93] Valerie Whenham and Alain Holeyman. Load Transfers During Vibratory Driving. (October 2012), 2012. doi: 10.1007/s10706-012-9527-0.

[94] Richard D Woods. *Dynamic effects of pile installations on adjacent structures*, volume 253. Transportation Research Board, 1997.

[95] Richard D Woods and Larry P Jedele. Energy—attenuation relationships from construction vibrations. In *Vibration problems in geotechnical engineering*, pages 229–246. ASCE, 1985.

[96] Xian Jian Yang. Evaluation of man-made ground vibrations. 1995.

[97] Tokimatsu.J Yoshimi.Y and Ohara.A. N. In situ liquefaction resistance of clean sands over a wide density range. 44:479–494, 1994. ISSN 0016-8505.

[98] T Leslie Youd and Izzat M Idriss. Liquefaction resistance of soils: summary report from the 1996 nceer and 1998 nceer/nsf workshops on evaluation of liquefaction resistance of soils. *Journal of geotechnical and geoenvironmental engineering*, 127(4):297–313, 2001.

[99] T.L Youd. Packing changes and liquefaction susceptibility. volume 103, No. GT8 of *Journal of the Geotechnical Engineering Division, Proceedings of the American Society of Civil Engineers*, pages 918–922, 1977.

[100] Guo Qing Yu, Zi Li Wang, Zhi Zong Tian, and Bao Sen Zhang. Implementation of data mining in sluice safety monitoring. In *Applied Mechanics and Materials*, volume 71, pages 4329–4332. Trans Tech Publ, 2011.